Unraveling the projection-stratified anatomical and molecular organization of the Deep Cerebellar Nuclei

Inauguraldissertation

zur Erlangung der Würde eines Doktors der Philosophie

vorgelegt der Philosophisch-Naturwissenschaftlichen Fakultät

der Universität Basel

von

Staci Thornton

2022

Genehmigt von der Philosophisch-Naturwissenschaftlichen Fakultät

auf Antrag von

Professor Dr. Silvia Arber, Professor Dr. Flavio Donato, Professor Dr. Mackenzie Mathis

Basel, 22 March 2022

Prof. Dr. Marcel Mayor

The Dean of Faculty

Table of Contents

Acknowledgments

Most importantly, I would like to thank Professor Silvia Arber for her support and mentorship during my Ph.D. Her passion, curiosity, and knowledge of the motor system are truly inspirational and admirable. Her drive to understand the nervous system provides a phenomenal scientific environment of rigor and urgency. Furthermore, I cannot thank her enough for her understanding during the difficult and extraordinary times within the last year of my Ph.D.

Secondly, I could not have done anything in the lab without the amazing organization, patience, and support of Markus Sigrist, Monika Mielich, Elisa Cacciatore, and Rose Marie Suter. To them, I extend a tremendous thanks. I also want to extend my thanks to Professor Flavio Donato for his role on my committee, whose advice and direction have been extremely beneficial. Additionally, I would like to thank Professor Mackenzie Mathis as the External Expert in my committee.

I would also like to thank the members of the FMI and University of Basel, Biozentrum Facilities that allowed my projects to run smoothly and were always there to answer questions and support me. In particular, I owe a remarkable gratitude to Charlotte Soneson and Michel Stadler of the Bioinformatics Facility, Hubertus Kohler of the FACS Facility, and Sirisha Aluri and Sebastien Smallwood of the Genomics Facility. Furthermore, I extend many thanks to Laurent Gelman and Laure Plantard of the FMI Imaging Facility for their scientific and general support. I have learned so much from them about microscopy, both with my student job and in questions related to my project. Lastly, I cannot thank enough the support of the FMI Animal Facility, in particular Giséle, who made all of the mouse work possible.

An immense thank you goes also to the members of the Arber Lab, current and past, especially Kevin, Elisa, Wuzhou, Rita, Chiara, Riccardo, Ludwig, Paolo, Andrés, and Haohao. I cannot emphasize enough how much I valued our time, as both friends and colleagues. Especially to Kevin, seems like ages ago we met in Boston - thank you for being my “rock” in the lab. Thanks to Sivan, Tiago, Martina, Alissa, Zeynep, Kai, and Alex for our friendships, you mean the world to me.

I also would like to thank the many *women in STEM* who have paved the way for the current generation of women in science, many of whom I have had the pleasure of being mentored by or collaborating with. In addition to Silvia, several Women scientists who have been highly influential and inspirational in the past years of my scientific path include Professor Nilay Yapici, Professor Elaine Lee, and Dr. Caroline Escoubas.

"Unfortunately, nature seems unaware of our intellectual need for convenience and unity, and very often takes delight in complication and diversity."

—Santiago Ramón y Cajal, 1906 Nobel lecture The structure and connections of neurons

Summary

Movement is the main output of the central and peripheral nervous systems. Our daily lives depend on the precise coordination and execution of movements involving multiple limbs. The neuronal circuits which mediate and coordinate movement span throughout the brain and involve the integration of information across the brain's motor centers to modulate execution, learning, and action planning. Recently, groundbreaking work in the brainstem, cerebellum and motor cortex has provided a framework for developing methods, designing experiments, and conjuring hypotheses to understand how movement is controlled. Research dedicated to delineating spatially intermingled neuronal populations in the mouse brainstem gave rise to the work that will be described in this thesis. Specifically, we describe how neurons in the deep cerebellar nuclei (DCN), the sole output of the cerebellum and a structure canonically known as devoted to online motor control, are connected to the brainstem and thalamus. We find a high degree of synaptic specificity concerning target regions innervated by different subpopulations of DCN neurons. Using a myriad of genetic, viral, and molecular tools, we identify previously uncharacterized anatomical and molecular cell types in the deep cerebellar nuclei and brainstem.

Introduction

Cell types in the motor system

A “cell-type” is a continuously developing, and often ambiguous, term to describe how a group of cells *can be* classified similarly based on morphological, functional, or molecular properties. In the case of neuronal circuits, cell types are incredibly helpful for reducing the complexity of the tremendous number of neurons and heterogeneity in the nervous system. In the case of neurons, the above properties can be further adapted to reflect developmental origin, connectivity, and function. Professor Ed Lein of the Allen Institute for Brain Science argues that a “testable definition of “cell type” is a set of cells with common transcriptomic signature and low variation in other phenotypes (including connectivity)” (Lein, 2017). It is by this definition that many systems neuroscience questions have evolved.

Advances in viral and genetic tools have enhanced the ability to resolve patterns in connectivity within, and between, brain regions. Higher-throughput, cheaper cost, and standardization in molecular techniques and analysis have led to a deeper understanding of the RNA, protein, and epigenetic profiles of neurons within their circuits. The combination of connectivity and molecular properties provide a rationale for categorizing neurons into cell types.

Along with these advances in technologies, advances in the characterization of cell types in the motor system have risen in parallel. One such example in the motor system is the subthalamic nucleus (STN) which is a region involved in motor and limbic functions. Using a transgenic mouse line where *pitx2-cre* is expressed in the STN, six gene clusters were identified which mapped to specialized compartments within the STN, verified with *in situ* hybridization. With the molecular cell types identified, one can now characterize the heterogeneous STN populations also by anatomy and function within the context of motor control (Wallén-Mackenzie et al., 2020).

Identified cell types can also be used to assess how neuronal circuits have evolved. The deep cerebellar nuclei (DCN) are a set of nuclei are the sole output of the cerebellum and act in a feed-forward fashion in motor control (Ito, 2006). Single nuclei RNA sequencing and spatial transcriptomics of DCN in humans, mice, and chickens revealed that one of the DCN is expanded in humans one cell class at the expense of another. Furthermore, the same methods

of projection-defined DCN revealed 15 region-specific excitatory cell types and 3 region-invariant inhibitory cell classes. Taken together, these data show a shift in projection pattern and an emergence of cell classes within the DCN across species, providing insight into anatomically, molecularly, and evolutionarily distinct cell types of one key hub of the motor system. (Kebschull et al., 2020).

While these examples provide insight into the molecular, anatomical, and evolutionary classes of cells in two regions of the motor system, a recent consolidated effort to elucidate the motor cortex has provided grounds for highly detailed and technically unmatched elucidation of cell types in the motor system. This consensus study has combined transcriptomic, epigenetic, morphological, physiological, and projection patterns to define and link cell types in the motor cortex. This massive effort arose as part of the BRAIN Initiative Cell Census Network composed of research groups around the world to put pieces of a puzzle together to describe a cell type census of one brain region.

The cortex is a unique example in the brain as it is organized into layers defined by several features including transcriptomic and morphological properties. Spatial mapping using MERFISH, and morpho-electrical property elucidation using Patch-Seq revealed that cortical layers can be defined as unique cell types based on such features. Clustering analysis of the MERFISH expression profiles showed 95 cell clusters in the MOp (primary motor cortex), which corresponded to the previously shown single cell or single nuclei RNA sequencing data. Interestingly, although the layers are very clear, there appeared to show a continuous gradient consisting of gradual changes in expression profile along the depth of the layers. The authors then sought to determine if these cell type data could be similar with connectivity from the cortex to the subcortical regions. Applying retrograde tracers, and further integrating these data with the spatial results from MERFISH, showed that the three canonical regions received inputs from multiple cell clusters owing to the idea that “projections of MOp (primary motor cortex) neurons do not follow a simple ‘one cell type to one target region’ pattern”. (Bakken et al., 2020; Callaway et al., 2021; Chen et al., 2015; Scala et al., 2021; Zhang et al., 2020; Zhang et

al., 2021). This raises the question of whether a cell type can be defined by one, or even two, strict classification(s)?

By combining retrograde tracing and epigenomic profiling, authors were able to identify methylomes of over 2000 projection neurons. These molecular data matched classes of projection neurons where cortico-cortical, cortico-striatal neurons are enriched in IT subclasses in layers 2/3, 4, 5, and 6 of the cortex and cortico-subcortical projecting neurons are more prevalent in L5 ET layers of the cortex. (Zhang et al., 2021).

In summary, these recent studies in the motor system together provide a data-driven definition of cell type, which gives rise to the idea that neurons can cluster together based on one or two features, such as molecular and anatomical profile, which will likely correlate accordingly to its functional and morphological features as well. **It is this that gives rationale for further elucidation of two key regions in the motor system whose anatomical and molecular cell types have yet to be clearly elucidated.**

The Brainstem

What is the brainstem?

The brainstem is a conserved structure in the caudal half of the brain. It is phylogenetically the oldest structure of the brain but remains largely understudied especially in humans, and only recently has undergone fine-grained elucidation in mice. In descending order, it is comprised of the midbrain, pons, and medulla oblongata. Together, these three regions have often been grouped into one, as the brainstem, and referred to as a relay station that connects subcortical brain regions to the spinal cord, where the final motor output for body movements is generated. The brainstem has been proven critical for movement across species such as frogs, mice, cats, and primates (Bjursten et al., 1976; Hinsey et al., 1930; Roh et al., 2011; Whelan, 1996). However, these studies have largely been based on lesion experiments, therefore omitting key information on how projection and connectivity patterns may influence components of a motor program. The brainstem regions, or targets used for such experiments, have been defined by the common use of a three-dimensional stereotaxic atlas, which guides researchers to specific populations based on *morphological* features. (Franklin, 2019). While

this has been a long-standing gold standard, new atlases have arisen providing more data and information into the regions within the brain, such as a cell types database, brain connectivity atlas, developing mouse brain atlas, human brain atlas, as well as disease-related expression data (Schizophrenia, sleep, and autism). One such example is the Allen Mouse Brain Atlas, whose goal has been to provide a common platform for researchers to investigate the mouse brain at multiple systems-scale levels. The Atlas, which details 132 coronal and 21 sagittal sections sectioned at either 100um or 200um, respectively, provides grounds for studying molecular, cellular, and behavioral components of the brain (Allen Institute for Brain Science. Allen Brain Atlas API. Available from: brain-map.org/api/index.html). The combination of these two atlases has been paramount for the tremendous escalation of atlases including cell type, connectivity, developmental atlases of the mouse and human brains.

These atlases have provided vast amounts of information to help define and guide anatomical tracing, registration, and functionally interrogative experiments, as well as have a reference framework for brain research.

Developmental properties of the brainstem

As described in the previous section, molecular and morphological features of the brain have aided in defining cell types, however, one approach to defining cell types is by understanding the developmental origins of the structures. During embryonic stages of development, distinct classes of neurons develop and differentiate into unique zones and positions along the neural tube. These classes generate distinct cell positions and fates in the spinal cord. (Jessell, 2000). The expression of *Shh*, strikingly, spreads from ventral to dorsal in a gradient where one can see the impact on differentiation highest closest to the floor plate and weakening in gradient fashion towards the roof plate. These signals patterning the neural tube correspond and generate spatial segregation of functional distinct neurons in the spinal cord (Dessaud et al., 2008; Dessaud et al., 2007). Interestingly, *Shh* mediates the expression or repression of a set of homeodomain proteins including *Pax* and *Dbx, Nkx* genes, at different concentrations. These together correlate to the *shh* gradient of expression in dorsal-ventral patterning. (Briscoe et al., 2000; Jessell, 2000; Pituello, 1997). Dorsal pattern factors include members of the BMP signaling family, and dorsalin-1 (Basler et al., 1993; Liem Jr et al., 1995). In addition to the

dorsal-ventral patterning, also the rostro-caudal axis needs to be patterned as well as the medio-lateral axis in the spinal cord. Moreover, there is further subdivision of cell types in the lateral motor column which targets limb muscles. This structure itself is segmented such that the medial part projects to the ventral limb muscles, and conversely, the dorsal limb muscles receive input from the lateral division. (Landmesser, 1978a; Landmesser, 1978b).

The developmental organization of the spinal cord described here, shapes unique connectivity patterns and likely motor circuits which direct motor programs. These motor programs are dependent on supraspinal centers in the brainstem, and these developmental programs and progenitor domain origins aid in subpopulation specification (Arber, 2012; Grillner et al., 2005).

It can be hypothesized that similar developmental rostral-caudal, medio-lateral, ventral-dorsal patterns exist in the brainstem, which can be correlated to connectivity and morphological features.

Indeed, abundant work has been done to define the boundaries of the brainstem, canonically defined into **midbrain, pons, and medulla**. There are 12 segments of the hindbrain, based on developmental ontology including the isthmus and 11 rhombomeres. This is based on the gene expression of transcription factors, and does not align with the more traditional and current view of gross divisions of the pons and medulla. (Alonso et al., 2013; Puelles et al., 2013; Watson, 2010; Zervas et al., 2004). This model based on developmental origin indeed creates brainstem boundaries defined by genes mentioned to define the spinal cord, where *Otx2* defines the midbrain, *Fgf8, Gbx2* define the isthmus and R1 of the pons, and R2 to R11 of the pons and medulla are defined by expression of *hox* genes (Puelles et al., 2003; Puelles et al., 2004; Puelles et al., 2015; Watson et al., 2017).

While these studies provide a model of organization along the rostral-caudal axis, it remains open to what extent these developmental origins and molecular organization can be linked to connectivity and functional identity, therefore defining cell types or patterns in the brainstem. Moreover, there is also abundant cell migration along the rostro-caudal axis in the brainstem, such that developmental origin does not pair necessarily with adult cell position in space (Alonso et al., 2013).

Functional and Anatomical cell types in the brainstem

There has been a long-standing theory that the function of the brainstem is as a controller of breathing, heart rate, and sleep. (Ángeles Fernández-Gil et al., 2010; Brown et al., 2012), as well as a relay station due to its central location connecting it to subcortical centers and spinal cord centers. While it had seemed that the brainstem's function had been elucidated, in more recent years, the field of systems neuroscience has developed to take a deeper look at understanding how **cell types and subpopulations** within previously defined structures (described above) can actually be **stratified by projection** and shift the framework for defining functional subpopulations of motor circuits.

The efforts to further stratify subpopulations according to connectivity and function, two major properties to define neuronal cell types, have revealed patterns of connectivity along the medio-lateral axis of the brainstem. Populations within these connectivity-defined patterns modulate highly specific components of motor programs.

For example, a small region in the medulla has been shown to mediate different aspects of whole-body behavior based on neurotransmitter identity and structure. Excitatory neurons in the lateral paragigantocellular nucleus (LPGi) were required for high-speed locomotion, while activation of GlyT2 neurons in gigantocellular alpha (GiA) (a region very near to the LPGi) and LPGi resulted in behavioral stalling (Capelli et al., 2017).

A more rostral region more (LatRM: Lateral rostral medulla) and the medullary reticular formation dorsal or ventral part (MdD/V) has been shown to control a diverse range of forelimb behaviors, including reaching and handling (Ruder et al., 2021). This small structure can be divided anatomically and functionally by its connectivity. Spinally projecting LatRM neurons elicit unilateral reaching when activated optogenetically. Regions in the caudal medulla (MdD and MdV) also receive input from LatRM and have different function. MdD projecting LatRM can induce grooming or hand to mouth movements, and MdV-projecting LatRM can elicit reach-to-grasp or tapping movements of the forelimb (Ruder et al., 2021).

Lastly, the mesencephalic locomotor region (MLR) of the midbrain is a structure that is anatomically defined as a structure in the midbrain composed of the pedunculopontine nucleus (PPN), cuneiform nuclei (CN), and mesencephalic reticular formation (mRT) (Ferreira-Pinto et al., 2021). Furthermore, it is classically known to function in full-body locomotion, with a correlation between speed and stimulation intensity. (Noga et al., 1988; Opris et al., 2019). The MLR has been described to promote exploratory behavior as well as speed control, and movement initiation (Caggiano et al., 2018; Josset et al., 2018). Most recently, the MLR's function has been further clarified through the elucidation of projection-stratified populations and cell-type specific control of behavioral paradigms. Here, authors found that medulla and spinal cord projecting MLR neurons differ in function from an *Rbp4*-transgene positive cell type projecting to the substantia nigra. The MLR neurons which project to the spinal cord are tuned to full body motions, such as rearing and body extension, while the *Rbp4*-MLR sub type is tuned to forelimb movements. (Ferreira-Pinto et al., 2021).

Together, it is clear that within the brainstem along the rostro-caudal, and medio-lateral axis, neuronal populations reside which can be categorized into different cell types based on neurotransmitter identity, connectivity, morphology, and function. However, many questions remain open about how the brainstem is modulating movement. One such question is how descending information from the cerebellum to executive motor centers in the brain such as the brainstem and spinal cord, can influence movement. This will be discussed in the next section.

The Cerebellum

Thus far, we have discussed cell types in the motor system as well as a more detailed look at developmental and functional cell types in the brainstem. It is next important to ask how the movements previously described to be mediated by brainstem subpopulations may be *learned* or *coordinated* by its input, and therefore we turn our attention to the cerebellum. The control of movement is dependent on a vast network of neuronal circuits mediating appropriate motor neuron activity and respective muscle engagement. Not only does this coordination of many muscles depend on the descending commands directing movement through spinal networks but is reliant on continuous feedback aiming to optimize the motor output. This continuous

feedback can be called “online motor control.” This precise control and coordination are affixed to proper integration of multiple complex networks. The overall sensory system which provides this feedback arises from multiple pathways including visual, proprioceptive, and tactile pathways.

A forward model of sensorimotor adaptation

Given the nature of the feedback from the sensory system, one must ask to what extent the feedback is passed forward to descending circuits. This, likely excitatory feedback, gives rise to an internal forward model. The forward model, or central monitor, would function to use the information of motor commands to distinguish the sensory consequences of the performed action. (Azim and Alstermark, 2015; Azim et al., 2014; Conner et al., 2021; Thanawalla et al., 2020)

Therefore, a central monitor, or internal forward model, is proposed to exist in order to integrate and transform the information on these motor commands into a prediction of the outcome, further distinguishing the sensory consequences of our own actions. Not surprisingly, this sensory feedback can produce temporal delays leading to inaccurate motor output. The predictions can be used to compensate for delays in sensory feedback and create a form of online motor control to produce precise trajectories (Azim et al., 2014). The cerebellum is a structure in the brain whose role has been analogous to reducing these temporal delays, by predicting movement outcome through the implementation of internal copies of motor commands within the aforementioned forward model. The **forward model** can be shaped to circumvent mismatch between what is predicted and what is actually occurring, which can be defined as **sensorimotor adaption**. The forward model of the forelimb could predict the upcoming state, including parameters of movement such as position or velocity in a trajectory, given the current state and desired motor command. (Wolpert et al., 1998). When the sensory information is delayed, corrections may not be carried out and therefore produce an inaccurate representation of the current status of the peripheral motor system.

Where is the sensory information originating?

If the cerebellum is considered analogous to maintaining online motor control, then it must constantly integrate motor commands with ongoing sensory feedback. There are two pre-cerebellar systems which are thought to transmit the external and internal information to the cerebellar cortex in a way that modulates motor function, and movement. One of these two systems is the mossy fiber system, largely attributed to the transmission of sensory feedback from several structures discussed next. The most prominent and well-studied structures in the first pre-cerebellar system include the lateral reticular nucleus (LRN), external cuneate, and basilar pontine nucleus. (See Figure 1). These input structures collateralize in the deep cerebellar nuclei (the sole output of the cerebellum) in addition to projecting to the cerebellum proper (Altman and Bayer, 1987). Interestingly, there are differences about the degree to which this collateralization occurs: Less than half of the basilar pontine nucleus axons send collaterals (Parenti et al., 2002; Shinoda et al., 1992) to the deep cerebellar nuclei but almost the entirety of the LRN axons collateralize in deep cerebellar nuclei (Wu et al., 1999). The pontine nucleus is the largest of the pre-cerebellar nuclei. It has been shown to receive motor information from the motor cortex, in particular upper body motor cortical centers, and is the main mossy fiber input to the cerebellum carrying these signals. Pontine stimulation during a skilled movement resulted in disrupted cortico-cerebellar communication, and specifically altered kinematic parameters of the movement, suggesting that this loop is important for proper movement execution. Additionally, the pontine converges on sensory pathways from the external cuneate nucleus (Guo et al., 2021; Guo et al., 2020; Huang et al., 2013; Leergaard and Bjaalie, 2007). The external cuneate nucleus is a major source or proprioceptive input to the cerebellum, which receives signals from tactile nerve fibers and has been shown crucial for sensory computation processing. This nucleus then is postulated to modulate primary afferents to higher structures, via mossy fiber input to the cerebellum (Altman and Bayer, 1987; He et al., 2021; Yamada and Hoshino, 2016).

Lastly, the LRN, is another structure key to the pre-cerebellar system carrying sensory information. Neurons in the cervical spinal cord (C3-C4 propriospinal neurons) receive input from motor centers ascending to the LRN. In turn, this information is then sent to the mossy

fiber input to the cerebellum (Alstermark and Isa, 2012; Alstermark et al., 2007; Azim and Alstermark, 2015; Pivetta et al., 2014).

The second pre-cerebellar system is the climbing fiber system, wherein the climbing fiber neurons are located primarily in the inferior olive in the medulla oblongata region of the brainstem. The inferior olive is a highly compartmentalized structure which receives input from the cerebral cortex, red nucleus, and spinal cord. The excitatory projections terminate at the purkinje cells. (Altman and Bayer, 1987; Ruigrok and Teune, 2014; Yamada and Hoshino, 2016). When stimulated, the inferior olive has been shown to activate climbing fibers (Hounsgaard and Midtgaard, 1989). The Inferior olive innervates purkinje cells in the cerebellum in a highly structured way, such that there are five modules within the olivo-cerebellar-medial deep cerebellar nuclei circuit (Fujita et al., 2020).

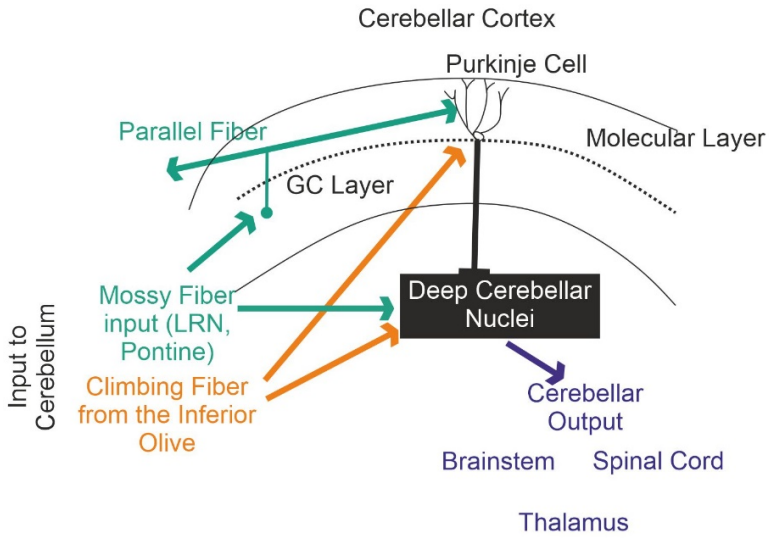

Figure 1: A model of the cerebellum, where the cerebellum is divided into the three layers, including the granule cell (GC layer), purkinje cell, and molecular layer. Mossy fibers originate in the pontine nuclei, LRN and project onto the cerebellar nuclei and in the granule cells in the granule cell layer. Granule cells connect to the molecular layer and collateralize in the opposite direction. These parallel fibers synapse with the Purkinje cells, which project to and inhibit the deep cerebellar nuclei. Climbing fibers originate in the inferior olive and project into the cerebellar nuclei and purkinje cells. The deep cerebellar nuclei descend to the brainstem, spinal cord, and thalamus. (adapted from https://nba.ugh.tmc.edu/neuroscience/m/s3/chapter05.html) Professor James Knierim, Johns Hopkins University.)

How are the internal copies processed within the cerebellum?

As shown in Figure 1 and discussed in the previous section, the cerebellar cortex is composed of the molecular layer, purkinje cell layer, and granule cell layer (Ito, 2006). These layers work closely together such that the Purkinje cells receive internal copy and sensory input from

granule cells. The granule cells communicate with the purkinje cells via parallel fibers found in the molecular layer. The input from mossy and climbing fibers that convey sensory information, will shape timing of the cerebellar neuronal activity through inhibition. The decisions of the purkinje cells which affect the final motor outcome is elicited through the deep cerebellar nuclei which project and target extra-cerebellar structures (Chan-Palay, 1977; Thanawalla et al., 2020).

Therefore, the cerebellum is vital for motor coordination and integration of sensory and motor feedback. The importance of the cerebellum has been seen clinically as well in animal experiments, where loss of motor coordination is defined as ataxia, and is a readout of cerebellar damage (Holmes, 1917; Sprague and Chambers, 1953). Specifically, Spinocerebellar ataxia type 1 (SCA1) is a fatal autosomal dominant neurodegenerative disease caused by a CAG trinucleotide repeated expansion within the coding region of the *ataxin-1* gene (Orr et al., 1993). MRI scans of SCA1 patients show atrophy and neurochemical abnormalities within the cerebellum and brainstem. The clinical symptoms include gait and limb ataxia, dysarthria, dysmetria (Bürk et al., 1996; Genis et al., 1995; Joers et al., 2018).

Of course, there are limitations in studying human and clinical data, therefore it is important to note that cerebellar ataxia has also been studied in mice. Homozygous *reeler* mutants show a severely ataxic gait, with mice having difficulties to maintain the hind limbs upright as well as poor performance in common behavioral tasks such as rotarod, beam, and water maze tests (Hamburgh, 1963; Lalonde et al., 2004). *Reeler* mice have has a sever neuropathology in the cerebellum, exemplified by an altered connectivity and morphology. (Terashima, 1983). Another model of cerebellar ataxia is the *purkinje cell degeneration (pcd)* mutant mouse. This model exhibits neural degeneration in postnatal development and is restricted to cerebellar purkinje cells. *Pcd* mice have locomotor deficits with specific multi-joint, inter-limb, and whole body coordination (Machado et al., 2015). Both *reeler* and *pcd* mice share similar abnormal cerebellar circuitry, with differences in synaptic connectivity in the brain and cerebellum, as well as distinct and shared features of gait ataxia.

The final channel of cerebellar signaling

This tremendous task of the cerebellum is carried forward by its sole output, a group of structures called the **deep cerebellar nuclei.** The deep cerebellar nuclei (DCN) project broadly to many regions but little is known about the organization and function of the descending pathways from DCNs to brainstem and spinal cord motor centers. Descending systems can be characterized by their origin (location of cells at the origin of the circuit), trajectory (location of neurons receiving terminations from the pathway), and collaterals ("other supraspinal targets innervated by axon collaterals from the circuit" (Sugiuchi et al., 2005)), pattern (number and distribution of fibers in the pathway. The quantity of axon collaterals can help to determine the complexity or focus of behavioral paradigms mediated by such circuits. One example is that the highly collateralized vestibulospinal tract axon system can promote coordinated movements. (Sugiuchi et al., 2005). The neurotransmitter or modulator released at the terminals of the circuit, as well as the molecular identity of neurons in the circuit are also valuable information. (Lemon, 2008).

These components provide a framework for identifying unique DCN cell types which give rise to understanding the functional role of the DCN in complex behaviors.

As described in previously, recent work from our lab has identified diverse neuronal populations in the brainstem controlling specific aspects of movement (Capelli et al., 2017; Ruder et al., 2021), but it is not known whether and how DCN inputs modify or control these descending pathways in the brainstem neurons and if so, in which behavioral context these inputs play a role.

The Deep Cerebellar Nuclei

Morphological and physiological properties of the DCN

The DCN contain a mixture of both excitatory and inhibitory neurons, equally dispersed throughout the structure (Baumel et al., 2009; Beitz and Chan-Palay, 1979; Kumoi et al., 1988). Excitatory projection neurons constitute approximately 50-60% of the population. These excitatory projections are numerous, and include perhaps most prominently, the projection to the cerebral cortex via the thalamus (Dacre et al., 2021; Dum and Strick, 1991; Gao et al., 2018; Guo et al., 2017; Kebschull et al., 2020; Kelly and Strick, 2003; Kuramoto et al., 2009; Low et al.,

2018a; Middleton and Strick, 2001). 30-35% of the neurons in the DCN are inhibitory projection neurons. The classical theory for decades has been that these inhibitory projections are exclusive to the inferior olive (Ito, 2006; Tolbert et al., 1976), however, recent work has described inhibitory projections to regions other than the inferior olive, including the brainstem, thalamus, and red nucleus (Judd et al., 2021). The remaining 10% of the DCN neurons are local inhibitory neurons (Chan-Palay, 1977; Czubayko et al., 2001). As mentioned, the DCN are the sole cerebellar output, and receive inhibitory input from the Purkinje cells. Purkinje cells are arranged in stripes which align with terminal fields of mossy fibers and climbing fibers, which vary in protein expression and the sub-nuclear target localization (Sugihara and Shinoda, 2007). The parasagittal zones of the cerebellum have the characteristic expression of the enzymatic marker zebrin II (aldolase C) (Apps and Hawkes, 2009; Leclerc et al., 1990; Leclerc et al., 1992). These stripes are continued in their DCN target, where Purkinje cell stripe projections to DCN have been described to be non-overlapping, thus, correlating the purkinje cell molecular zones to their projection target in the DCN. (Hawkes, 1997; Ito, 2006; Ito and Itō, 1984). However, it remains unclear to this point how exactly these Purkinje cell – DCN stripes can be considered unique modules. A individual Purkinje cell is postulated to innervate approximately 30-40 DCN neurons, while each DCN neuron receives input from 600-900 Purkinje cells (Baumel et al., 2009; Chan-Palay, 1973a; Chan-Palay, 1973b; Mezey, 1977; Palkovits et al., 1977). While the largest percentage of synaptic connections on the DCN is formed by Purkinje cells (60-85%), an important input arises from olivo-cerebellar fibers (5%) (Chan-Palay, 1973c; De Zeeuw and Berrebi, 1996; Mezey, 1977; Palkovits et al., 1977; Van der Want et al., 1989), but the weight of interneuron and mossy fiber synapses to the DCN projection neurons remains unclear. DCN neurons, which range in size from 15-35 microns or 5 – 20 microns (excitatory or inhibitory, respectively) (Baumel et al., 2009), fire spontaneously at over 10Hz, and firing rates are modulated by either sensory or motor activation. This modulation can be either increased or decreased (Eccles et al., 1974a, b; Rowland and Jaeger, 2005, 2008; Strick, 1983; Thach, 1968, 1975). Glycinergic neurons in one set of DCN have been shown to fire between 35-60 HZ, and both excitatory and inhibitory neurons in that nucleus

maintain sustained firing at physiological rates, suggesting a role in online control which perhaps helps to shape motor output.

Molecular Compartmentalization of the DCN

Ramon y Cajal, over a century ago, identified key characteristics of the brain, pivotal to current cerebellum research. This groundbreaking work identified one neuronal type in the cerebellar nuclei. As challenges turned into small hurdles, thanks to the advent of many new technologies, later the cerebellar nuclei were categorized into six types based on morphology only. (Chan-Palay, 1977) These neuronal types span the entirety of the DCN, which are organized into three major, and post well-studied, divisions including the Medial (Med), Interpositus (Int), and Lateral (Lat) DCN. These can further be segregated into eight minor subdivisions along the rostral-caudal and medial-lateral axis (Lateral, LatPPC, IntA, IntDL, IntP, Medial, MedDL, MedL**)**.

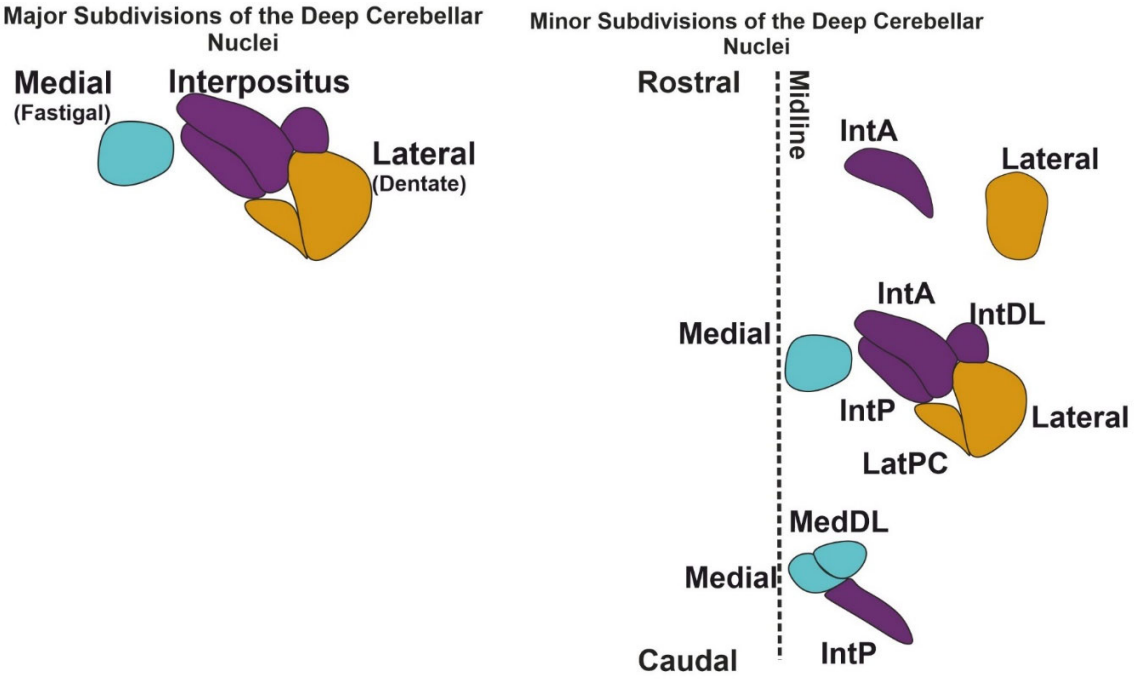

Figure 2: The major and minor divisions of the deep cerebellar nuclei, along the 3 rostral – caudal levels.

Within these divisions, there is a tremendous amount of neuronal complexity, which is striking, given the seemingly homogenous distribution of excitatory and inhibitory projection neurons and local interneurons. The molecular composition of the Purkinje cells has aided in determining to which DCN neurons Purkinje cells project. Axons from Purkinje cells generally

terminate in a specific area in the DCN, and axons from neighboring Purkinje cells within the same *aldolase c* compartment project to the same area on the DCN (Sugihara and Shinoda, 2007). Therefore, one could imagine that the molecular composition of the DCN can match cell types that are stratified by their cerebellar input. In the last two decades, this has started to come to light, primarily in concurrence with deeper molecular characterization of Purkinje cells. Effectively all neuronal types in the primate cerebellum contain at least one of three calcium binding proteins calretinin, calbindin, and parvalbumin (Fortin et al., 1998). Members of the cadherin family are expressed in unique patterns along the parasagittal stripes of the cerebellar cortex. These are also maintained in parts of in of the deep cerebellar nuclei. (Neudert et al., 2008). A detailed molecular map of the compartmentalization of the DCN revealed markers for medial, Int, and Lat, where markers for Int and Lat are shared in several cases**.** These *in situ* data revealed expression within each DCN including six expression domains in the medial nucleus (M1 to M6) where three genes are exclusively labeling the medial DCN (*GlyT2, Tbr1, ebf2)*. The interpositus nucleus can be segregated into four subdomains characterized by the expression of *Glyt2*, *Tbr1*, *ebf2,* HNK1, PLCβ4. The first domain (I1) is characterized by the absence of PLCβ4, and the horizontal sections stained for HNK1 and PLCβ4 from the second domain. The second domain (I2) is distinguished by the expression of HNK1. The third domain (I3) contains a small cluster of cells in the posterior Int labeled by *Ebf2-lacZ.* The fourth domain (I4) does not contain *GlyT2-EGFP, Ebf2-lacZ,* or Tbr1-immunoreactive neurons, but does contain neurons expression *thy1-YFP,* PLCβ4, and HNK1. The Lateral DCN can be divided into two molecular domains, where the first group (L1) can be compartmentalized by the presence of *thy1-YFP,* PLCβ4, and HNK1, and absence of *glyT2-EGFP, Ebf2-lacZ* and Tbr1 expression. Neurons in the second domain (L2) do not contain *thy1-YFP.* While these domains within the DCN have been identified, it is important to note that generally speaking two genes PLCβ4 and *HNK1* are expressed almost exclusively in Int and Lat, but not medial. *Tbr1* and *ebf2* are exclusively expressed in Medial. **This suggests a sort of molecular similarity between Int and Lat (Chung et al., 2009).** These expression data give rise to a first glance of the molecular complexity within the DCN, and a rationale for the need to identify cell types within the DCN that further explore their complex molecular heterogeneity. As mentioned before, it has been

speculated that the Purkinje cell projections lie in individual stripes, or micro-zones, where each has a private DCN terminal field. These *in situ* data, however, show many fewer expression compartments or domains than would make up the number of targets for the Purkinje cell stripes (20). Therefore, it is possible that there are indeed overlapping projection zones from the Purkinje cells to the DCN targets. While there are limitations with this study, being a targeted *in situ* screen, it suggests that there is a need to further categorize DCN cell types in both a molecular and anatomical manner (it is still unclear how the expression domains in the DCN correspond with the axonal terminal fields of the described Purkinje cell stripes). One could also wonder how and if the molecular cell types within the DCN correspond to the target in which the DCN project.

Anatomical Compartmentalization of the DCN

While the data presented in the previous section of this thesis describe a molecular means to a characterizing the expression profiles of the DCN into compartments, it remained unclear to what extent these molecular compartments can be correlated to anatomical projection profiles. In the most recent publication aimed to fully characterize the DCN, Kebschull et al., characterized the transcriptomic cell type, spatial organization, and projection profile of the three major DCN divisions (medial, interpositus, and lateral, hereby denoted Med, Int, and Lat). Anterograde tracing revealed that all three DCN, with the exception of Lat, innervate the spinal cord and all three innervate large portions of the ipsilateral (ipsi) and contralateral (contra) brain (125 ipsi and 140 contra brain regions), with largely similar regions in the thalamus, and brainstem. While similar, they noticed shifts in the relative density of terminations such that Int and Lat are more similar to each other than the Med projection patterns. Using single cell transcriptomics, they revealed four clusters, including three *Gad1* positive inhibitory clusters and one largely *Slc17a6* excitatory cluster, where there were only 5 inhibitory cell types and 15 nucleus-specific excitatory cell types distinguished by marker gene sets. They further identified two classes of excitatory neurons, where Class A and Class B vary expression and electrophysiological properties. While they have identified anatomical and molecular subtypes of the DCN, in which the molecular profiles are also spatially organized as verified by *in situ* methods, precise characterization is limiting with respect to the following key questions. It

remains unclear if and how the projection-stratified neurons in the DCN are transcriptionally related. It also is not known to how many targets a single DCN neuron projects. This information is vital for understanding and defining DCN cell types according to both molecular and projection/anatomical profile. This paper also showed that Int and Lat are more evolutionarily similar to each other than the medial. This similarity between Int and Lat has been shown in another study as well. The researchers show a striking segregation of Int and Lat from Medial based on specific transcription factors, where Int and Lat expressed *Brn2* while Medial expressed *Tbr1* (Fink et al., 2006).

While this study took an in-depth look at the classic divisions of the DCN, Med, Int, and Lat, Med, the phylogenetically oldest DCN, has been dissected further. Medial DCN has been divided into two distinct zones along the rostral to caudal axis, which differ in their electrophysiological properties and projections (Ito and Itō, 1984; Thach, 1975). The more rostral nucleus is thought to mediate adaptive control of full body behaviors, such as balance and posture by their projections to the vestibular nuclei and reticular formation (Lu et al., 2013) The more caudal fastigial (MedL and MedDL, Figure 2) have a role in cortical function, oculomotor control (Noda, 1990) and project to the thalamus and brainstem (Fujita et al., 2020). In primates, Med activity has been shown to influence a horizontal movement, and accuracy, within a saccade. It has also been shown to be required for saccadic adaptation and learning to fine tune behaviors (Batton III et al., 1977; Buttner et al., 1991; Noda, 1990). This more rostral Med nucleus has been shown to contain glycinergic neurons projecting ipsilateral to the brainstem vestibular and reticular nuclei , and excitatory neurons projecting contralateral to the brainstem and reticular nuclei (Bagnall et al., 2009). One can speculate that this means that these parallel output channels help to assist in cross-midline coordination, like postural adjustments, which would be required in a myriad of tasks where multiple limbs and/or the trunk is involved. As discussed, only around 30% of the projection neurons in the DCN are inhibitory and nearly exclusively project to the inferior olive. However, recent data suggest a critical role in of the Med glycinergic projections to the ipsilateral brainstem and indicate a further cell type diversity within the DCN (Bagnall et al., 2009)

As mentioned in the Introduction, neuronal cell types are best categorized by the combination of their transcriptomic type, anatomical/projection pattern, and functional relevance (either physiological or behavioral). To this end, cell types within excitatory neurons in the Med have also been elucidated, in the context of morphology, expression, and input-output connectivity. As seen in Figure 2, Med can be subdivided into the rostral, caudal, and dorsolateral protuberance (Med, MedL, MedDL), each of which has been linked with distinct sets of Purkinje cells, aligning with previously described notions that the well categorized Purkinje cells target distinct, largely non-overlapping, DCN targets. These three zones also align with district inferior olive nuclei (Batton III et al., 1977; Sugihara and Shinoda, 2007; Sugihara et al., 1999; Teune et al., 2000). As expected from work described in the previous section, many neurons were immunopositive for calbindin and calretinin proteins, but also included five populations of the Medial DCN which could be delineated by marker gene expression and anatomical distribution, where the more rostral Med was divided into three regions dorsal to ventral, and the caudal Med could be divided into two regions in the same manner. These regions were classified largely by the presence of three proteins, SNCA, SPP+, and CALB2. Single cell qPCR of the Med cells revealed four neuronal cell types (F1 – F4, with F1 being divided into two subgroups), which project to unique descending and ascending targets. The caudal Med (F2 and F4 subgroups) project differentially to the thalamus where the more medial and ventral region projects to the ventromedial thalamus preferentially, while conversely, the more dorsal and lateral region of the caudal Med projects to the ventrolateral thalamic nuclei. Based on the identified projection targets, which do have largely overlapping regions, the authors categorized the molecular, anatomical defined Med categories into also functional categories where F1 projects to either posturomotor or oro-motor regions (spinal cord, MdV, SubC, LPGi or IRt, PCRT, 7N respectively), F2 projects to brainstem and midbrain regions described in orienting behaviors, F3 correlates to output zones involved in positional-autonomic functions, and F4 output targets are involved in vigilance (Fujita et al., 2020). The extensive molecular and anatomical classification, and speculative functional classification, of these subclasses of Med provide groundbreaking insight into the high complexity of neuronal cell types within the DCN. It remains unclear, however, if and to what extent the expression profiles of the projection-

stratified neurons are unique. It also remains unclear to what extent these same projection-stratified neurons function in the speculated behavior based on projection target. The first remaining question could be addressed using a combination of the retrograde sequencing approach they have used for anatomical mapping, plus single neuron sequencing, where one can identify the transcriptomic profile of the projection-stratified neurons in the overall population of transcriptomic types in that region of the Med. In the same way, one could use retrograde tracing in combination with genetic silencers or activators to manipulate specifically these projection specific domains in the expected, or unexpected behavioral task.

The DCN and skilled behaviors

Medial DCN has been shown to be a center of gating/modulation required for learning (Gao et al., 2018; Sathyamurthy et al., 2020; Wang et al., 2020b). Specifically, silencing contralateral cervical spinal cord projecting medial DCN had no effect on skilled limb control reaching task, but could not sustain skilled locomotion on a rotarod. This effect was only seen when silenced prior to having learned the task (Sathyamurthy et al., 2020). The vermis-Medial DCN pathway has also been implicated in modulation of the amplitude of eyelid closure during a delay eyeblink conditioning task, a task often used to study mechanisms for associative tasks where the motor response is precisely timed with respect to sensory input (Wang et al., 2020b). Lastly, perturbing the medial DCN disrupted correct responses but not movement execution, but was required for maintenance of cortical preparatory activity. (Gao et al., 2018)- While the role of the medial DCN is not entirely clear, **Interpositus DCN** is inarguably critical for forelimb control.

Endpoint precision in a reaching task: Neuronal recordings of Interpositus revealed peak activity near the endpoint of a skilled reaching task. *Activation* of excitatory neurons in the Interpositus DCN resulted in a reduced upward and outward velocity of the reaching phase of the skilled forelimb program. Therefore, success was impacted given the expected outcome was perturbed by the neuronal manipulation. Conversely, *inhibition* of these neurons elicited an increased upward and outward velocity in the reach (Becker and Person, 2019). Similarly, an excitatory subpopulation within the IntA nucleus is required for efficacy of a skilled reach. Ablation of these neurons resulted in a decreased accuracy of the reach, where the mice reached farther than the expected termination before retrieving the pellet, compared to

control mice. While it was not analyzed in this paper, one would hypothesize that these data match the previously described study, where there is an increased velocity with silencing and therefore produce this over-reach phenotype. Interestingly, ablating these neurons in a locomotor task has a strong impact on the positioning of the forelimb movement (stride duration and stance duration) during locomotion (Low et al., 2018a). Most recently, the cervical spinal projecting population in Interpositus DCN has been shown to be required for a skilled reaching task, when silenced before and after learning. This suggests these spinally projecting neurons are required for online control of the forelimb during skilled movement. (Sathyamurthy et al., 2020) These data taken together, suggest that the temporal and spatial positioning of forelimbs are heavily mediated by Interpositus DCN.

Precise placement in a locomotor task: While we have focused largely on skilled forelimb movements in the context of a reaching task, it is important to note that Interpositus DCN is also required for adaptation to a split-belt treadmill assay. This assay probes the function of Int in a paradigm where one side of a treadmill increases its speed before the other side. Purkinje Cells directly innervating medial, Interpositus, lateral DCN were activated. This activation leads to inhibition of the respective DCN. Interpositus injected animals showed impaired step-length adaptation contrary to medial, lateral and controls. Interestingly, unlike the mildly ataxic *pcd* mice previously described, Interpositus-silenced animals were able to maintain the baseline perturbation in locomotion, suggesting the requirement of Int specifically in adaptation of a new task (Darmohray et al., 2019).

The **Lateral DCN** has been shown to ramp activity predictive of the timing and direction of self-initiated saccades (Ichinohe et al., 2000; Prevosto and Sommer, 2013). Furthermore, projection specific domains of the DCNs have been functionally interrogated, including a medial-brainstem pathway mediating locomotor learning and a cervical spinally-projecting Interpositus pathway required for performance in a forelimb task (Sathyamurthy et al., 2020; Wang et al., 2020b). (Figure 3).

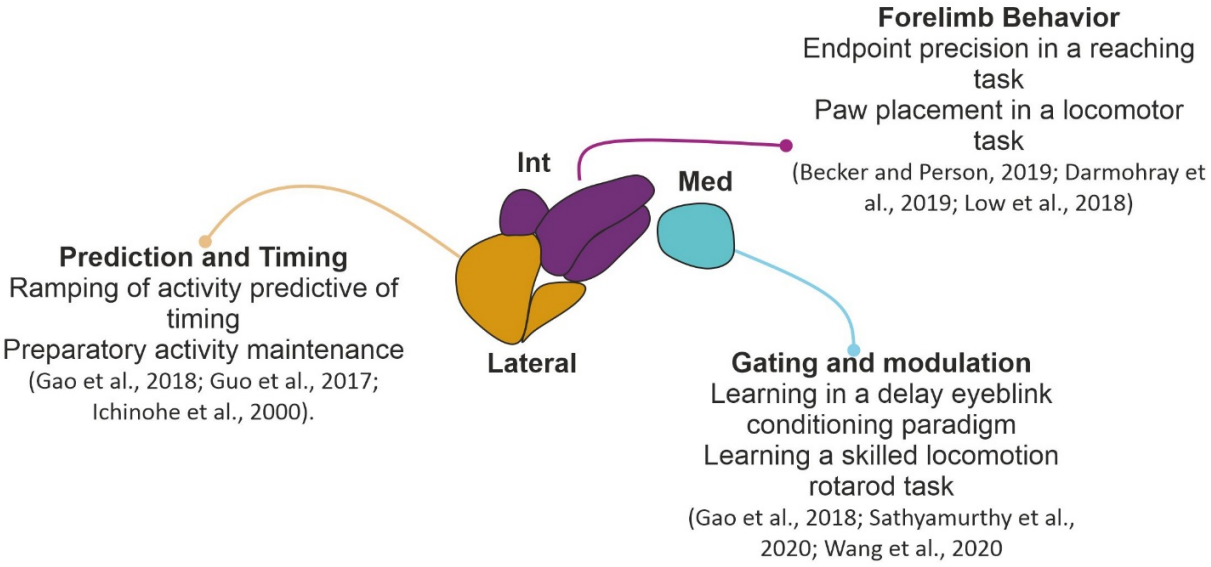

Figure 3: Abbreviated summary and categorization of the classically defined DCN according to recent literature

Therefore, the DCN have been broadly studied but these studies were largely restricted to the overall medial, lateral, and interpositus DCN subdivisions despite the knowledge and growing evidence of additional organization and diversity within these nuclei, as well as their minor subdivisions (rostral medial, caudal medial, medDL, medL, IntA, IntDL, IntP). Recent studies have begun to explore the function of subpopulation specific domains (cervical-spinally projecting and MdV projecting DCN), as well as unique molecular profiles (medial, medDL, medL) (Sathyamurthy et al., 2020; Wang et al., 2020b)

There is still a lack of extensive and precise anatomical, behavioral, and molecular mapping of the excitatory populations largely with respect to brainstem and spinal cord projecting populations. This knowledge is essential for understanding the cell types within the DCN and crucial for clarifying the numerous complexities of the DCN.

The DCN as a node in multiple brain-wide loops

Thus far we have described the complexity of molecular, input-output, and functional cell types that the neurons of the DCN embody. However, it is important to also note that the DCN have been described and further speculated to play key roles in two brain wide loops. These large “loops” are critical for the integration of signals, either motor or sensory, which ultimately mediate the optimal final motor output.

DCN and Red Nucleus

The Red Nucleus (RN) is a structure of the midbrain, which is composed of two (known) domains, the parvocellular and magnocellular zones. The magnocellular (mRN) is the more caudal region, while the parvocellular (pRN) is the more rostral region, where large sparse neurons make up the former while medium-sized neurons make up the latter (Onodera and Hicks, 2009; Ulfig and Chan, 2002; Yamaguchi and Goto, 2008). In a similar way that was described for defining cell types of the DCN, domains within the RN have been delineated based on connectivity patterns. The mRN has been shown to project to the contralateral spinal cord and inferior olive. The RN receives specific input from the DCN, where Lat projects to the more rostral RN and Int projects largely to the caudal RN (Basile et al., 2021; Kennedy and Humphrey, 1987; Ruigrok and Teune, 2014; Swenson and Castro, 1983). This raises the obvious question as to what information are these two divergent pathways, Med versus Int and Lat, sending to their respective RN regions and where then is this information being passed further. It is well established that the DCN play a role in forelimb behaviors, where Int encodes kinematic related parameters of limb movement (Becker and Person, 2019). It has also been shown in primates that the RN neuronal activity encodes kinematic parameters as well. The activity of the structure correlates with timing and magnitude of upper limb muscle activity (Kennedy and Humphrey, 1987; Kohlerman et al., 1982; Miller and Houk, 1995). It can therefore be speculated that these timing-related signals are being sent from the DCN. Indeed, experiments in turtle models have shown that there is positive feedback between the RN and Int, as seen when the selective inactivation of RN reduces activity in Int and, conversely, inactivation of Int reduced activity in RN (Keifer, 1996).

With the advent of anterograde tracing methods, it has been found that the mRN innervates the cerebellar cortex minimally, and maximally to the DCN, compared to the basilar pontine nucleus, a known source of mossy fiber carrying motor information to the cerebellum. This mRN preference to targeting to the DCN puts the mRN in a position for modulation of Int integration of Purkinje cell inputs, giving rise to the hypothesis that the DCN and RN constitute a processing module independent, or semi-independent, of the cerebellar cortex. This has been shown recently with optogenetic tools that Int inputs projecting to the mRN show strong

excitation but not inhibition, suggesting that Int is under afferent control independent of the cerebellar cortex (Beitzel et al., 2017a). One could therefore speculate that recurrent feedback exists between mRN and Int which is important for maintaining muscle recruitment, by way of interaction also with the cervical spinal cord, supporting key kinematic parameters throughout the movement (Beitzel et al., 2017a).

The DCN as a node in the cerebello-thalamo-cortical loop

The DCN project to the cortex via thalamic nuclei, but the exact role, and precise tracing to identify which DCN and which thalamic nuclei are involved in the thalamo-cortical loop, and to what extent they are required for given tasks remains unclear despite several recent studies addressing these questions.

Both the DCN and the cortex have been shown to be critical for “goal-directed” movements, as well as learning tasks ranging from skilled locomotor learning, skilled reaching, and licking (Darmohray et al., 2019; Gao et al., 2018; Guo et al., 2020; Low et al., 2018b; Sathyamurthy et al., 2020; Schäfer et al., 2020). Cerebellar activity has been shown to contribute to preparatory activity in the motor cortex, where silencing the lateral DCN caused suppression of preparatory activity in the anterolateral motor cortex (Chabrol et al., 2019). Combinatorial viral tracing strategies allowed for the identification of DCN-recipient motor thalamic (MThal) regions, such that retrograde tracing in the caudal forelimb area (CFA) of the cortex, plus anterograde tracing in the combined Interpositus and Lateral DCN (Int/Lat) resulted in a near 100% overlap in the Ventrolateral (VL) thalamic nuclei. This tracing approach suggests that Int/Lat projects to the CFA via VL. In order to assay the functional requirement of these three nuclei within the cerebello-thalamo-cortical loop, they applied gain and loss of function, plus neuronal recordings, in either the DCN, MThal, or CFA. These manipulation experiments, in addition to the recording data, are limited in concrete conclusions likely owing to the fact that both the manipulation and recordings are not projection specific, but rather, merely manipulate the regions that have been implicated to be connected via anatomical tracing. Likely, this is due to a limitation of viral techniques. Nevertheless, they argue that, during a cued-forelimb push task (head-fixed) which asks how these three regions convey a motor timing signal, in which 210/248 Int/Lat recipient MThal neurons encode push related activity, either by increasing or

decreasing prior, or increasing or decreasing after the reward. Activation of axon terminals over DCN recipient MThal or MThal recipient CFA triggered full lever push movements. Conversely, silencing of each nucleus along the pathway blocked movement initiation, suggesting that the Int/Lat-thalamo-cortical pathway is required for maintaining a learned forelimb movement initiation (Dacre et al., 2021).

In a similar way, the Medial DCN—thalamo-cortical loop has also been studied in the context of preparatory activity, where mice performed a sensory discrimination task using short-term memory to plan a figure directional movement by licking. Both Med and the frontal cortex encoded preparatory activity, similarly to the previously described work where Int/Lat, and CFA activity was observed prior to the movement onset (Dacre et al., 2021). Silencing of the frontal cortex led to lack of preparatory activity in the Med, and conversely, Med was required for preparatory activity in the frontal cortex. While this work focuses on the relation of the Med and Cortical areas, notably, they observe that the Med projects preferentially to ventromedial MThal, while (in a similar way to the previous work) the Lateral DCN projects primarily to the more dorsal ventrolateral MThal. This Med-recipient MThal overlaps largely with their frontal cortical region (anterior lateral motor cortex) projects to in the thalamus. Again, this paper merely mentions that the DCN and cortical areas of interest make up nodes in the thalamo-cortical loop, by way of the VM MThal, but do not directly address the function of the thalamus in this node (Gao et al., 2018).

As mentioned, there are limitations with the conclusions from both studies, as neither interrogates, nor records in a projection-specific nor cell-type specific manner. These data conclude on the necessity of the nodes to learn a movement related task, as well as the symbiotic relationship of either the Int/Lat and CFA or Med and ALM in preparatory activity and success within the tasks, but the information which is sent remains a mystery. Interestingly, the Lateral DCN was used as a control for the Med-VM-ALM project, where they saw no preparatory activity in their task. Of course, the first study combined Int and Lat and assayed a different task, potentially giving rise to the conflicting data, but these are confounding results which need to be addressed. From these data, the DCN are critical for coding future movement and timing of movement, in the motor cortex by way of their respective motor thalamic nuclei.

Given what we know about the DCN projections to the brainstem, it is critical to address the question of if projection stratified DCN project to both the brainstem and MThal. It remains unclear to what extent DCNs embedded in the thalamic loop influence brainstem neurons and whether DCN neurons projecting to the thalamus also influence the brainstem directly. Furthermore, it would be beneficial to know exactly to which region of the motor cortex is targeted by the DCN via thalamus, using viral strategies which jump one synapse to the next.

Chapter 1

Introduction

Thus far, we have discussed how neuronal cell types can be defined, from molecular, anatomical, and functional approaches. We have discussed the brainstem, the most caudal region of the brain just before to the spinal cord which acts as a command center for motor programs. We have introduced the cerebellum, which integrates internal copy signals from several other regions of the brain to help optimize and correct for errors. We have further introduced the Deep Cerebellar Nuclei, the sole output of the cerebellum. And we have touched on the role of the deep cerebellar nuclei in two brain-wide loops. While many conclusions have already been made on the DCN, they remain a key structure in the motor centers of the brain that remains largely unexplored with respect to the much necessary combination of molecular, anatomical, and functional methods, especially with respect to the brainstem. This is critical for understanding how the DCN are coordinating motor output, and maintaining online motor control, especially in the context of DCN-brainstem connectivity following recent fine-grained functional elucidation of the brainstem's role as an executive motor center. Therefore, in this Chapter 1, we have four main aims in the characterization of the anatomical cell types of the DCN, in the context of their connectivity to motor centers in the brain.

Aim 1: Map the excitatory output of the DCN to the brainstem and motor thalamus

Significance: A complete characterization of the excitatory output to key motor centers in the brain, the thalamus and brainstem, is lacking. While the DCN have recently been shown to project to the motor thalamus as well as the caudal medullary region of the brainstem (Wang et

al., 2020b), a complete characterization to descending motor centers is missing. Given the complexity of the DCN, we hypothesize that the classic divisions of the DCN project to unique zones in the brainstem, which spans across the rostral to caudal axis (from 5N to 12N, described in the following sections).

Approach: Anterograde viral tracing using viruses containing Flex or Frt AAV Synaptophysin plus a fluorescent Tag (Flex-AAV-SynTag or FRT-AAV-SynTag) in transgenic mice to determine synaptic terminal density patterns in the brainstem and motor thalamus. We target either Medial DCN or the combination of Interpositus and Lateral DCN, hereby called Med or Int/Lat respectively.

Brief Conclusion: The classically defined DCN can be redefined by projection patterns, where the Medial DCN descends nearly exclusively to the contralateral medial brainstem and Int/Lat DCN descend to both the contralateral medial brainstem and the ipsilateral lateral brainstem, with a higher terminal density to the ipsilateral lateral brainstem. This medio-lateral patterning is consistent in the ascending direction to the motor thalamus, where the ventromedial nucleus receives a higher weight of input from the Medial DCN, and the ventrolateral nucleus receives a higher weight of input from the Interpositus/Lateral DCN.

Aim 2: Characterize a genetic cell-type of Interpositus DCN

Significance: One major caveat to precision mapping of the DCN is the small size of the structures. The transgenic line, *ntsr1-cre*, expresses cre recombinase in a subset of excitatory Interpositus and lateral DCN. While this line has been used in recent work to characterize the Interpositus nucleus in a skilled reaching task, the anatomical characterization of the line is lacking. This line would add great value to precise targeting of the Interpositus and Lateral DCN, but it is critical to know to where and what extent the *ntsr1-cre* positive DCN cells project to in the thalamus and brainstem.

Approach: Using retro-orbital (Systemic, flex-PhP.eB) viruses (Chan et al., 2017), we quantify the distribution of *ntsr1-cre* positive cells compared to *vGlut2-cre* positive cells in the DCN. Using anterograde -*cre* dependent viruses, we compare the synaptic output of the *ntsr1-cre* positive cells to *vGlut2-cre* positive cells in the brainstem and motor thalamus.

Brief Conclusion: ntsr1-cre positive DCN neurons are located nearly exclusively in Interpositus and Lateral DCN, whereas the distribution of excitatory *vGlut2-cre* positive DCN are evenly distributed across the DCN. *ntsr1-cre* positive Int/Lat neurons project similarly to the *vGlut2-cre* positive Int/Lat neurons with respect to the brainstem and motor thalamus, but project preferentially in a way that suggests they are a minor subset of excitatory Int/Lat neurons.

Aim 3: Identify projection-stratified organization within the DCN

Significance: As discussed in the introduction, the DCN have been classically divided into three main structures (Medial, Interpositus, and Lateral), whose relative structural shape changes along the rostral-caudal, dorsal-ventral, and medial-lateral axes. Further discussed in the introduction was a molecular compartmentalization defined by expression patterns giving rise to more fine-grained cell type divisions within the classically defined DCN. With this, in addition to the patterns of connectivity from Aim 1, we hypothesize that there may be a projection-stratified topographical organization within the Int/Lat.

Approach: Using a -cre dependent retrograde virus, tagged with a fluorescent tag (rAAV-Flex-Tag) we focus on the rostral medulla, 7N region of the brainstem and retrogradely infect either the medial or lateral rostral medulla (defined in the Results section). We then quantify the number of retrogradely labeled neurons and align the distribution to a 3D brain registration (Wang et al., 2020a) to visualize the spatial organization.

Brief Conclusion: In accordance with the results from Aim 1, we see a spatial organization of projection-stratified neurons in Int/Lat, delineated by projection to either medial or lateral rostral medulla, and the laterality of the projections.

Aim 4: Map the collateralization patterns of the Int/Lat DCN

Significance: While it is known that the DCN have a vast amount of descending and ascending projections, it has remained largely unclear if projection-stratified neurons project to multiple regions, in particular, the multiple regions in the brainstem and thalamus described in Aim 1. This is critical for understanding the anatomically defined cell types within the DCN, because it provides insight into how and what signals are being integrated across nodes which comprise key motor circuits.

Approach: Combinatorial viral tracing, using flex-retrograde tagged with a reporter (rAAV-cre-Tag) into either the contralateral medial rostral medulla (MedRM) or ipsilateral lateral rostral medulla (LatRM) (further defined in the Results sections) or contra motor thalamus plus anterograde Flex-AAV-SynTag and anterograde Flex viruses which fill the axons tagged with a fluorophore (Flex-AAV-cTag) into either the ipsilateral or contralateral Int/Lat will allow visualization of collaterals in the brainstem or motor thalamus.

Brief Conclusion: Projection-stratified Int/Lat neurons collateralize at multiple regions in the brainstem and thalamus, such that contra MedRM projecting Int/Lat collateralize minimally into the ipsilateral LatRM, and conversely the ipsi LatRM projecting Int/Lat collateralize into the contra MedRM. MThal projecting Int/Lat collateralize to both the contra MedRM and ipsi LatRM, but with preference to the dorsal PCRt region of the LatRM.

Results

Deep Cerebellar Nuclei defined by excitatory output to motor centers

As discussed in the introduction, the deep cerebellar nuclei (DCN), are set of three classically defined nuclei, which are comprised of both excitatory and inhibitory neurons. This neurotransmitter composition of the medial, Interpositus, and Lateral DCN neurons is relatively similar across the DCN (Figure 1A)**.** Recent work has verified with *in situ* and RNA-sequencing that the distribution of *Gad1* and *Slc17a6* and *Slc6a5* classical inhibitory and excitatory markers to be evenly spread throughout the medial, Interpositus and lateral DCN (Kebschull et al., 2020). While the relative neurotransmitter composition of the DCN is not composed of striking patterns of distribution, the canonical perception has been that, with the exception of the inferior olive in the caudal medulla, broad DCN output is nearly *exclusively excitatory*. Recent work has countered that long-standing theory (Judd et al., 2021), therefore in order to re-address this question, we employed an anterograde viral tracing strategy to map the output of all excitatory and inhibitory DCN neurons in the brainstem and motor thalamus regions of the motor system within a mouse of specific genetic background. We chose to focus on the brainstem and motor thalamus (MThal) based on current literature and current work in the lab, as discussed in the Introduction. Anterograde tracing using a Flex-Synaptophysin Tag (Flex-SynTag) virus injected into the excitatory DCN (n=3) of *vGlut2-cre* transgenic mice (Figure 1B)

reveals widespread synaptic terminations across motor regions of the brain, similar to what has been described before in the thalamus and brainstem (Figure 1C,D,G) (Fujita et al., 2020; Judd et al., 2021; Kebschull et al., 2020). Anterograde tracing using FRT-Synaptophysin Tag (FRT-SynTag) or Flex-Synaptophysin (Flex-SynTag) virus into the inhibitory DCN (n=2) on the other hand, revealed little to no synaptic terminals in motor centers of the brain, with the exception of the expected Inferior Olive in the 12N region, as well as the superior periolivary nucleus in the 5N region. (Figure 1D-G). We further put focus on regions of the brainstem defined according to motor nuclei clusters (5N, 7N, and 12N), which segment the brainstem along the rostral to caudal axis. These regions have been described as three main regions of the brainstem, delineated by function (Esposito et al., 2014). Furthermore, these zones represent anatomical, morphological, and functional boundaries of the brainstem caudal to the beginning of the 5N and continuing caudal to the 12N (Alonso et al., 2013; Franklin, 2019; Puelles et al., 2013). Synaptic terminals were imaged using a bespoke (FMI, FAIM Facility) spinning disk confocal (See Methods) and terminals were quantified using Fiji TrackMate and Imaris quantification (Ershov et al., 2021). The excitatory synapses were vast in all three brainstem zones as well as the motor thalamus, defined as the ventromedial and ventral lateral thalamic nuclei, with synapse number averaging between 20000 and 30000 puncta (Average at the Rostral Medulla level of 27907 terminals. N=3, SEM = 2786) (Figure C,D,F,G). In contrast, the number of inhibitory synaptic terminals remained significantly lower (1748 at the Rostral Medulla Level (N=2, SEM=596), again with puncta restricted to Inferior Olive at the 12N region. (Figure 1E,F,G). Mapping the excitatory output revealed a widespread distribution. However, we identified unique patterns in laterality of projection where we saw contra and ipsilateral biases, where the contralateral pontine reticular nucleus, caudal part (PnC), medullary reticular nucleus, ventral part (MdV), gigantocellular reticular nucleus (Gi), intermediate reticular nucleus (Rt), and ipsilateral Irt, medullary reticular nucleus, dorsal part (MdD) and parvicellular reticular nucleus (PCRt) had the most striking patterns of synapses. Strikingly the more medial regions mentioned, (PnC, MdV, Gi), contain proportionally more contralateral terminals from the DCN while the more lateral regions mentioned (PCRt, IRt, MdD) contain proportionally more ipsilateral terminals (Figure 1C,G). In the thalamus, the largest number of synapses were

found in the contralateral ventrolateral thalamic nucleus (VL), ventromedial thalamic nucleus (VM), and centromedial/centrolateral thalamic nucleus (CM/CL). The ipsilateral CM/CL thalamic nuclei are also densely labeled (22586 terminals, n=3, SEM 7618).

Given our interest in the motor system, and hypothesis that the DCN contribute to online motor control of motor programs controlled by brainstem and motor thalamic regions, we therefore decided to explore further to what extent the classically observed excitatory neurons in the DCN contribute to the excitatory projection patterns revealed in Figure 1, neglecting inhibitory DCN in further analysis.

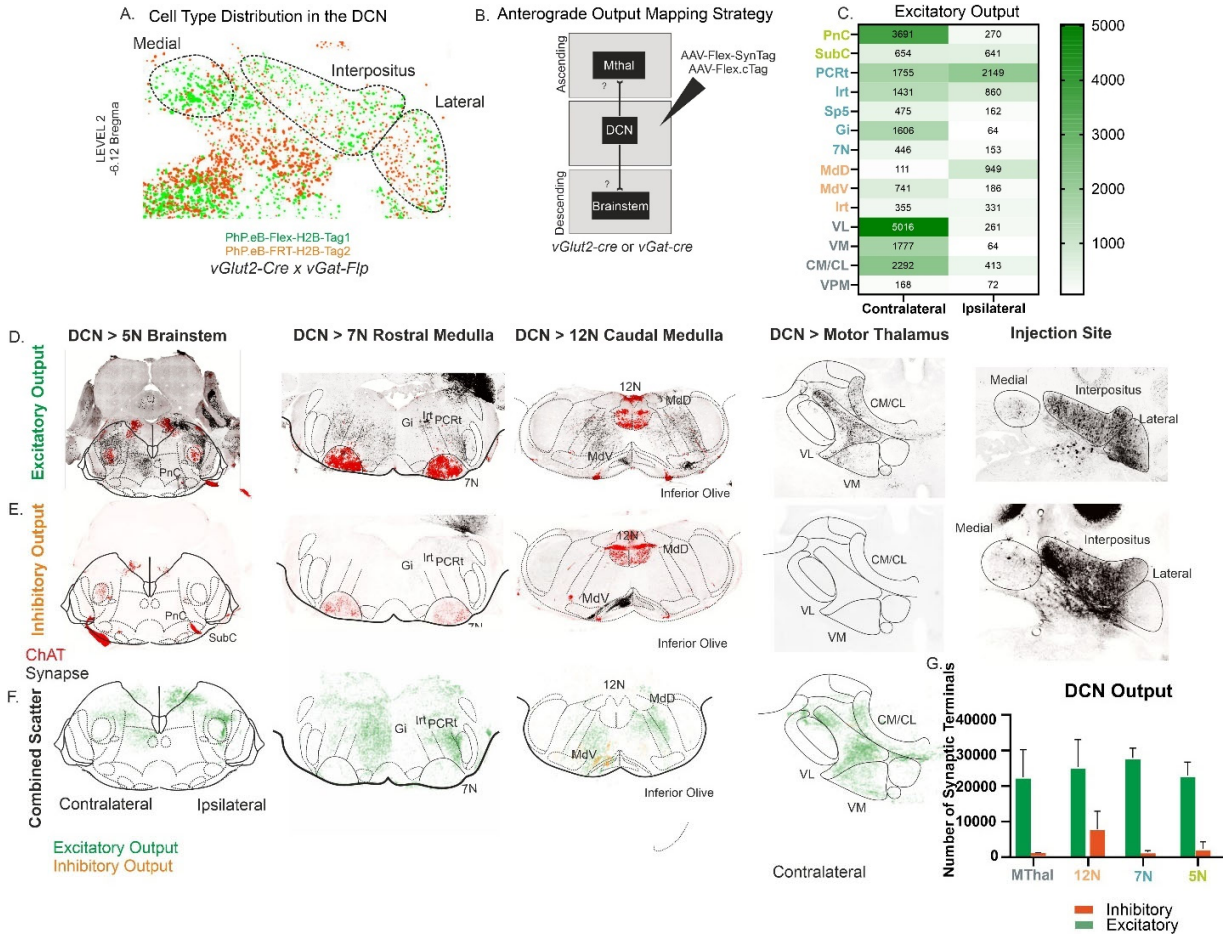

Figure 1: Anterograde mapping of excitatory and inhibitory output neurons. A). Excitatory (green) and Inhibitory (orange) nuclei of the Medial, Interpositus, and Lateral DCN by co-injection of a PhP.eB Flex-H2B-Tag and a PhP.eB FRT-H2B-Tag into a *vGlut2-cre x vGat-flp* transgenic mouse line. B). Experimental strategy for anterograde tracing from excitatory or inhibitory neurons C) Distribution of synaptic terminal quantification in heat map format where red represents the highest number of terminals and blue represents the lowest. D, E). Confocal images of the 5N, 7N, 12N levels of the brainstem plus MThal where Acetylcholine (ChAT) is in red to define the 5N, 7N, or 12N. Synapses are labeled in black. Boundaries are drawn according to the Mouse Brain Atlas. F). Scatter plot representation of the dual anterograde injection into *vGlut2-cre x vGat-flp* mouse line, where each dot represents one synapse (orange in inhibitory, green in excitatory). G). Quantification of synaptic terminals in the motor thalamus (MThal) and 12N, 7N, 5N regions of the brainstem. Bars represent the average number plus SEM. (n=3 excitatory (n=2 *vGlut2-cre,* n=1 *vGlut2-cre x vGat-flp* and n=1 inhibitory in *vGat-cre*). Note* Dot representations are quantified through the Z Stack.

DCN redefined by medial-lateral patterning in descending output

Thus far anterograde output mapping of the DCN (combined Medial, Interpositus, and Lateral) revealed widespread excitatory projections to the brainstem and thalamus. We next asked to what extent these classic divisions of the DCN, as described in the Introduction, contribute to projection patterns. Figure 1 reveals that the DCN project to many regions of the brainstem, spanning the 5N to 12N regions of the brainstem in both contralateral and ipsilateral directions. We focused our injections of AAV-Flex-SynTag on Medial (Med) and Interpositus and Lateral DCN. Due to difficulty with precision targeting, and the combined information described in the introduction where Lat and Int are molecularly more similar to each other than the medial DCN (Fink et al., 2006; Kebschull et al., 2020), plus the recent work to combine Int and Lat based on similar projection to the motor thalamus (Dacre et al., 2021), we pooled Interpositus and Lateral DCN together, henceforth named (Int/Lat). (Figure 2A, B). We first focused on the 7N Brainstem (Rostral Medulla, RM) where we found that Int/Lat projects preferentially to the ipsilateral lateral rostral medulla (LatRM), with a smaller proportion of terminations in the contralateral medial rostral medulla (MedRM). **LatRM** is a region composed of the canonical boundaries PCRt, SP5, IRt (shown in Figure 1D) and also described Ruder et al., 2021 (Ruder et al., 2021). MedRM is composed of Gi, LPGi, and Gi alpha. This is further defined in Figure 5. Of the total terminals quantified across the RM, 56.8% (n=4, SEM =4.1) were located in ipsi LatRM and 31.8% (n=4, SEM=3.7) were in contra MedRM. 4.9% were in the ipsi MedRM (n=4, SEM=1.2) and 6.7% were found in the contralateral LatRM (n=4, SEM=2.0). On the contrary, the Med DCN projected almost exclusively to the contralateral MedRM. Of the total terminals quantified across the RM, only 4.1% (n=4, SEM=1.3) were located in ipsi LatRM and 67.2% (n=3, SEM=5.7), were in contra MedRM. 11.1% (n=3, SEM =6.1) were in the ipsilateral MedRM and 14.4% (n=3, SEM 2.9) were in the contralateral LatRM. We visualized this using contour density and kernel density plots (Figure 2D,E). These shown representative injections are reproducible across experiments (Figure 2F). Visualizing the synaptic distribution by percentage of synapses per RM region (contra LatRM, contra MedRM, ipsi LatRM, ipsi MedRM) over the totality of synapses of the RM reveals that Int/Lat DCN neurons are preferentially targeting the ipsilateral LatRM and due to the lack of ipsilateral LatRM neurons receiving input from Med, *this suggests*

that Int/Lat are required for the contribution of excitatory DCN output to the ipsilateral LatRM. In contrast, while Int/Lat do project to contralateral MedRM, *Med DCN is the main contributor of the DCN to this contralateral descending circuit, with widespread and dense contralateral terminals* (Figure 2C).

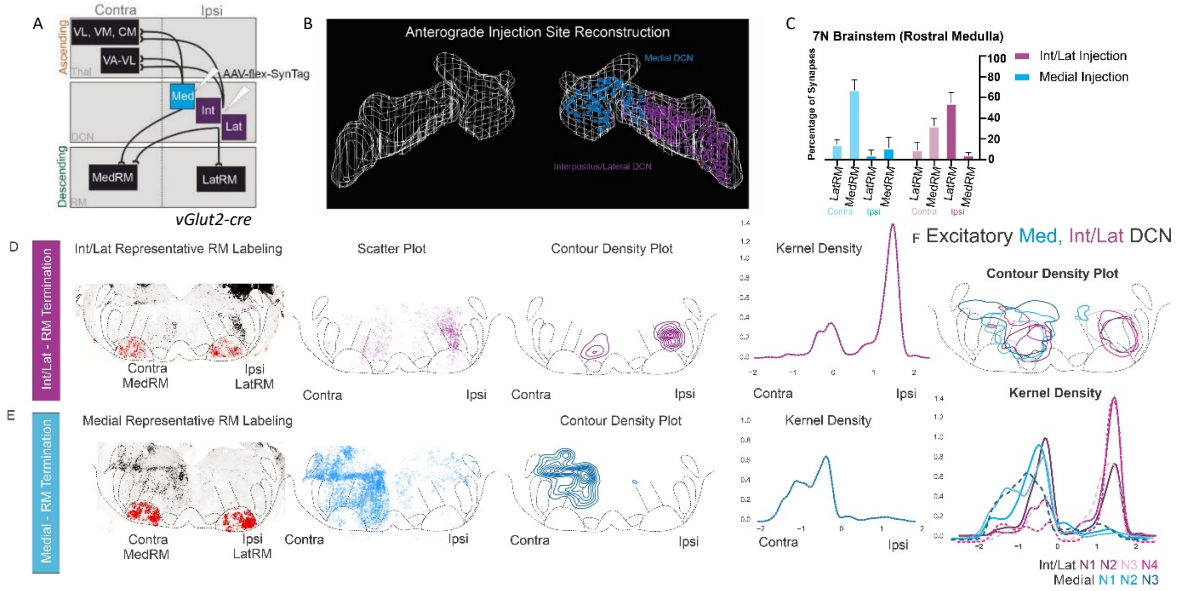

Figure 2: Anterograde mapping of the excitatory medial and Int/Lat DCN A) Experimental strategy to label classically defined DCN. Medial DCN is shown in cyan, while Int/Lat DCN is shown in purple. AAV-flex synaptophysin Tag virus was injected into either of these two regions of the DCN regions of the MThal and 7N Brainstem were assessed. B). 3D reconstruction of a representative medial and Int/Lat injection into the DCN. 16, 80um slices spanning the entire DCN were reconstructed, where each dot represents the location of one anterogradely infected nuclei. C). Quantification of synaptic output, where bars represent the average percentage of terminals in the contralateral or ipsilateral Lateral or Medial regions of the 7N, RM brainstem of the medial (n=3) and Int/Lat (n=4) plus the SEM. D and E). Representative confocal images of the Rostral Medulla sections of the brainstem with ChAT in Red, and synapses in black. Confocal images followed from left to right by scatter plot map of the synaptic output where each dot represents one synaptic terminal. Contour and kernel density plot representation of the synaptic output of the respective Int/Lat or Med injection sites. F). Pooled contour and kernel density plots for n=3 Med and n=4 Int/Lat Injection Sites.

DCN-Brainstem projection patterns are maintained along the rostral-caudal extent of the brainstem

These data thus far reveal that Int/Lat DCN project preferentially to and is required for the excitatory output to the ipsilateral LatRM, while Med is the most relevant DCN in terms of abundance of synaptic contribution for the contralateral MedRM projection. We therefore wondered whether the medio-lateral patterns revealed here are maintained across the rostral to caudal axis of the brainstem, which we defined to range in our work from the 5N to 12N zones of the brainstem. As discussed in the introduction, many years of research have gone into elucidating cell types in the spinal cord based on the spatial organization of transcription factors

expressed. Genes have been shown to be expressed specifically in the dorsal or ventral, or medial or lateral dimensions of the spinal cord according to spatial distributions of neurons. (Briscoe et al., 2000; Jessell, 2000; Pituello, 1997) Figure 2 reveals that there is a medial and lateral pattern in projection target from the Med and Int/Lat DCN to the medial and lateral regions of the rostral medulla. One can imagine that the medial and lateral organization, albeit with gene expression or projection pattern which is seen in the spinal cord and now also with the DCN-RM connectivity is maintained over the rostral-caudal axis of the brainstem. Therefore, we quantified and assessed the projection patterns of the same Med and Int/Lat anterograde tracing experiments from Figure 2, for the 5N and 12N regions of the brainstem (Alonso et al., 2013; Puelles et al., 2013; Watson et al., 2017; Zervas et al., 2004) (5N Brainstem and 12N Brainstem Caudal Medulla). To properly address the spread of virus, we measured the spread of the Flex-SynTag virus in the three rostral to caudal domains of the DCN described in the Introduction. Med (n=3) and Int/Lat (n=4) injections consistently labelled the medial (slightly into the more medial portion of Int) or the Interpositus and Lateral DCN (Figure 3A). Indeed, the laterality patterns revealed in Figure 2 are maintained across the rostral to caudal zones of the brainstem, where Int/Lat labeling is required for the ipsilateral Lateral projections and Med labeling is required for preferential and vast contralateral Medial projections. (Figure 3B – D). For the 12N segment of the brainstem, from the Int/Lat injections 64.8% of the terminals are located in ipsilateral lateral region (containing largely MdD and IRt), while 16.7% are in the contralateral medial region (containing mostly MdV) (N=4, SEM 6.7, 2.99 respectively). Conversely, at the 12N level for Med cohort, 67.6% of terminals are located in contra Medial region and 3.2% in ipsi Lateral region (N=3, SEM 2.1, 1.0 respectively). The same pattern persists at the level of the 5N (Figure B,D,E).

It can be noted that the third N of the Int/Lat injection samples, is near completely restricted to the Lateral DCN with the exception of a few labeled cells in the lateral portion of IntA and remains consistent in projection pattern across the brainstem. One injection in the Int/Lat cohort (N2) contains a slight contamination into the vestibular, just ventral to the Int (Figure 3A), but does not affect the distribution of terminals in MedRM or LatRM. This provides rationale, in our given context of connectivity mapping to the brainstem and thalamus, that Int

and Lat can be pooled together. The results thus far indicate that Int/Lat and Med DCN have unique projection patterns to the descending brainstem, maintaining a medio-lateral organization. Therefore, we hypothesized that similar patterns may exist to the motor thalamus.

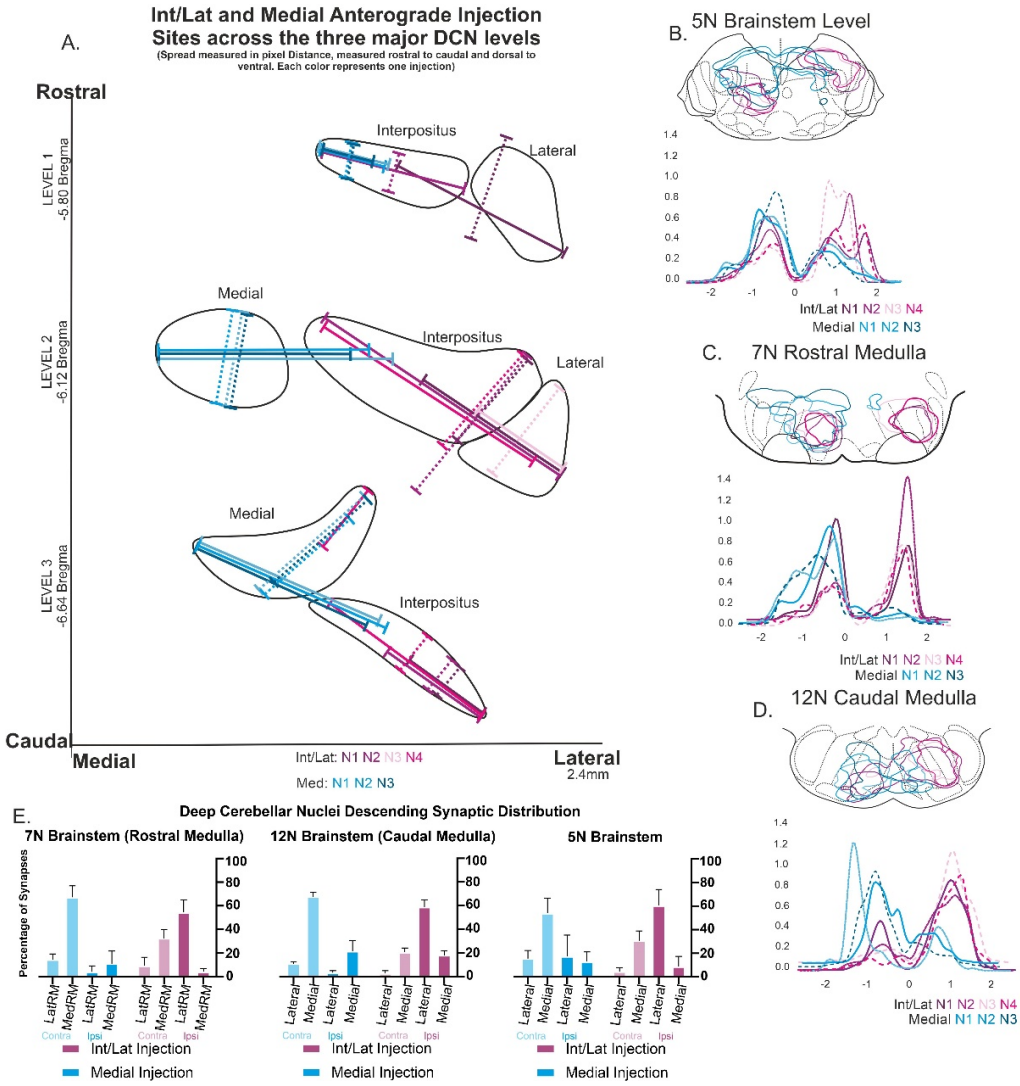

Figure 3: Mapping the excitatory output of the DCN along the rostral caudal axis. A). Injection site mapping of anterograde injections of either Medial (n=3) or Int/Lat (n=4) across the three rostral to caudal divisions of the DCN (defined in the introduction). Solid lines represent the spread from medial to lateral boundaries, and dotted lines represent the dorsal to ventral spread at the center of the injection defined by the medial – lateral spread. B – D). Contour density (represented by outline of density plot) and kernel density of the Medial or Int/Lat Injections mapped in A). E). Quantification of synaptic output, where bars represent the average percentage of terminals in the contralateral or ipsilateral Lateral or Medial regions of the 7N, 12N, or 5N brainstem zones. of the medial (n=3) and Int/Lat (n=4) plus the SEM.

DCN medial-lateral patterning is maintained ascending to Motor Thalamus

While it is clear that the excitatory DCN output descends to the brainstem in medial-lateral organization, as well as with contralateral or ipsilateral preference, we sought to explore to what extent the Med and Int/Lat DCN contribute to the widespread motor thalamic output seen in Figure 1. Since much of the more recent DCN literature in the context of the cerebello-thalamo-cortical loop has had sparse anatomical characterization (largely due to the focus on functional topics) has defined motor thalamus simply as DCN-recipient at an overall level, we wanted to confirm and validate previous literature which has shown that Lat and Int both project to VL (Bohne et al., 2019; Dacre et al., 2021; Ichinohe et al., 2000; Middleton and Strick, 1997) and Med projects to VM (Gao et al., 2018; Ito, 2006). Using the same cohort of injections from Figure 3, we quantified the synaptic distribution in the contralateral VM and VL, the most canonical motor thalamic nuclei studied, and most prominent projections revealed in our data from Figure 1. While there are not entirely discrete patterns between the two DCN zones, scatter and contour plots reveal that Int/Lat projects more heavily to the VL thalamic nuclei. When again analyzed based on the percent coverage of either VL or VM, out of the totality of synaptic terminals of the two regions, Int/Lat and Med DCN project preferentially to MThal nuclei, where VM and VL were assessed based on the Allen Brain Atlas boundaries, plus the assistance of the antibody detecting Calbindin (Arai et al., 1994) (Figure 4B), which labels specifically VM and CM/CL, excluding VL, therefore providing an additional method to determine VM and VL boundaries. 69.1% of the terminations are in the VL (n=4, SEM=2.36), and 30.99% of the terminals are found in the VM (N=4, SEM 2.39). On the other hand, Med projects preferentially to the VM thalamic nuclei, with 72.93% of terminals located in VM (N=3, SEM 3.34) and 27.067% of terminals found in VL (N=3, SEM 3.34). (Figure 4A – C). Interestingly, and which will be discussed in the Discussion section of this Chapter, the projections from Int/Lat in VM are more dorsally located while the projections from Med to VM are more evenly distributed. Due to limitations with number of infected cells, there may be a difference across samples of the relative distribution in VM, but for the purposes of this thesis to identify patterns between Med and Int/Lat, we focus our results on the general distribution differences

between Int/Lat > VL and Med > VM.

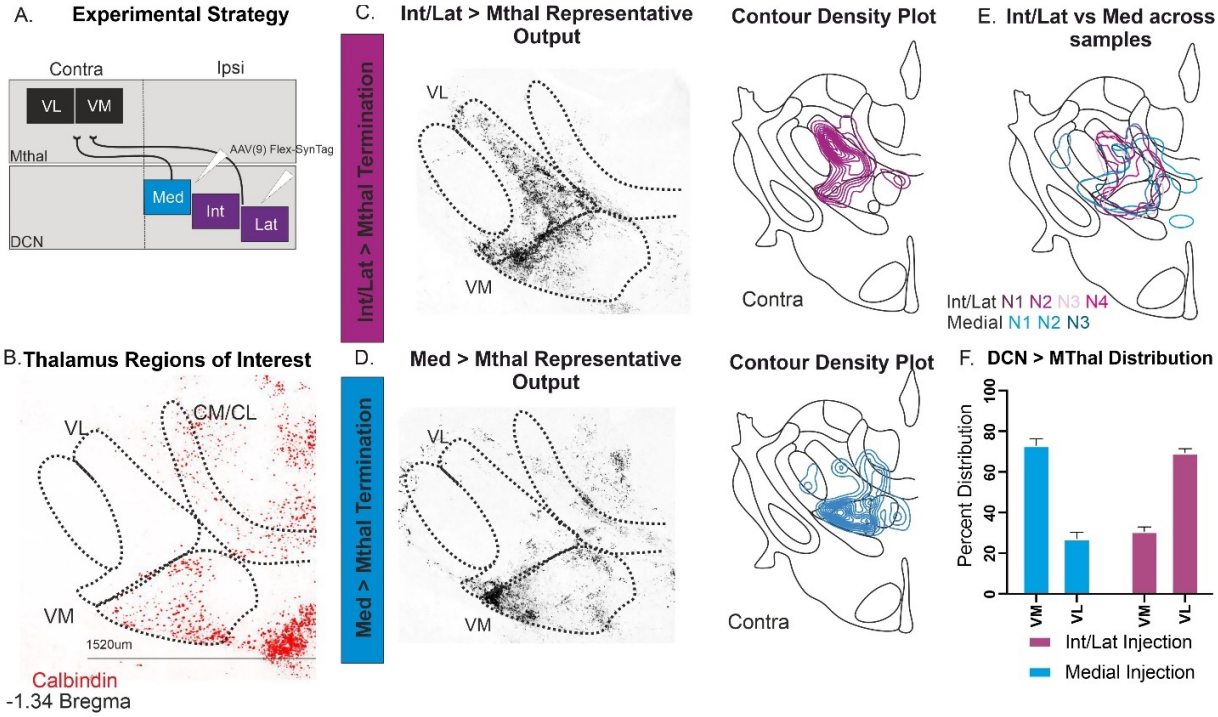

Figure 4: Mapping the excitatory DCN-MThal projections A). Experimental strategy to anterogradely inject the DCN and identify terminals in the contralateral MThal, VL or VM. B) Representation of the thalamic regions of interest, compiled from literature described in the introduction. Calbindin shown in red which labels the VM and CM/CL. The edge of the VM is at approximately 1520um from the midline. C, D). Left panels: Confocal images (zoomed of representative terminations from either Int/Lat or Med in the VM or VL thalamic nuclei. Right panels: Contour density plots of representative samples. E). Outer most boundary of the contour density plots from each of the injections (Med, n=3 in cyan. Int/Lat, n=4 in purple). F). Quantification of synaptic output, where bars represent the average percentage of terminals in the VM or VL of the contralateral MThal of the medial and Int/Lat injections plus the SEM

A DCN-Rostral Medulla boundary

Thus far in Chapter 1, we have focused to further characterize the excitatory output of the DCN and have concluded that a gradient in the DCN exists where the Med and Int/Lat project to the brainstem and Motor Thalamus in a concordant medial-lateral pattern, and additionally reveal a bias in contralateral versus lateral projection preference. From this, we define and further characterize the DCN connectivity based on the division of the RM into contralateral Med-MedRM and ipsilateral Int/Lat-LatRM projecting (Figure 5). These data reveal patterns of connectivity from the DCN which have not yet been described before, that define anatomical cell types based on connectivity patterns. These striking medial-lateral patterns will be able to aid in the characterization of the functional contribution of the Med and Int/Lat DCN to motor control.

In summary, these results indicate synaptic output patterns of the DCN based on projection target. We reveal that the Int/Lat DCN is necessary for the ipsilateral LatRM excitatory projections. Given the role of LatRM in skilled forelimb behavior (Ruder et al., 2021) we continued our focus in characterizing these Int/Lat neurons in more detail.

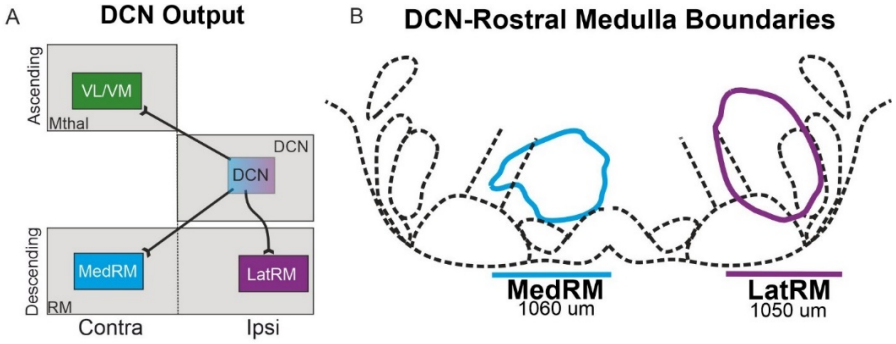

Figure 5: Brainstem boundaries defined by anterograde DCN tracing A) Conclusion scheme of the Medial versus Int/Lateral DCN output. B). based on the tracing from the above figures, regions of the brainstem pertaining to DCN output can be defined as MedRM or LatRM, where MedRM is contralateral to the affected DCN and LatRM is ipsilateral to the affected DCN.

Validation of Combining Interpositus and Lateral

As mentioned throughout the previous sections, the molecular, developmental, and connectivity research of the Int and Lat have given rationale for our inclusion of the two as one entity which make up components of the ipsilateral and contralateral patterning across the rostral to caudal axis of the brainstem. We therefore thought to compare our most precise lateral injections, which again include label very sparsely the IntDL, but have the same patterning at our levels of interest in the brainstem and motor thalamus. This can be seen in the contour plots in Supplemental Figure 1, where in orange are the more lateral biased injections and the shades of purple contain more cells in the Interpositus.

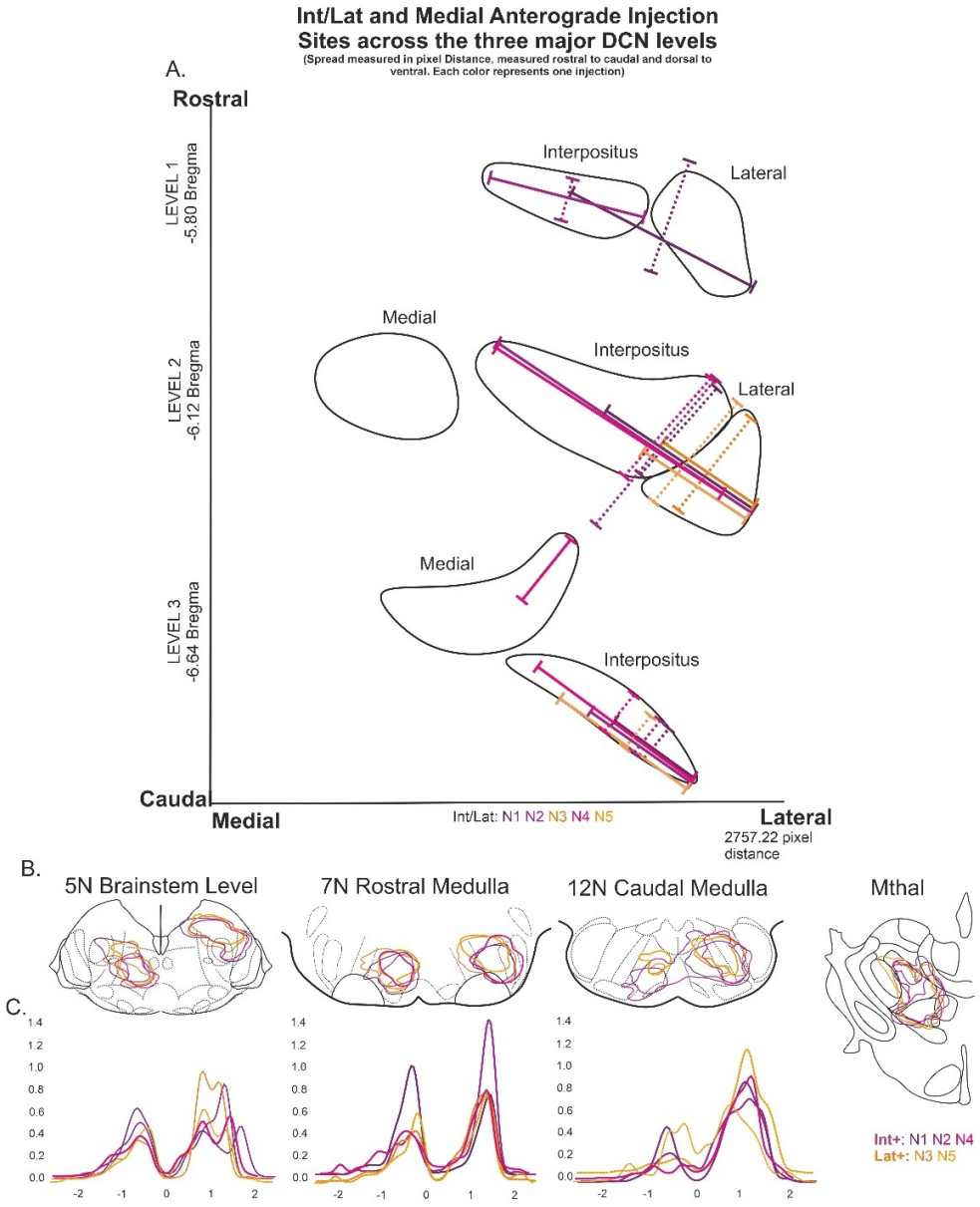

Supplemental Figure 1 A) Injection mapping of the Interpositus plus Lateral Injections. B). Contour plots of the 3 levels of the brainstem and Motor Thalamus plus contour density distribution of the terminals of the brainstem from rostral to caudal.

ntsr1-cre as a genetic entrypoint to characterize the Int/Lat DCN circuit

Previous research that has elucidated the function of Interpositus, specifically, have taken advantage of the transgenic line, *ntsr1-cre*, in which *cre* positive neurons are located specifically in Interpositus and Lateral DCN and are excitatory (Becker and Person, 2019; Beitzel et al., 2017b; Houck and Person, 2015; Judd et al., 2021). We therefore thought that this transgenic line could be a useful genetic entry point to interrogate specifically a subtype in the Int/Lat DCN population which we have characterized already in the *vGlut2-cre* background; however, the output of these neurons has not been fully characterized in the context of the rostral medulla. Interestingly, these neurons were shown to be required for proper kinematics in a skilled forelimb task, but results remained consistent with the same experiments in a Wildtype mouse where presumably both excitatory and inhibitory Int/Lat neurons were manipulated. This raises the question of why this excitatory subset would yield similar functional results as a genetically un-defined population of Int/Lat neurons. We hypothesized that a further characterization of these *ntsr1*-cre neurons could additionally answer this confounding result (Becker and Person, 2019). Using PhP.eB systemic viruses injected into either *vGlut2-cre* or *ntsr1-cre* we quantified and compared the distribution of *cre* positive neurons in the Lateral, medial, or Interpositus nuclei. These results show that *vGlut2-cre* neurons are generally evenly distributed along the three DCN (30.067% lateral, 30.7% Medial, 39.233% Interpositus, n=3, SEM 4.4, 1.7, 2.7 respectively) with a slightly higher percentage of nuclei residing in the Interpositus, however, the mean percentage of nuclei in Interpositus of the *ntsr1-cre* line is 94.0%, 5.0% lateral, 0.995% Medial (n=2, SEM=2.7, 2.9, .23 respectively). (Figure 6A). The distribution was reconstructed in 3D to the Allen Brain Atlas and the sparsity of the *nstr1-cre* labeled DCN neurons can be visualized accordingly (Figure 6B). Furthermore, to show that the line is indeed highly specific for Int/Lat, we analyzed confocal images of the PhP.eB systemic injections of either *vGlut2-cre* or *ntsr1-cre* neurons (Figure 6D). Expression of *nstr1-Cre* is limited to the DCN, with the exception of a few cells in lateral paragigantocellular nucleus, alpha part. The average number of DCN neurons labeled by the *vGlut2-cre* systemic viral tracing approach is 5648 (n=3, SEM 967) and *ntsr1-cre* is 1622 (n=2, SEM 172), thus the percentage of *ntsr1*-cre positive DCN neurons is just 28.7% of the average number of *vGlut2-cre* DCN neurons visualized with systemic injections. This is valuable because the lack of cre positive neurons dorsal or ventral to

the DCN greatly reduces the difficulty of injecting the Int/Lat, therefore making this *ntsr1-cre* line a genetic tool to assay Int/Lat specifically and without contamination elsewhere.

We conclude that *ntsr1-cre* labels a subset of Int/Lat DCN neurons, but it remains open as to whether these neurons maintain the projection pattern of the *vGlut2-cre* Int/Lat to the brainstem and MThal shown in the previous figures.

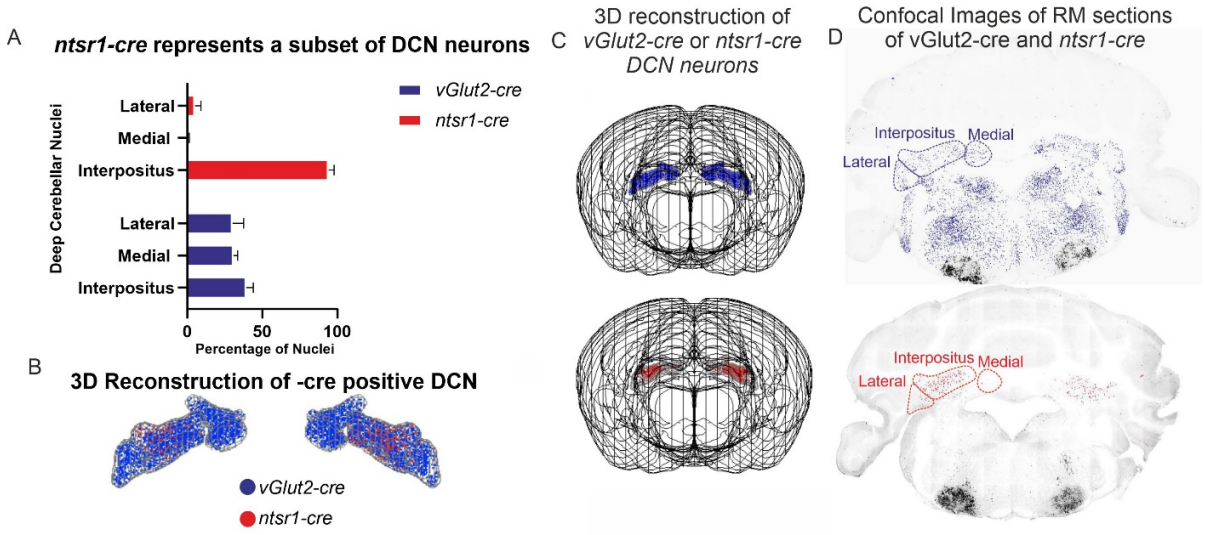

Figure 6: *ntsr1-cre* positive neurons label Int/Lat neurons A) Quantification of *ntsr1-cre* and *vglut2-cre* positive neurons where bars represent the percentage of nuclei represented in either lateral, interpositus, or medial DCN out of all of the neurons labeled. *vGlut2-cre* (n=3) in blue and *ntsr1-cre* (n=2) in blue. Neurons labeled by Flex-PhP.eB virus into the respective transgenic line. B and C). 3D reconstruction of the *vGlut2-cre* or *ntsr1-cre* positive DCN neurons. D). Confocal images at the RM level of brainstem where each dot represents one nuclei labeled.

nstr1-cre Int/Lat neurons terminate preferentially to ipsilateral LatRM

In order to map the output of the *ntsr1-cre* DCN neurons, we injected AAV-flex-SynTag into Int/Lat and compared this to the *vGlut2-cre* Int/Lat anterograde injections described above (Figure 7A ,B). Synaptic quantification revealed that *ntsr1-cre* project with a high proportion to the ipsilateral LatRM, in a similar pattern to the *vGlut-cre* Int/Lat, but with a more localized density in the PCRt region of the LatRM (visualized in the contour plot, Figure 7F). *ntsr1-cre* DCN neurons project to the contralateral MedRM but is densest and more tightly bound to the midline, whereas the *vGlut2-cre* Int/Lat neurons project to a less centralized area of the contra MedRM (Figure 7 C to F). Despite the slightly different pattern in density seen in the contour density plots of the RM, the actual synaptic terminal number represented as a percentage per region of the total number of synapses in across the RM slice, does not vary between *vGlut2-cre*

and *ntsr1-cre*. 54.4% (n=4, SEM 5.1) of the terminals from the *vGlut2-cre* neurons project to the ipsi LatRM and 32.4% (n=4, SEM=3.8) to the contra MedRM, while 56.6% (n=3, SEM=1.5) of the terminals from the *ntsr1-cre* neurons project to the ipsi LatRM and 34.5% (n=3, SEM=2.9) to the contra MedRM (Figure 7H). As described in Figure 4, vGlut2 Int/Lat neurons terminate in both VM and VL thalamic nuclei, however when comparing the percentage of terminals distributed across the two regions, there is a larger percentage found in the VL. In the same way that we compared *vGlut2-cre* and *ntsr1-cre* output in the rostral medulla, we then asked how the *ntsr1-cre* neurons project in the thalamus. We used *Calbindin* (Figure 7G) to differentiate between VM and VL, and quantified the number of terminals using TrackMate plugin, in Fiji. We found that *ntsr1-cre* DCN neurons project to VM and VL, but with proportionally more terminals in VM. As mentioned before, 69.1% of the MThal output from *vGlut2*-cre Int/Lat neurons lie in the VL (n=4, SEM=2.36), and 30.99% of the terminals are found in the VM (N=4, SEM 2.39). On the contrary, 63.66% of the *ntsr1-cre* Int/Lat neurons terminations in MThal are VM while 36.33% are found in VL (N=3, SEM = 2.39) (Figure 7E,F,H). Because VM and VL project to both thalamic structures, we can speculate from this that the *ntsr1-cre* neurons are a subset of excitatory neurons which project preferentially to the (likely *vGlut2-cre* positive) terminals in VM and a subset of (likely *vGlut2-cre* positive) terminals in VL. This suggests a heterogeneity in the VL which has not been identified before.

We have now described an additional component to the cell types within the DCN, where in addition to medio-lateral projection organization into the brainstem and MThal, we have a genetically defined subset of neurons within Int/Lat.

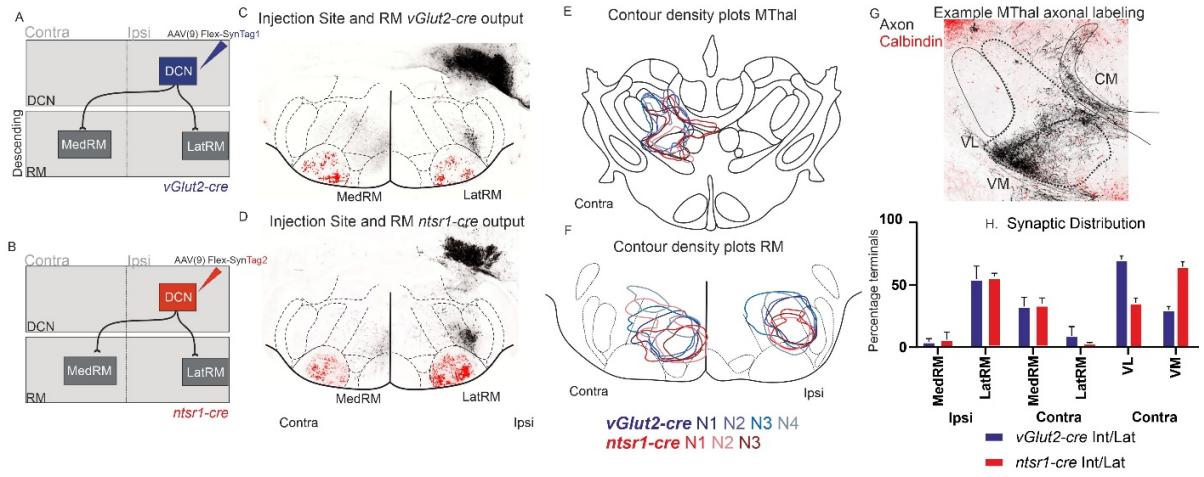

Figure 7: *ntsr1-cre* positive Int/Lat neurons project preferentially to ipsilateral LatRM A and B). Injection strategy to anterogradely label from either *vGlut2-cre* (blue) or *ntsr1-cre* (red) nuclei with AAV(9) flex syn-Tag virus. C and D) Confocal images of the output of either *vGlut2-cre* or *ntsr1-cre* nuclei with ChAT in red and synapses in black. E and F) contour density plot representation, where each line represents the outer most density ring in the RM or MThal per each animal injected (*ntsr1-cre* n=3, *vGlut2-cre* n=4). G). Example of the VM and VL axonal labeling from the *ntsr1-cre* representative injection where axons are labeled in black and Calbindin (marking VM and CM) antibody staining is labeled in red. G) Synaptic distribution as a percentage, where each bar represents the average percentage of synapses in that region of the RM (ipsi MedRM, ipsi LatRM, contra MedRM, contra LatRM) or MThal (contra VL or contra VM) per the entire RM or MThal, plus the SEM.

In situ validation of *–cre* and *slc17a6* reveals minimal transcript overlap

In the previous sections, we compared the output of the *ntsr1-cre* positive Int/Lat neurons and the *vGlut2-cre* positive neurons. We assumed, based on the number and distribution of *–cre* positive neurons identified from systemic injections (Figure 6), that *ntsr1-cre* represents a subset of excitatory neurons in Int/Lat. However, with the results from the anterograde tracing, we sought to further clarify to what extent the *ntsr1-cre* transgenic line labels a subset of excitatory neurons. To address this question, we performed RNAScope, a commercialized and robust *in situ* hybridization method (Wang et al., 2012), to quantify the *cre* positive transcripts and *vGlut2 (Slc17a6)* transcripts in the *ntsr1-cre* transgenic mouse line, in combination with the viral tracing of systemic PhP.eB virus. We looked at the three different levels described before for the DCN, along the rostral to caudal axis, and see labeling at the two more caudal levels (Bregma -6.64 and Bregma -6.24) (Figure 8a, A,B). By visualizing both *cre* and *slc17a6* single molecules, with the systemic virus, we show that *cre* and virally labeled cells are minimally expressed compared to *Slc17a6.* Quantification reveals that at the Bregma -6.12, 11.7% of the *Slc17a6* positive neurons co-express *cre* and 13.5% of the *Slc17a6* positive neurons co-express the systemic virus. At the more caudal level, the percentage increases to 20.5% and 21.55% co-

expressing either *cre* or the virus (respectively). (Figure 8a, D). Quantifications were done using a semi-automatic Fiji Plugin, Trackmate with size of 13 for the object diameter and a threshold of 3. Cells that are positive for a particular gene contain at least 3 transcripts, and quantified at the maximum projection of the image. (Figure 8b). This percentage of *cre* labeled cells compared to *Slc17a6* labeled cells is similar the comparative number of neurons labeled in the systemic injections in previous figures where the total number of *ntsr1-cre* neurons labeled by systemic injection is only 28.7% of the total number of neurons labeled by the systemic injection in *vGlut2-cre* transgenic mice. The slight difference in percentage between the *in* situ and systemic viral injections can likely be attributed to variable nature of the viral tracing strategy. These data further suggest that the *ntsr1-cre* mouse line labels a highly specific subset of Int/Lat neurons which give rise to the likely represent the excitatory population which mostly to the VM motor thalamic structure and ipsilateral LatRM, while slightly to the contra MedRM and to a very small extent the VL thalamus region. This will be discussed later in Chapter 1: Discussion.

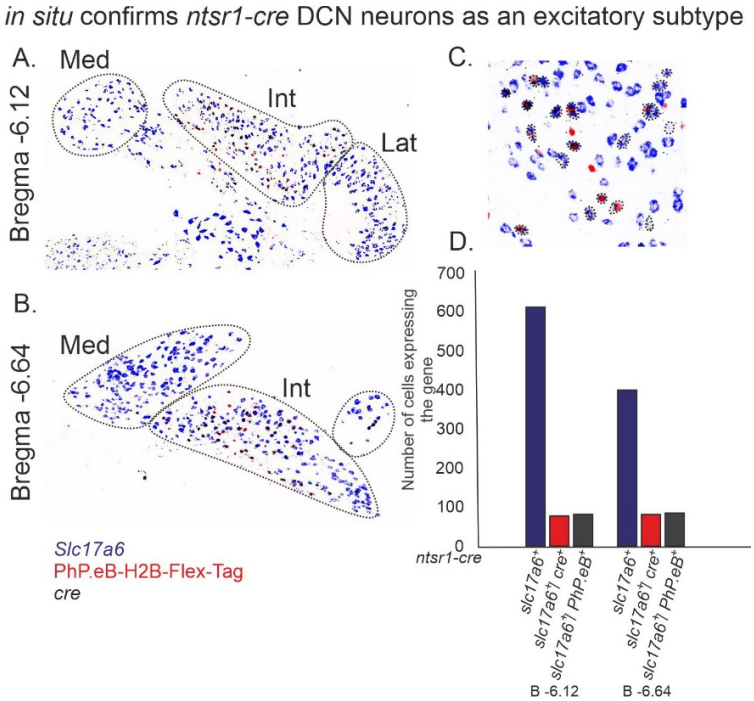

Figure 8a: ntsr1-cre positive neurons represent a minor subset of the excitatory DCN neurons. *In situ* hybridization using RNAScope at two levels described previously. Transcripts for *slc17a6* are shown in blue, *cre* positive transcripts are shown in black, and PhP.eB systemic labeled neurons are in Red. (A,B,C). Where A and B depict the medial and caudal levels of DCN and C shows a close up of the colocalization. Panel D, shows the number of neurons expressing either gene or the systemic virus.

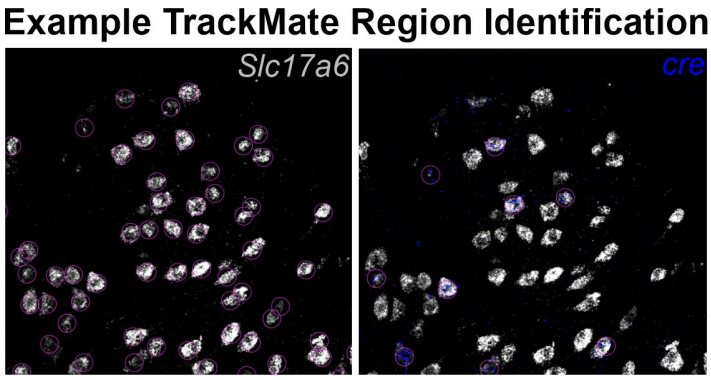

Figure 8b: Example region identification using TrackMate, where the purple circle denotes a positive cell according to the density of transcripts (*Slc17a6* in gray and *cre* in blue). TrackMate parameters used were the Laplacian of Gaussian Filter, average nuclei object size of 13. Both were used with a quality threshold of 3, pre-processed with the median filter, and sub-pixel localization. Quantifications at the Maximum Intensity Projection, using 40x oil objective and 0.6 z depth, binning of 2.

Redefining Int/Lat by projection stratified neurons

Retrograde tracing reveals spatial organization within IntA/Lat

To answer the question as to whether there is projection-stratified organization within Int/Lat, we infected regions of the RM previously established with anterograde tracing to be relevant to Int/Lat connectivity with a virus exhibiting retrograde targeting potential (Tervo et al., 2016). We injected retrograde AAV-Flex-Tag viruses into either MedRM or LatRM based on the areas identified in anterograde tracing, in *vGlut2-cre* mice (Figure 5) and identified a specific organization within Int/Lat, with ipsilateral LatRM projecting Int/Lat residing only on the most lateral portion of Int, plus IntDL, as well as in the Lateral DCN (Figure 9A). Ipsilateral MedRM projecting Int/Lat neurons are less specifically situated, where ipsilateral Int projecting are located more densely in the more lateral region of IntA (Figure 9B). Strikingly, and which has been observed before (Sathyamurthy et al., 2020) , is the cervical spinal cord projecting population in the most medial stripe of IntA (Figure 9B). To fully observe the span of retrogradely labeled neurons, we performed a 3D reconstruction of the volume of the DCN to easily visualize the distribution patterns. The patterns match the anterograde tracing results described above, with respect to contralateral and ipsilateral patterning. Notably, when LatRM and MedRM were injected on the same side with different viruses, there was a clear emphasis on contralateral connectivity between Med DCN and MedRM and the ipsilateral connectivity between Int/Lat and LatRM (Figure 9C, D). Given these data, we quantified the number of neurons retrogradely labeled in the DCN, this time separating Int into IntA and IntDL to

determine whether there is topography between these two nuclei as well. Figure 9E shows the number of retrogradely labeled neurons from either MedRM or LatRM. The number of contralateral Med DCN labeled from MedRM dominates the other DCN retrogradely labeled in these injections (1603 neurons, N=2, SEM 4.0). The number of ipsilateral labeled DCN from MedRM is minimal (Figure 9E). The next most striking pattern, as with what matches the anterograde tracing, is the ipsilateral retrogradely labeled neurons from the LatRM injections where Ipsi IntA, IntDL, and Lateral make up the largest numbers of cells (293.3, 192.67, 255.67. SEM=49.1, 57.7, 38.8 respectively for N=3). In order to analyze in a way done in the previous sections, with regards to normalizing across injections, we looked at the percentage distributed of the neurons where we see the following results. 79.1% of the total **contralateral projecting-MedRM** labeled neurons are found in Med, 9.6% are found in Int, and 11.3 % are found in Lat (n=2, SEM=2.9, 0.16, 3.1, respectively). In contrast the **ipsilateral projecting-MedRM** distribution is more distributed where 46.7% of the total ipsi projecting neurons are found in Med, 38.79% in Int, and 14.48% in Lat neurons (n=2, SEM= 4.4, 1.6, 6.0, respectively). As expected from the anterograde tracing, there are a number of medial DCN neurons projecting to **contralateral** LatRM. 77.7% of the total **contralateral projecting-LatRM** retrogradely labeled neurons are found in Med, while 12.97% are found in Int, and 9.6% are found in Lat (n=3, SEM=7.4, 5.4, 2.1 respectively). However, of the **ipsilateral LatRM-projecting** population, Int/Lat makes up the largest population of the ipsilateral projecting LatRM neurons. 63.05% are found in Int, 1.49% in Med, 35.45% in Lat. (n=3, SEM=0.8, 7.1, 7.8 respectively).

In summary, these data reveal a unique organization of projection-stratified neurons in the DCN, especially with respect to Int/Lat projections to MedRM and LatRM, where the ipsilateral projecting DCN reside largely in Int/Lat while the contralateral projecting reside largely in Medial. It can be noted that, in these retrograde tracing data included in this thesis, plus off-target injections across the 5N to 12N brainstem regions we have not seen any unique patterns between Int and Lat, therefore giving rationale for having pooled Int and Lat as one entity, which matches the anterograde data presented in previous figures. Because we used nuclear-tagged viruses, these experiments were primarily aimed at identifying neuronal distributions

within DCN, and did not yet address whether projection-stratified neurons can project to multiple regions.

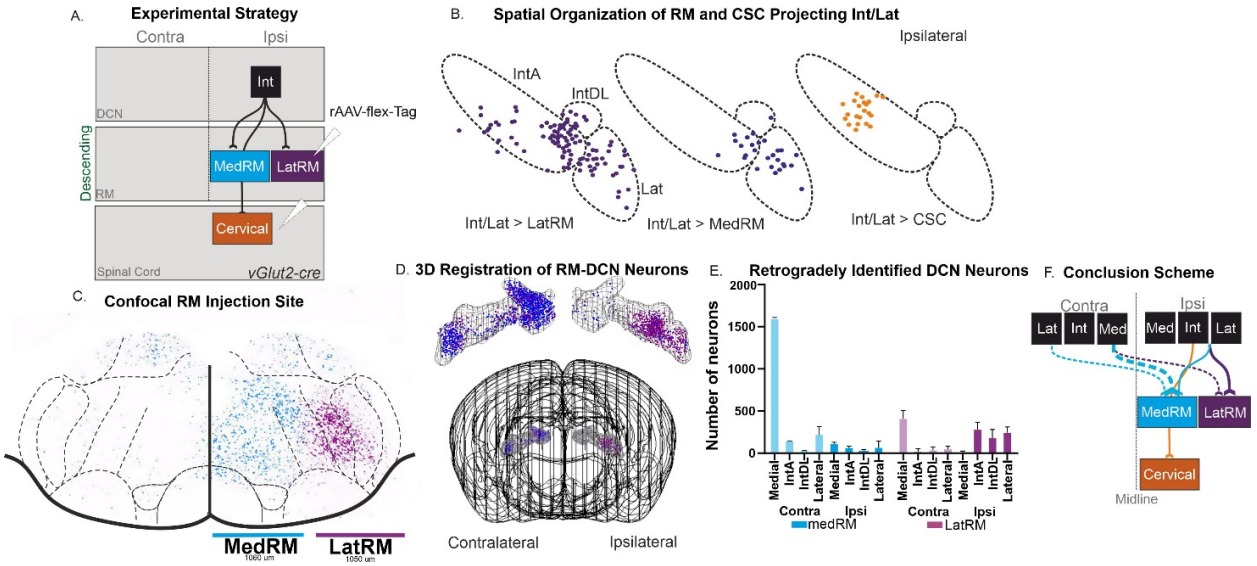

Figure 9: Retrograde viral tracing reveals projection-stratified, spatially organized Int/Lat neurons A). Experimental strategy to retrogradely label MedRM, LatRM, and spinal cord projecting Int/Lat DCN neurons. B). Spatial representation of rertogradely labeled DCN where each dot represents one retrogradely labeled nuclei C). Confocal image of representative RM injection site and labeled DCN when MedRM and LatRM are infected retrogradely in the same animal. D). 3D Registration of RM projecting DCN neurons. E). Quantification of retrogradely labeled DCN neurons, where IntA, IntDL, Lateral, Medial are quantified separately, both ipsilateral and contralateral to the RM injected region. (MedRM, n=3. LatRM, n=3). F). Conclusion Schematic, where the thickness of the line represents the weight of the percentage projecting from a specific DCN to its descending target. Dotted lines indicate contralateral projections.

MedRM and LatRM projecting DCN are largely non-overlapping

There are two main methods to address whether projection-stratified neurons can project to multiple targets, one of which is quantifying the number of double positive retrogradely labeled DCN neurons. While in the previous figure, we injected MedRM and LatRM in the same side of the RM, in order to assess the contralateral versus ipsilateral patterning, we injected MedRM and LatRM on the opposite sides of the RM and asked what percentage of retrogradely labeled nuclei are double positive (Figure 10A). This tracing strategy mimics the pattern of contralateral and ipsilateral retrogradely labeled cells seen in the previous figure but also reveals a small percentage of neurons in Interpositus, Lateral, or Medial are double-positive cells. These data were calculated by measuring the percentage of MedRM, LatRM, or double positive neurons in either Lateral, IntDL, IntA, or Medial DCN. The four bars on the left denote the DCN projecting

Ipsi to LatRM and Contra to MedRM, while the bars on the right denote DCN projecting contra to LatRM and ipsi to MedRM (Figure 10D). From this we can argue that indeed there are a minor population of dual projecting Int/Lat neurons, but few. While the percentage of double positive neurons is low, there are caveats with this strategy. While this approach has been used in previous papers in the lab (Ferreira-Pinto et al., 2021), we cannot exclude the limitations in virus efficiency and potential variation between batches of production. We have done a control experiment by co-injecting both retrograde AAV-flex-Tag (rAAV-flex-Tag) viruses in one site (Figure 10C), and while a large percentage are double positive, there is a difference in efficiency (Tag 2 is between 65.8 – 71.2% efficient in labeling as Tag2). We therefore employed the second approach to strengthen our results, which takes advantage of a combinatorial viral tracing strategy.

To continue to probe whether projection-stratified Int/Lat neurons project to multiple targets in the RM, and MThal, we next took advantage of combinatorial viral tracing strategies to identify collateralization patterns.

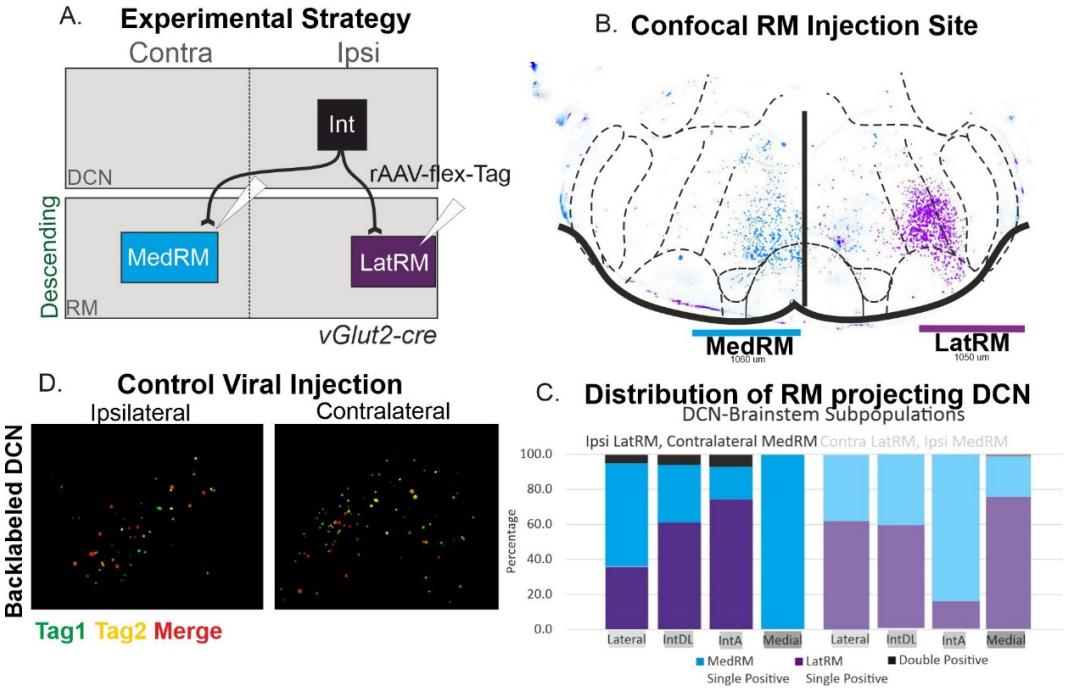

Figure 10: Retrograde viral tracing reveals minimal dual-projecting projection-stratified Int/Lat neurons A). Experimental strategy to identify double positive, dual-projecting DCN neurons by injecting contralateral MedRM and ipsilateral LatRM with retrograde AAV-flex-Tag viruses. B). Confocal image of injection site of the retrograde virus into MedRM or LatRM of the RM. C). Distribution of retrogradely labeled DCN neurons as a percentage, where each color within the DCN (Lateral, IntDL, IntA, Medial) denotes the percentage of that nuclei labeled by either MedRM (purple), LatRM (cyan), or both (black). D). Control injection where the two Flex-Tag viruses are co-injected into the LatRM. Images shown are retrogradely labeled ipsilateral Int/Lat and contralateral Medial DCN, from two different co-injections into LatRM.

Projection-stratified Int/Lat-LatRM neurons collateralize in MedRM and MThal

As mentioned, limitations exist between both the retrograde and combinatorial anterograde-retrograde approach, however the combination can be more informative. We therefore injected a retrograde AAV-cre (rAAV-cre) into the descending or ascending target of Int/Lat plus an AAV-Flex-SynTag and AAV-Flex-cytosolic-Tag (AAV-Flex-cTag) for visualizing axons. (Figure 11A). Retro-cre into LatRM plus Flex-SynTag injected into ipsilateral Int/Lat reveals some collaterals in MedRM but significantly less than what is in the ipsi LatRM (1559 terminals in contra MedRM versus 4192 terminals in ipsi LatRM, n=1). Conversely, retro-cre into MedRM plus Flex-SynTag injected into contralateral Int/Lat reveals few collaterals in ipsi LatRM (999 terminals in Ipsi LatRM, 11600 terminals in contra MedRM, n=1). Retro-cre in the contralateral VL and VM of the MThal reveals dense and fairly similar numbers of synaptic terminals into both contra MedRM and ipsi LatRM. These can be visualized as well with kernel density plots. (Figure 11B-D).

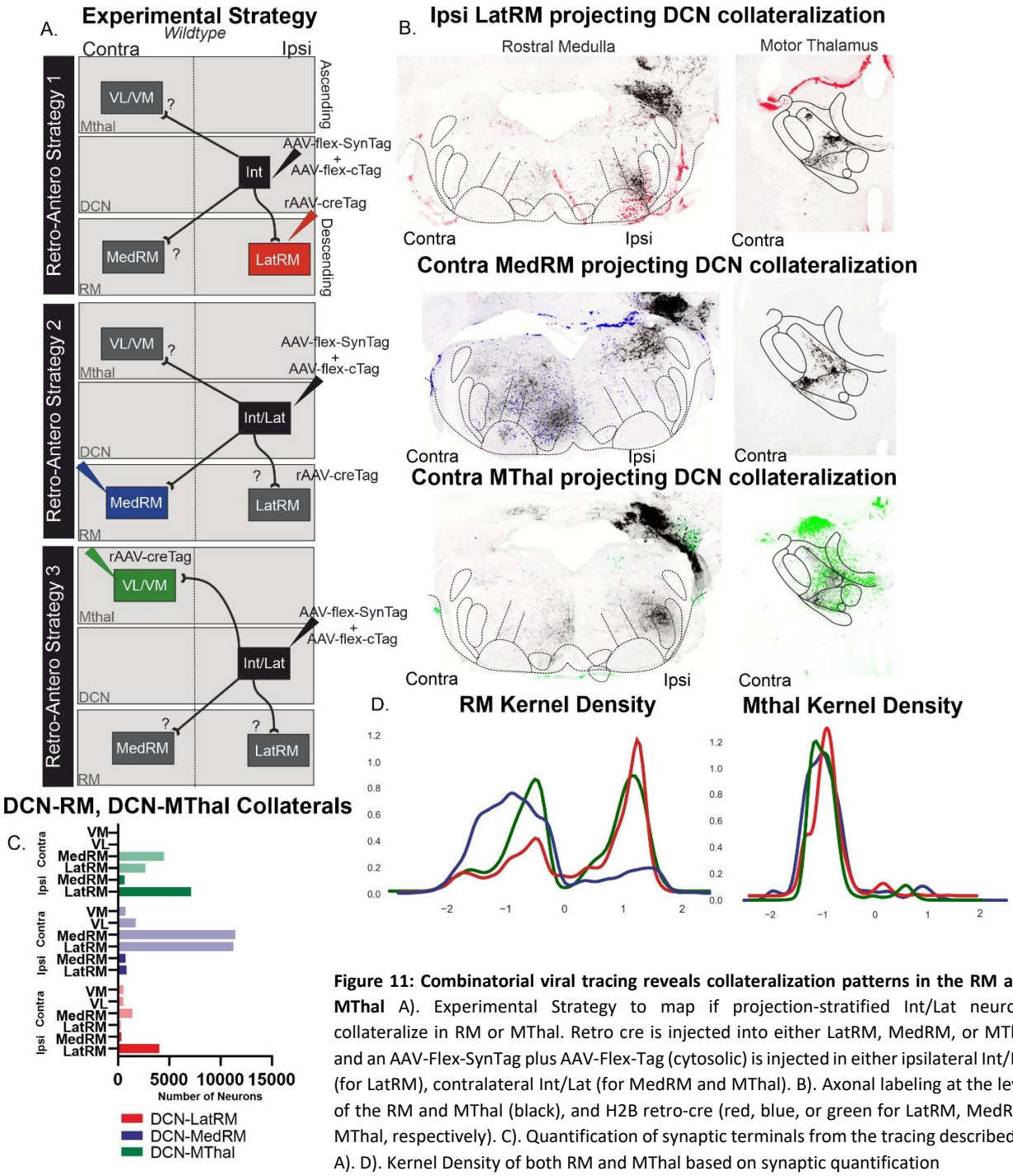

Figure 11: Combinatorial viral tracing reveals collateralization patterns in the RM and MThal A). Experimental Strategy to map if projection-stratified Int/Lat neurons collateralize in RM or MThal. Retro cre is injected into either LatRM, MedRM, or MThal and an AAV-Flex-SynTag plus AAV-Flex-Tag (cytosolic) is injected in either ipsilateral Int/Lat (for LatRM), contralateral Int/Lat (for MedRM and MThal). B). Axonal labeling at the level of the RM and MThal (black), and H2B retro-cre (red, blue, or green for LatRM, MedRM, MThal, respectively). C). Quantification of synaptic terminals from the tracing described in A). D). Kernel Density of both RM and MThal based on synaptic quantification

Conclusion

Our combinatorial tracing strategy identifies collateralization patterns at the level of the RM and the MThal, where ipsilateral LatRM projecting Int/Lat collateralize slightly into the contralateral MedRM. Conversely, the contra MedRM projecting Int/Lat collateralize minimally to the ipsi LatRM. The MThal projecting Int/Lat collateralize to a larger extent to the ipsi LatRM, but also the contra MedRM. Interestingly, the Int/Lat > MThal population collateralizes in a more dorsal region of the LatRM (Figure 11 and 12). Recent work from the Arber Lab showed different functionalities between the dorsal and ventral regions of the LatRM where the dorsal region was more handling tuned, while the ventral region was tuned to reaching, and these populations were projection-stratified (caudal medulla receiving input from the dorsal, the ventral LatRM projected to the spinal cord) (Ruder et al., 2021). We can therefore speculate that perhaps that the DCN projecting to both the MThal and the LatRM have highly specific functionalities depending on where in the LatRM they are collateralizing, adding another level of complexity.

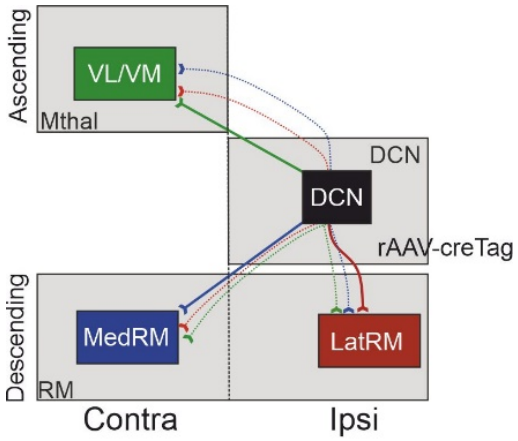

Figure 12: Conclusion schematic from Figure 10.

Discussion

The data presented in this first chapter provide an approach to defining anatomical and projection-stratified cell types within the DCN. With the advent of viral tracing and genetic tools, there has been a rise in DCN research, however these data are rather inconsistent, with work describing multiple functionalities of the individual DCN. Both lateral and medial DCN have been shown to have a role in timing, learning, and modulation of movement. Interpositus

has been shown to contribute to both skilled locomotion and skilled forelimb behavior (Becker and Person, 2019; Darmohray et al., 2019; Low et al., 2018a; Sathyamurthy et al., 2018). This wide range of roles of the DCN might be attributed to the fact that these studies have largely been restricted to assaying the full neuronal populations within the DCN, therefore not addressing the likely critical role that the projection-stratified subpopulations have in motor control. With the exception of the cervical-spinal cord projecting Int neurons, the brainstem projecting DCN have not been described with respect to connectivity, function, and molecular properties. Additionally, the DCN have been studied recently in the context of the cerebello-thalamo-cortical loop, but a complete anatomical characterization of the individual DCN to motor thalamic regions is lacking.

We therefore had the goal here to more deeply characterize the excitatory output of the DCN to the brainstem and motor thalamus, in hopes to define DCN cell types categorically by anatomical and connectivity characteristics. The combination of viral tracing strategies employed here reveal laterality patterns of connectivity to the brainstem and thalamus, where we see the following:

Anterograde tracing reveals that the medial DCN preferentially targets the contralateral medial brainstem and contralateral ventromedial motor thalamus. Interpositus and Lateral DCN are required for the DCN excitatory output to the ipsilateral lateral brainstem and terminate in the ventrolateral and ventromedial motor thalamus, but is the required nucleus for a high density of termination in the VL motor thalamus. Given these data, we can hypothesize that the confounding and unclear results from the compilation of DCN publications might potentially be explained by the previously unelucidated complexity of the DCN output. For example, given the previously described role of LatRM and Interpositus in skilled forelimb behavior, we speculate that LatRM projecting Int/Lat neurons are a key neuronal population contributing to online motor control of the skilled reach previously shown to be elicited by LatRM. We postulate that if LatRM neurons are directionally tuned, that the LatRM projecting DCN neurons might contribute to online motor control required for this directional tuning, precision and learning of the task. One could imagine that this subpopulation is engaged when the animal must learn to reach properly or adjust when a reach is inaccurate and therefore require correction due to

such an error. Conversely, the medial region of the rostral medulla (Gi, LPGi) is required for more full-body like behaviors such as head turning, and speed control. Medial DCN has been shown to function in timing and modulation, as well as required for learning of a full body task such as the rotarod, which however is also considered as a skilled task, but involving the whole body. We therefore believe that that the contralateral MedRM projecting medial DCN make up the neuronal population required for learning these full body tasks and maintenance of online motor control and adaptation during the tasks. One could imagine that this subpopulation is engaged when the animal must increase speed, stop, or turn the head at the beginning of a full body turn. Importantly, while we can speculate on this, we have also revealed a portion of the RM projecting DCN to collateralize in other regions of the brainstem, as well as in the thalamus, such that LatRM projecting DCN collateralize to some extent in the contralateral MedRM. Conversely, the contralateral MedRM projecting DCN collateralize to some extent in the ipsilateral LatRM. While the extent of collateralization is minimal, we can speculate on the potential function in the context of a skilled forelimb task. In the reaching task described for LatRM, mice reach with one hand through a slit in a reaching box. One can imagine that the mouse has to adjust its posture from the start of the reach and when bringing the food back to complete the task, where the mouse handles. We therefore hypothesize that the majority of LatRM projecting DCN which are not dual-projecting are required for the learning and adaptation of this task but the LatRM projecting DCN which collateralize in the contralateral MedRM function to maintain postural control and adjust for the full body functionality of the skilled reaching task. We present here a map of Med versus Int and Lat combined, a combination that has been done before (Chung et al., 2009; Dacre et al., 2021; Kebschull et al., 2020). These suggest that Int and Lat are evolutionarily, and functionally similar. Furthermore, the output at the level of the rostral medulla and motor thalamus, in our hands, two injections nearly inclusive to Lateral (sparse labeling in IntDL, N3 from Figure 3 and 4, and supplemental Figure 1) are consistent with the output from Int (ipsilateral LatRM and contralateral MedRM, plus contralateral VM and VL). This does not exclude the possibility that Lateral DCN's output is entirely similar to Interpositus, however, for the scope and patterns revealed in this thesis, we

believe the two to able to be pooled when considering a purely anatomical characterization to the brainstem and thalamus.

The extent of literature describing the DCN in the context of the cerebello-thalamo-cortical loop has focused on how neurons in the three regions are timed in behaviors such as licking (Guo et al., 2017). The activity of the neurons is time locked in a way that the DCN-recipient MThal neurons send information to cortical neurons (Economo et al., 2018; Gao et al., 2018; Guo et al., 2017) but what information is being passed in this circuit is unclear. The cortex has been extensively shown to be critical for learning (Arlt et al., 2021; Gerraty et al., 2018). The thalamic function in motor programs is less clear, however one theory is that it acts as a "super integrator" of signals, where it receives signals from the cortical layer 5 on the initial motor program (Kakei et al., 2001), the cerebellum on the state of the body (in a way, proprioception) (Eccles, 1973), and from the basal ganglia on motivational context of the action sequence ((Redgrave et al., 2010). With these signals, the motor thalamus then processes the information and projects such a refined motor plan back to the cortex to update new parameters of the motor program. While this is just a theory, it is an interesting way to speculate the thalamic function, also in addition to the many open questions remaining in if and how the basal ganglia and cerebellar input to MThal neurons are impacting the motor programs (Bosch-Bouju et al., 2013). Therefore, we speculate that DCN inform neurons in the cortex, via VM or VL thalamic nuclei, that an error has occurred and that the motor program needs to be updated.

Once this information is within the context of the cortex, where is the signal sent? Because the cortex has been shown to project to the spinal cord and brainstem, the command and executive centers of the brain, specifically in goal-directed and skilled movements (Nelson et al., 2021; Wang et al., 2017) we hypothesize that if the cortex receives updated information from the DCN via MThal, then the cortex sends the updated signal to the brainstem where the correction is made and the precise movement is performed.

Importantly, we show that RM projecting DCN collateralize in the thalamus and MThal projecting DCN collateralize in the RM. This cannot be understated and therefore we can also speculate further about the function of the brain-wide loop in motor control. In a similar way as with the RM projecting DCN, the same combinatorial tracing approach in the VL and VM regions

of the MThal revealed collaterals of MThal projecting DCN into the ipsilateral LatRM and contralateral MedRM. I hypothesize that when the dual-projecting DCN neurons receive an error signal, they send a stop signal to the RM (for example, in the case of a missed reach), and simultaneously sends signal to the cortex to update the motor action via VL thalamic nuclei. The cortex then sends this updated signal to the respective brainstem region to continue the motor program with the further optimized action. It remains unclear where exactly in the regions of the motor cortex which send output to the brainstem, that the DCN project. We hypothesize that there is a spatial preference of the Medial versus Int/Lat DCN projecting to the cortex via MThal, however this question remains to be addressed. We further hypothesize that if there were Med and Int/Lat specific projection patterns in the motor cortex, then they are transmitting differential information back to the brainstem. However, likely both signals are needed to update the motor program after an error signal was sent to the DCN. A major caveat of these speculations is that they are based on our data, plus recent papers which address the cerebello-thalamo-cortical loop, which are not necessarily targeting the same thalamo-cortical areas. For example, the work describing the role of the DCN in either preparatory activity or movement initiation investigate Med-VM-ALM or Int/Lat-VL-CFA. In our lab, the region of the motor cortex studied is also named and located slightly more caudal than these regions. It would be informative to map the overall DCN output to the cortex via MThal, and then further narrow down the extent of projection across the motor cortex, and how the DCN project via MThal to ALM and CFA, and if these are overlapping. Furthermore, we have shown that Int/Lat project preferentially, but not exclusively to VL, and Med projects preferentially but not exclusively to VM. Therefore, we cannot forget that there is potential for different information processing between these pathways. In the case that the thalamus, either VL or VM, is “simply” a relay station, perhaps VM and VL are relay different information from the DCN to the cortical regions they target.

If, however, the target in the cortex is overlapping, one could imagine that the signals from the DCN-MThal converge at the level of the cortex prior to signaling an updated command to the brainstem.

Characterization of a transgenic line labeling a subset of DCN neurons: We have further characterized a transgenic mouse line that has been studied in the context of Interpositus DCN research, but limited in anatomical elucidation with respect to output at the level of the brainstem. We therefore first characterized the neurons labeled by this line using a combination of viral tracing and *in situ* hybridization. Systemic viral tracing in combination with RNAscope *in situ* hybridization revealed that *ntsr1*-cre mouse line labels a subset of excitatory neurons in the Interpositus and Lateral DCN. Systemic viral tracing enabled the visualization and quantification of differences in distribution of *ntsr1-cre* neurons versus excitatory *vGlut2-cre* neurons, as visualized in the 3D rendered brain, across the divisions of the DCN. Next, in order to ask to what extent the *ntsr1-cre* line can be used to target this presumably excitatory subset of DCN neurons, we performed RNAScope *in situ* hybridization in the *ntsr1-cre* mouse line to compare the number of cells labeled with *cre* transcripts and the *vGlut2* gene *Slc17a6* transcripts. Cells with more than 3 transcripts were considered positive for that gene of interest. This quantification revealed that all *cre* positive cells were also *Slc17a6* positive, but less than one-fifth of the *Slc17a6* positive neurons were also *cre* positive or positive for the PhP.eB virus. Therefore, the ntsr1-cre line labels a small subset of excitatory neurons in the DCN.

The absolute number of *cre* positive neurons in RNAScope may differ than the absolute number of systemically labeled neurons for several reasons, but the conclusion remains the same. Such reasons include limitations with the viral tracing approach, including variability in efficiency across mice, which provided rational for quantifying neuronal distribution based on percentage in a way to normalize for variability. RNAScope does not have the same variability and is highly robust. Technically, immunostaining following systemic viral injection is performed on 80um slices and quantified through the z dimension, while RNAScope is performed on 20um slices and quantified at the maximum projection. That being said, the main conclusion is that in fact the -*cre* positive neurons in the *ntsr1-cre* line are all *Slc17a6* positive but make up a small percentage of the *Slc17a6* neurons and therefore are a small subset. Ongoing experiments to solidify the results from Figure 6 and 8, is ISH with the combination of systemic injection in the *ntsr1-cre* line plus RNAScope of *Sl17a6*.

Thus far, we have shown that the neurons labeled by the *ntsr1-cre* line in the DCN are a subset of excitatory neurons, therefore we sought to compare the output of these neurons to the output revealed in *vGlut2-cre* anterograde tracing from Int/Lat. At this point, we have decided to focus on the Int/Lat DCN. Anterograde tracing from the Int/Lat of the *ntsr1-cre* line revealed similar output to the Rostral Medulla, however, a visually more restricted density more close to the midline in the contralateral MedRM and a smaller distribution in the ipsilateral LatRM (Figure 7 contour plots). This is not surprising, given the previously described role of both *ntsr1-cre* and LatRM in skilled forelimb movement. We can further speculate that these excitatory *ntsr1-cre* neurons may play a role in online motor control of the motor programs mediated by LatRM.

In addition to comparing output of the *vGlut2-cre and ntsr1-cre* to the RM, we postulated that the two neuronal populations would project similarly to the motor thalamus regions, VL and VM. As we have discussed, anterograde tracing from *vGlut2-cre* positive Int/Lat neurons revealed projections of excitatory neurons to both VL and VM. The percentage of terminals is indeed more pronounced, and of higher quantity than the number of terminals in VM. Tracing from *ntsr1-cre* Int/Lat, however, showed a larger number of terminals in VM, and limited number of terminals in VL compared to what we see with the *vGlut2-cre*. This information in combination with our ISH data suggests that *ntsr1-cre* positive Int/Lat neurons represent a subset of DCN neurons targeting a specific population of neurons in VL and VM, perhaps representing a specific output channel to the motor thalamus that comprises a role in skilled forelimb motor programs. (Supplemental Figure 2).

Our data align with the recent literature which shows that the *ntsr1-cre* neurons project to the VM (Judd et al., 2021) and VL (Houck and Person, 2015), however a quantitative comparison of output from the DCN to each of these regions has not been done. Additionally, our data mirror recent literature that shows that the *vGlut2-cre* Int and Lat project to the VL thalamic nuclei (Bohne et al., 2019; Dacre et al., 2021; Ichinohe et al., 2000;

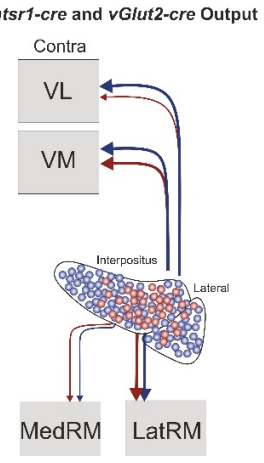

SUPPLEMENTAL FIGURE 2: *NTSR1-CRE* VERSUS *VGLUT2-CRE* OUTPUT

Middleton and Strick, 1997), and medial projects to the VM thalamic nuclei (Gao et al., 2018; Ito, 2006).

So what can this mean? The thalamus is a very large structure in the brain whose functions are of some debate. While at least we can divvy the thalamic nuclei into motor and intralaminar, the thalamus remains somewhat of a black box. As we have discussed, there are several theories on the function of the motor thalamus, as a relay center or integration hub of information from multiple motor center inputs. The elucidation of its anatomical and cell type heterogeneity, and the link between the two, has been underwhelming. Recent work has shown in the VM, that there are compartments delineated by input from regions of the SNr likely correlated to specific components of behavioral modulation. (Lee et al., 2020). This could also be the case for the cerebellar input to the VL and VM, where we see either *ntsr1-cre* or *vGlut2-cre* DCN projecting slightly differently to regions within the VL and VM. To what extent this plays a role in function, or further patterning to the cortex (and further sending signals to the brainstem) remains to be elucidated.

Retrograde tracing from the Rostral Medulla has revealed a spatial organization in the DCN. Especially, the Interpositus and Lateral DCN where retrograde tracing from the medial rostral medulla labels extensively the contralateral medial and lateral DCN, largely omitting the Interpositus DCN. Retrograde tracing from the lateral rostral medulla labels neurons most heavily in the ipsilateral Interpositus and Lateral DCN. Furthermore, the LatRM projecting DCN are spatially organized in the more lateral region of the IntA and IntDL, and lateral DCN. This is just adjacent to the cervical spinal cord projecting DCN in the most medial stripe of IntA. While we have included the spinally projecting population, we have not completely addressed these neurons, given our focus on the brainstem and thalamus. However, it is important to note that It remains unclear if the spinally projecting population are dual projecting to regions of the rostral medulla or thalamus, and this needs to be addressed.

It is of course important to note that we have only focused on one level of the Rostral Medulla for these retrograde tracing experiments. With further retrograde mapping at more rostral regions of the brainstem, such as in the 5N region, we are likely to identify further spatial organization of projection-stratified neurons in the DCN. For example, while we also focused

largely on Int/Lat, in our hands, we also see topography in the medial DCN. This is not too unexpected, given the segregation of rostral and caudal medial DCN where it was speculated and shown in previous literature to be highly diverse from anatomical, molecular standpoints (Fujita et al., 2020) that the two have largely different functions. Triple retrograde experiments in the Arber Lab (unpublished) from the MLR, LatRM, and spinal cord show a segregation of retrogradely labeled nuclei in the caudal Medial DCN where MedDL projects to LatRM and MedL projects to MLR. These projection-stratified Medial zones exhibits yet another level of complexity of the DCN which remains unexplored.

Inhibitory circuits: we also mentioned in the Introduction that there are glycinergic projection neurons to a small region in the caudal medulla. While the data on inhibitory projection neurons are minimal, and the canonical ideas remain that the inhibitory DCN projections exclusively project to the inferior olive, it remains an interesting concept. These glycinergic projection neurons were found to project only to the ipsilateral side of the brainstem, while the excitatory project to the contralateral. It has been speculated that this balance of excitatory and inhibitory projections, and contra versus lateral, may have a role in mediating axial muscular opponency, and therefore have an interplay in motor targets of the projections which are lateralized for limb musculature (Bagnall et al., 2009; Prekop et al., 2018).

Red Nucleus Loops:

Lastly, I briefly described the DCN > Red Nucleus Loop in the introduction, and wanted to further expand here. Masao Ito in “The Cerebellum, Brain for Implicit Self” described in detail his view on how the cerebellum, and the DCN, comprise feedforward models. He therefore speculates on why the Int would project to the Red Nucleus and the Motor Cortex (via VL, (Toyama et al., 1970) two structures largely speculated to be “controllers”. He suggests that the system can be a sort of hybrid control system, where the reflex activity and can be active during voluntary activity where the RN is the former and the cortical loop is the latter. The reflex controller, would contain information on the peripheral input. This hypothetical is interesting because it again puts the DCN into the context of mediating multiple brain-wide loops and in this speculation, also omits the DCN projections to the brainstem. It remains unclear if DCN > Red Nucleus neurons collateralize in the brainstem, but would be a key information for

understanding what information is being transmitted from the DCN key for movement control. (Ito, 2006).

In summary, the combination of excitatory output patterns revealed from anterograde tracing, as well as the spatial organization revealed in the retrograde tracing, help to define cell types in the DCN categorized by anatomical connectivity and projection pattern. We have also described a genetic cell type in the DCN whose neurons represent an excitatory population of Int/Lat, with fairly similar projection profiles to the RM, but projects almost exclusively to the VM thalamic nuclei. It remains unclear whether this cell type collateralizes in a similar way as the *vGlut2-cre* Int/Lat neurons, but would be important to address in defining this as a cell type within Int/Lat. As discussed in the introduction, this is just one facet of defining cell types, however, it is extremely critical in order to properly evaluate the role of the DCN in online motor control.

Chapter 2

Introduction

The data in Chapter 1 reveals anatomically and projection-stratified cell types of the DCN, where Med and Int/Lat vary in their output to the brainstem and motor thalamus. While there has already been work to define molecular cell types of the DCN, there has not been transcriptomic profiling of projection-stratified DCN. It is crucial to link the molecular compartmentalization to the projection-stratified topography to define DCN cell types.

In an analogous way as the DCN, the transcriptional taxonomy of the mouse brainstem remains unexplored, especially with the comparison of the transcriptomic types between the midbrain, pons, and medulla. This is a key missing information, which could correlate to the different broad functionalities of the brainstem. For example, one can imagine that transcriptomic cell types within the midbrain, pons, and medulla help to define or further characterize functional cell types previously described (Esposito et al., 2014). Likely, the midbrain and pons which contains regions involved in locomotion or head turning, for example (Capelli et al., 2017; Cregg et al., 2020; Esposito et al., 2014), differ in transcriptomic profiles than those regions in the medulla shown to play a role in more skilled behaviors. (Ruder et al., 2021)

Continuously advancing RNA sequencing and viral tracing strategies allow us to address the following aims:

Aim 1: Elucidate the transcriptional profiles of the midbrain, pons, and medulla regions of the brainstem

Significance: The midbrain, pons, and medulla represent three regions of the brainstem which are developmentally and functionally diverse. The molecular heterogeneity within these regions has been left largely unexplored yet is critical for understanding the cell types within.

Approach: Using single nuclear RNA sequencing (snRNAseq) in combination with a suite of viral tools, we label, isolate, and FACS individual nuclei of either the full brainstem, or three regions within (midbrain, pons, medulla, isolated separately). Following this, we take advantage of a commercialized droplet-based single cell sequencing platform, drop seq and 10X Genomics (Macosko et al., 2015).

Brief Conclusion: snRNAseq furthered our understanding of the cellular heterogeneity of the brainstem. Of the 22497 nuclei to be sorted, sequenced (10X has around a 30% dropout rate of nuclei), and made it through the quality check (See methods), we identified 16 excitatory and 17 inhibitory transcriptomic types of the entire brainstem dataset. Furthermore, we found that the midbrain and pons are more closely related for inhibitory cell types, while the pons and medulla re more closely related for excitatory cell types.

Aim 2: Map projection stratified DCN transcriptional profiles to the overall DCN molecular map

Significance: While two major studies have identified molecular compartmentalization of the DCN using either *in situ* or single cell RNA sequencing, projection-stratified DCN neurons have not been profiled. This is vital for truly understanding the complexity of the cell types of the DCN.

Approach: We use a combination of viral tools to label, isolate, sort, and sequence the overall DCN population, plus a retrogradely labeled population (LatRM-projecting DCN). We used a modified version of the SmartSeq2 (Picelli et al., 2014) protocol by sorting single nuclei into 384 well plates, then processed on an automated liquid handling machine.

Brief Conclusion: We have identified 5 transcriptomic types in the DCN, as well as three LatRM projecting DCN transcriptomic types. When these experiments are pooled together, 8 transcriptomic types are revealed, where all clusters except one of the pooled data contain nuclei of both populations, however, the proportion of the nuclei represented from either experiment is mixed.

Results

Excitatory and Inhibitory Brainstem Subtypes

While the mouse brainstem's anatomical and developmental cell types have been a focus of some areas of research, the transcriptional diversity of the midbrain, pons, and medulla have remained largely unknown. The tremendous advances in single nuclei RNA sequencing methods and analysis, in combination with viral tracing strategies have provided an entry to point to ask how the three major regions of the brainstem (midbrain, pons, and medulla) are transcriptionally related. In order to address this question, we used nuclear (H2B Tag) PhP.eB systemic viruses to label all the excitatory and inhibitory populations of the double transgenic mouse line *vGlut2-cre* x *vGat-flp* and isolated either the whole brainstem (Figure 1A) or the midbrain, pons, and medulla (Figure 2A) of two genetically identical mice (See Methods for details). After dissociation of the brainstem (n=3), we verified the nuclei for markers specific to neurons, as well as per each cell type (*Slc17a6* for excitatory, or *Gad2* for inhibitory, (Figure 1B,E,F). We then analyzed each cell type separately to identify transcriptomic sub types within the two populations (Figure 1C,D), and revealed with a clustering resolution of 0.7 determined by a robust program designed for identifying optimal clustering parameters (Zappia and Oshlack, 2018) we identified 16 excitatory and 17 inhibitory subtypes of the 22497 nuclei collected. In the Supplemental Figure 3, we show the top 25 genes which account for 15.1% of the total counts. These genes share similar GO terms according to molecular function, mostly related to development and ion channel binding. Specifically, *lsamp* promotes the growth of limb neurons and mutant mice display an increased exploratory activation in novel environments (Catania et al., 2008). *Fgf14* has been shown to play a role in adult locomotor activity, where mutant mice suffer from ataxia and neurological deficits (Goldfarb et al., 2007). *Rbfox1* is required for mature motor function, where mutant mice display splicing changes which alter proteins required for brain development and neuronal function (Gehman et al.,

2012). *Pcdh9* has a potential role in in formation of neural circuits (Asahina et al., 2012). Other genes in the top 25 are related to synapse assembly, and calcium channel regulation or binding and include *nrxn3*, *nrxn1*, *Lrp1b*, *Tenm2*, *Lingo2, Lrrtm4, Lrrc4c. Grid2* is also highly expressed and encodes a glutamate receptor.

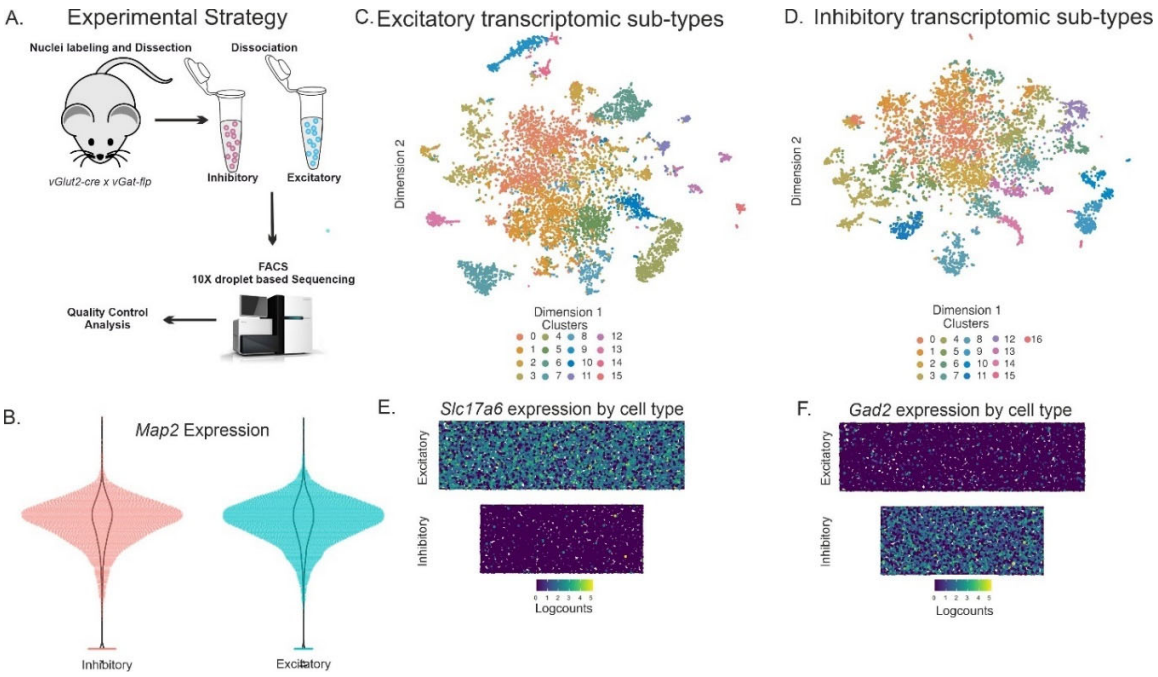

Figure 1: Transcriptional Diversity of the Mouse brainstem A). Experimental strategy to label, sort, and sequence the excitatory and inhibitory nuclei of the brainstem. B. Verification of FACS of only neurons by expression of *Map2* in both inhibitory and excitatory samples, where each dot represents one nuclei. C and D) *t-sne* representation of transcriptomic sub-types within either the excitatory or inhibitory neuronal populations of the brainstem E and F). Selected marker expression for verification of either excitatory or inhibitory expression where each dot represents one nuclei and the expression of either *Slc17a6* or *Gad2* in a log count scale.

For the regional data set, we sought to isolate the midbrain, pons, and medulla separately based on landmarks and measurements according to the Paxino's mouse atlas (Franklin, 2019). After dissociation of the three regions (pooled of the two mice), nuclei were labeled with DAPI to exclude doublets, and excitatory and inhibitory nuclei double positive for DAPI were FACS sorted according to their respective fluorescent tag. After 10X droplet-based sequencing, the single nuclei were analyzed. (Figure 2A). As proof of concept, we excluded nuclei that did not meet the expected quality and checked our excitatory and inhibitory populations for canonical markers according to neurotransmitter identity as well as neuronal markers, thus omitting any potential glial contamination. Excitatory nuclei of each region of the brainstem clustered

separately, but also had largely overlapping populations. This shared transcriptional identities (black) can be expected because, while there are known functional and developmental segregations along the rostral to caudal axis of the brainstem (midbrain to pons), there are indeed shared functionalities. Because there are many shared transcriptional identities of these data between the three regions, it can also be a limitation of the technique as 10X sequencing is fairly shallow (Zhang et al., 2019) as well as limitations with collection of *all* excitatory and inhibitory nuclei due to virus limitations in efficiency, and potential tropism of the viruses. A validation would be to sort and sequence the brainstem and its regions again, but isolating only based on expression of excitatory and inhibitory markers, rather than relying on the viral tagging approach (Figure 2B). Hierarchical clustering reveals that in the excitatory populations of the brainstem, the pons and medulla are more closely related while in the inhibitory the midbrain and pons are more closely related to each other (Figure 2D,E). Lastly, while these data revealed interesting results, the main goal of these experiments began as an attempt to develop the technical and analytical methodology. We therefore asked if we could map smaller populations back onto our larger, overall dataset. This full excitatory brainstem dataset provided a map for which we were able to map the excitatory regional data set back onto. (Figure 2C).

These data presented on the brainstem proved that indeed single nuclei RNA sequence can reveal transcriptional profiles of different regions in the brain, largely, to compare midbrain, pons, and medulla and establish methods, and techniques. We therefore wanted to apply these techniques to the Deep Cerebellar Nuclei, overall population, plus a projection-stratified population within the DCN.

The Midbrain, Pons, and Medulla transcriptional taxonomy

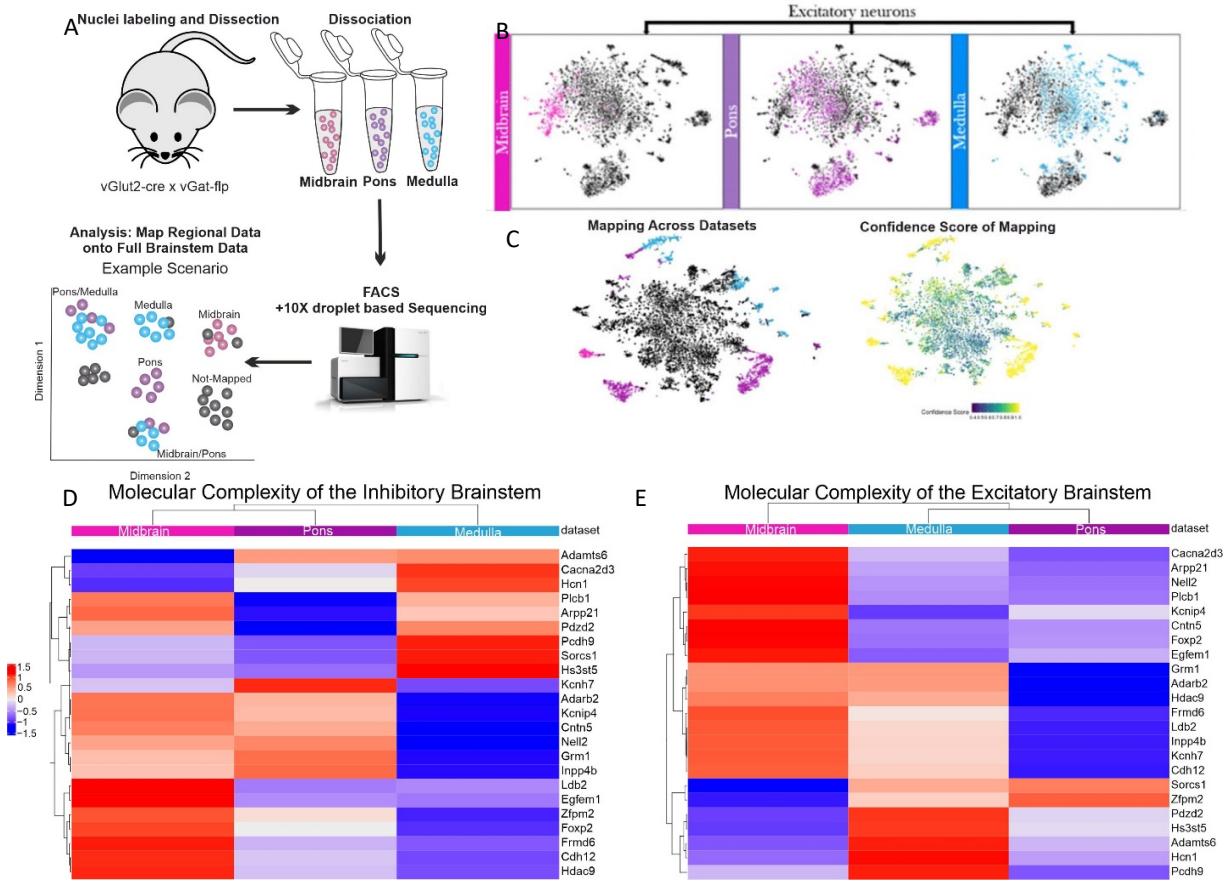

Figure 2: single nuclei RNA-sequencing reveals transcriptional diversity of the midbrain, pons, and medulla. A). Strategy for labeling nuclei, dissociation, to FACS and 10X sequencing. B). t-sne visualization of midbrain, pons, and medulla transcriptional profiles where each dot represents one nuclei. C). Mapping of the midbrain, pons, medulla nuclei back onto the overall excitatory population of the mouse brainstem, and confidence score of mapping back onto the overall dataset. D). Hierarchical clustering of the inhibitory and excitatory midbrain, pons, and medulla.

Projection-specific DCN represent a transcriptional subset of the DCN excitatory population

In order to compare the transcriptional profiles of the overall excitatory DCN population to a projection-stratified DCN population we employed two viral tracing strategies. We systemically labeled the entire exciatory DCN population using a PhP.eB Flex H2B Tag(1) virus. We then retrogradely labeled LatRM projecting DCN using a Flex H2B Tag(2) virus. We then isolated the DCN, dissociated the tissue, labeled with DAPI to exclude doublets, and FACS sorted according to fluorescent Tag. In the case of the DCN, we used the SmartSeq2 single-nuclei sequencing method (Picelli et al., 2014). This method of sequencing allows for greater sequencing depth, and the ability to sequence less nuclei (10X sequencing has a high drop out rate). We took advantage of a 384-well approach which allowed for automated processing, and therefore less

handling error than what would be with with usual 96-well SmartSeq2 approach. (Figure 3A). After sequencing, the nuclei were verified with excitatory markers, and pre-mRNA were clustered according to the SC3 analysis pipeline (Kiselev et al., 2017), and verified with the Seurat analyisis pipeline (Duò et al., 2018). These two types of analyses are the "gold standard" and allow for robust analysis. We determined which resolution of clustering should be performed based on consensus and silhouette plot verification. (Figure 2B). Nuclei from both the retrograde and straight DCN population were pooled together for analysis and *t-sne* representation reveals eight distinct clusters. (Figure 3C). Of the eight clusters, there is fairly spread distribution of the straight verus retrogradely labeled populations, but there are two clusters which have no or few retrogradely labeled DCN. This is very important to note, because indeed I only have collected LatRM projecting DCN. These other clusters with no retrogradely lebeled cells are likely from different projecgion populations. (Figure 3D). We were able to identify top marker genes for each cluster, either highly or lowly expressed, compared against all other clusters. (Figure 3E,F).

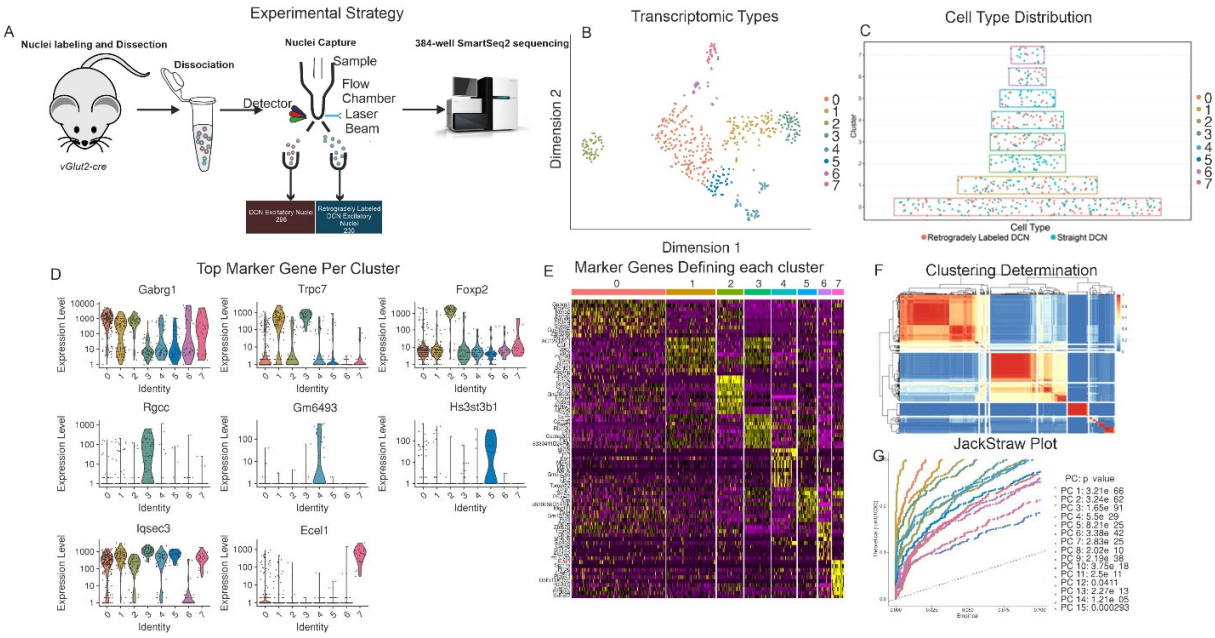

Figure 2: LatRM-projecting DCN represent a transcriptional subset of the overall DCN transcriptional profile A). Experimental strategy to isolate and sequence DCN and retrogradely labeled DCN neurons. B). *t-sne* visualization of the pooled, full-DCN and LatRM projecting DCN nuclei determination of clustering strategy C). Dot plot visualization of the distribution of straight versus retrogradely labeled DCN per each of the clusters from D). Violin plot representation of the top marker gene per each cluster where each color represents the cluster matching with B and C). and each black dot represents one nuclei. E). Expression heatmap for the clusters, with the top markers (maximum 20 per cluster). F) Consensus matrix to represent similarity between the cells based on averaging of clustering results from all combinations of clustering parameters, where a similarity of 0 (blue) dictates that the two cells are always assigned to different clusters, where 1 (red) means the two cells are always assigned to the same cluster. (SC3 source) G). JackStrawPlot to visualize the distribution of p-values for each PC with a uniform distribution. Significant PCS show strong enrichment features with low p-values in colored lines above the black dashed line.

Discussion

These data together give help to define molecular cell types in both the brainstem and deep cerebellar nuclei. Both datasets provide a framework to correlating molecular, and anatomical DCN and brainstem neuronal classes. snRNA-seq of the midbrain, pons, and medulla suggest that the expression of certain genes may arise in development. Because the pons and medulla are more closely related transcriptionally, and are functionally more advanced (skilled behaviors) than the midbrain (locomotor and phylogenetically older) then it could be interesting to isolate and sequence each region over the developmental time course of the animal, where specific behaviors arise. Furthermore, it is interesting that the inhibitory nuclei are most transcriptionally similar between midbrain and pons. It could be that the inhibitory molecular program does not expand through development. As mentioned, there is the limitation of depth of sequencing with the 10X sequencing method, so therefore, it could be

interesting to sequence with a deeper method where potentially more transcriptional types can be identified, further breaking up the large central cluster seen in Figure 2B, C. This project originally started in order to map back neuronal subpopulations which have been functionally elucidated. This would provide a functional, anatomical, and molecular means to truly identify brainstem cell types. For example, it would be interesting to sequence the different LatRM populations described in recent papers, which show different functionalities. I would hypothesize that, for example, spinally-projecting LatRM would be mapped onto one cluster in the medulla dataset described here. Likely, the full LatRM population would be spread onto several clusters. Conversely, likely one could identify LPGi, Gi, and MLR (for example) in distinct sets of clusters in this overall brainstem dataset. One could imagine that regions tuned to full-body behavior are more similarly related (could be elucidated by hierarchical clustering) to each other than to brainstem regions functionally shown to mediated skilled forelimb tasks. This is of course speculative, and also challenging with technical and analysis hurdles, and would therefore have to be addressed.

snRNAseq of the full DCN excitatory population reveals five transcriptomic types, while the LatRM projecting DCN are composed of three transcriptomic types. When pooled and analyzed together retrogradely labeled DCN can be identified in nearly all of the straight DCN populations with the exception of one cluster. This cluster (Cluster 2), when compared to clusters 3 and 4 which are an even distribution, contains 5 genes highly expressed including (*Zfhx3, Zfhx4, Tcf712, Nrgn, Gr3).* I would speculate that these genes are present in other projection-stratified subpopulations not targeted in this particular experiment. In other clusters, the proportion of retro nuclei to straight DCN are variable. I would hypothesize that the three LatRM projecting DCN can be anatomically matched to some of the populations revealed in the anatomical data presented in Chapter 1 when tracing retrogradely from LatRM. For example, I would hypothesize that within the three types, there are an ipsilateral Int/Lat population, a contralateral Medial, and contralateral Lateral population. This would have to be verified with *in situ* to identify the spatial location of these genes in the DCN.

The clusters with no or few retrogradely labeled nuclei is not surprising, because I have only sequenced one RM-projecting population. Likely, there are populations in the overall

population whose transcriptional identities may match with contralateral MedRM projecting DCN for example. While this thesis focuses almost exclusively on the rostral medulla, it cannot be forgotten that other regions of the midbrain, and medulla are receiving input from the DCN and likely have a unique molecular profile. As this is all speculative, the most logical next experiment which would align well with the defined anatomical cell types in Chapter 1 of the DCN, would be to label and sort both single positive contralateral MedRM and ipsilateral LatRM projecting DCN. It would be interesting to also collect the double positive, dual-projecting nuclei and compare the transcriptomic types to each other as well as map back onto the overall DCN population. Several genes from these data have also been described in the supplement of the recent DCN RNA sequencing paper described earlier (Kebschull et al., 2020), including genes *Sv2c, Acan, Hs3st3b1*, and *ecel1* which are found to be highly expressed in class B medial, Interpositus, and lateral DCN. *Foxp2* was also identified in both datasets which is highly expressed in class 1 medial DCN, according to this study. The gene *spp1* is found in both our dataset and the described dataset and was shown to be highly expressed in Int and Lat Class B neurons. Analysis to map our identified nuclei back to the data revealed in the mentioned paper is ongoing, using the SingleR package in Bioconductor which allows for unbiased cell type recognition across datasets (Aran et al., 2019) ; this will allow us to potentially identify clusters related to the DCN divisions based on recently published transcriptomic data.

Conclusions

As humans, we depend on our bodies, muscles, and neuronal circuits for optimally performing our daily tasks. From walking, biking, writing, and eating we rely on our brains ability to constantly adjust for any unexpected change that may occur. This can be a hole in the road in front of us, a slip on the ice, a change in expected shape of food – all require a circuit-wide adjustment and integration of signals encoding the unexpected versus expected.

The cerebellum has been described as the “little brain” owing to the tremendous role it has in essentially all movement. Most commonly seen with cerebellar damage in humans is an inability to maintain balance, coordinate movement, and learn movements. Mossy fibers and purkinje cells of the cerebellum deliver motor and sensory information to the deep cerebellar nuclei from regions of the brain and periphery (Glickstein, 1997). The sole output of the

cerebellum, is the deep cerebellar nuclei. These nuclei have vast projections to motor centers in the brain, including the motor thalamus and brainstem, two structures key for to the carrying out of motor programs. As one can imagine, the diversity of unique and specialized movements performed on a daily basis is enormous and would require specialized neuronal circuits to learn and optimize the many actions we call on. As systems neuroscience is recently dominated by efforts to elucidate neuronal circuits into their molecular, cellular, and organizational components, we had the aim to do just this strategy to explain the role of the DCN in online motor control, a term analogous to the concept of real-time adjustment in a motor program when comparing the expected versus unexpected.

We have explored the anatomical and molecular heterogeneity of the deep cerebellar nuclei based on the combination of excitatory output patterns and gene expression profile. We have revealed output patterns specific to Med and Int/Lat, wherein, the Int/Lat is required for ipsilateral projections to the LatRM region of the Rostral Medulla. Since both the Int/Lat and LatRM have been implicated in skilled reaching behavior, likely, the two regions are working in harmony to learn and maintain such a skilled motor program. We have identified molecular profiles of the DCN which, while need to be verified for spatial organization with *in situ* hybridization, reveal a molecular complexity of both the full and projection-specific DCN neurons.

An additional point of interest is how anatomical modules can relate to potential functional modules, a concept which has been shown in the cerebellum proper where modules have been used to describe basic operational units of the cerebellum. One can imagine this idea can be continued with the DCN and their output in such a way where there exists medial and lateral modularity, further relating to general function involving either full body (medial) or skilled forelimb (lateral) zones.

Methods

Single nuclei RNA sequencing of the brainstem

Processing, sorting, sequencing of the nuclei

Nuclei were labeled with either systemic PhP.eB-flex-Tag with two different fluorescent tags (FRT-tdTomato and Flex-GFP) via retro orbital injection into *vGlut2-cre* x *vGat-flp* mice. Brains were removed after deep anesthesia, and stored in Hibernate A solution to preserve tissue integrity. For the full brainstem dataset (three genetically identical mice, brothers of the same litter), the entire brainstem was collected after removing the cortex to visualize just rostral to the superior colliculus, at the boundary of the mRT. (5.5mm rostral to the caudal brainstem). Midbrain, pons, and medulla regions were isolated for the regional dataset according to Allen Brain Atlas calculations, in combination with using a brain slicer matrix with 100um intervals, and ability to visualize the 5N and 7N from the underside of the brain. Brain sections were collected in 1X ultrapure PBS. Tissue was homogenized using a tissue 3mL dounce-homogenizer setup, at 2000rpm. Homogenized tissue was centrifuged for 5 minutes at 4°C at 10000rpm, and supernatant was removed. The pellet was gently resuspended to a homogenous mixture with 1X PBS (molecular grade PBS in RNAase-free water), RNAase Out, and UltraPure BSA. (9.5mL, 25uL, 500uL respectively). This mixture was then passed through a 70um MACS filter, followed by a 20um filter. The homogenized tissue was then incubated with DAPI 10 minutes prior to FACS sorting. The samples were then FACS sorted, with either double positive for DAPI (singlet) and GFP, or double positive for DAPI (singlet) and tdTomato. Immediately after collection, 10X Genomics sequencing was performed on the nuclei.

Alignment, dimensionality reduction, marker gene identification

Sequencing metadata and gene annotations (gencode.vM19.annoation) were read using tx2gene and both spliced and premRNA were aligned. We used Cellranger, which is built on STAR program to estimate transcript abundance, but adds a component of UMI deduplication, the reads were quantified and genes annotated, the result is a UMI count matrix, where the matrix values display the number of molecules for each feature detected in each cell. Data then underwent quality control and filtering with scater (thresholds determined following the Seurat vignettes). (McCarthy et al., 2017; Stuart et al., 2019) where the features with over 2500 counts or under 200 counts were filtered out.(see example figures from Regional Dataset), maximum mitochondrial gene read count must be less than 5. After this, the data were normalized according to a global-scaling method “LogNormalize”, normalizing the feature expression measurements for each cell by total expression and multiplying the expression by a scale factor of 10000.Following normalization, dimensionality reduction for PCA, TSNE, UMAP were applied and SingleCellExperiment (SCE) (Amezquita et al., 2020) objects were created. Data were converted to Seurat objects (Duò et al., 2018), and a method to integrate data across experiments was applied (FindIntegrationAnchors) (Stuart et al., 2019), and clustering was applied on the integrated data based on the computation of nearest neighbor graph and SNN. Integrated data is in Ngenes x Ncells, where Ngenes is the number of highly variable gens included. These values are adjusted values on a log scale. Using a standard-in-the-field clustering approach was used (Clustree) (Zappia and Oshlack, 2018) we

determined the optimal clustering parameters to be with a resolution of 1.5. PCA and t-SNE were applied to the integrated data. Marker genes were determined by identifying gene with the most highly variable expression against all other clusters. (Supplemental Figure 3: A-F). For more details on the code analyzing these data, the Github code can be found at: https://github.com/stacci989/RNAseqdata_10x (when published online).

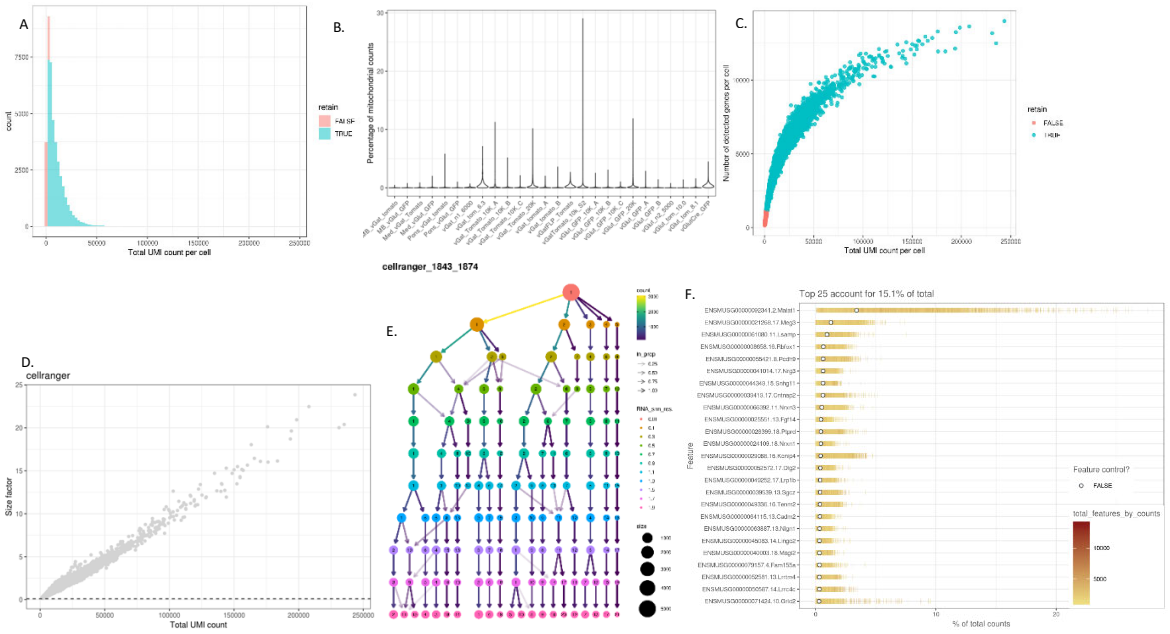

Supplemental Figure 3: A). Total UMI counts per nuclei sequenced. B). Percentage of mitochondrial counts per each 10X run. C). Total genes detected per cell versus the total UMI count per cell D). Size Factor over total UMI count. E). Hierarchical clustering determination. F). Top 25 genes based on percentage of the total counts.

Mapping regional dataset onto full dataset

In order to map the regional (midbrain, pons, medulla) dataset onto the full dataset, we measured the correlations of cells in the full dataset to pseudo-bulks in the regional dataset. For each cluster in the regional data, the average logcounts of each gene was calculated and the most highly correlated cluster for each cell in the integrated full brainstem data set were identified. We then determined the number of closest neighbors to consider for each cell.

Single nuclei RNA sequencing of deep cerebellar nuclei

Processing, sorting, sequencing of the nuclei

Nuclei were labeled with either systemic PhP.eB-flex-Tag or rAAV-flex-Tag via retro orbital injection or stereotactic injection into LatRM (as described Methods, Viral Tracing) of *vGlut2-cre* mice. Brains were removed after deep anesthesia, and stored in Hibernate A solution to preserve tissue integrity. The brain was mounted in a 4% agarose gel to be sectioned on a vibratome, on ice. 150um sections were collected in PBS, and the brainstem was removed. Tissue was homogenized using a tissue 3mL dounce-homogenizer setup, at 2000rpm. Homogenized tissue was centrifuged for 5 minutes at 4deg C at 10000rpm, and supernatant was removed. The pellet was gently resuspended to a homogenous mixture with 1X PBS (molecular grade PBS in RNAase-free water), RNAase Out, and UltraPure BSA. (9.5mL, 25uL, 500uL respectively). This mixture was then passed through a 70um MACS filter, followed by a 20um

filter. The homogenized tissue was then incubated with DAPI 10 minutes prior to FACS sorting. This protocol was developed by the Catherin Dulac Lab, and optimized for our experiments.

Individual, single positive fluorescent (plus DAPI positive, singlet), nuclei were sorted using a BD FACSAria instrument, and Aria Diva software, into individual wells of a 384-plate. To reduce batch effects between plates, plates were filled one half with one fluorescent Tag and the second half with the second fluorescent Tag. Parameters of FACS sorting Plates were then frozen at -80 until being processed using an automated liquid handling system adapted to the previously described SmartSeq2 Protocol. (Picelli et al., 2014). One row of each plate contained RNA spike-in controls.

Alignment, dimensionality reduction, marker gene identification

Sequencing analysis was developed and run in collaboration with Dr. Charlotte Soneson (FMI Bioinformatics). Sequencing metadata and gene annotations (gencode.vM19.annotation) were read using tx2gene and both spliced and premRNA were aligned. The gene abundances from the full length SmartSeq2 data were estimated using Alevin, which is built off of the Salmon quantification method (Patro et al., 2017; Srivastava et al., 2019) Salmon provides a means to estimate transcript abundance with “dual-phase statistical inference procedure” and a model that accounts for positional biases, fragment, GC-Content and sequence specificity. Sequence reads were aligned to genomic features using both Salmon and featureCount approaches (Liao et al., 2014; Patro et al., 2017). QC metrics were calculated according to a common standard (Ilicic et al., 2016; Stuart et al., 2019) with scater, and filtered according to total features (2500 to 5000), percent assigned to the genome (40), and total counts threshold (50000).

Data were subset into SingleCellExperiment objects (Amezquita et al., 2020) , normalized by calculating the logcounts, and dimension reduction was performed (runPCA, runTSNE, runUMAP), and saved as an object for further analysis.

Retrogradely labeled and the full DCN populations were, in the end, analyzed together from the SingleCellExperiment (SCE) objects created. Two analysis methods were followed, which are considered the golden standards including the Seurat Pipeline (Brennecke et al., 2013; Duò et al., 2018; Stuart et al., 2019) and Bioconductor SC3 Pipeline (Kiselev et al., 2017). Briefly, both methods were used to ensure a conservative, yet, meaningful clustering approach. Data were normalized with a global-scaling normalization method (LogNormalize) which normalizes the feature expression for each cell by the total expression, and is multiplied by a factor of 10,000, and log transforms the result. After this, highly variable features were calculated which models the mean-variance, and is used for dimensionality reduction in the following steps. Prior to linear dimensional reduction, the data are scaled with the application of a linear transformation (ScaleData), which shifts the expression of each gene to a mean expression across cells of 0 so that the variance across cells is 1. The weight is then equal for further analysis and therefore the highly expressed genes will not dominate. giving equal weight in downstream analysis such that most highly-expressed genes don’t dominate. Final clustering was performed with snn resolution of **0.7**. (Figure S2A-B). Marker genes were determined from this selected resolution and this list, with one element for each cluster, contained a dataframe with top markers for each pairwise comparison of that cluster to all other clusters. The p-value and false discovery rate (FDR) columns to aggregated p-values across all comparisons. Therefore, top genes are those that are unique to a given cluster, given the null hypothesis that the gene is not differentially expressed. Marker genes were identified for each cell, by comparing the most highly expressed genes in a cluster against all other clusters. For identifying markers specific to the retrograde-lacking cluster (cluster 2 in our data), we compared specifically cluster 2 to clusters 3 and 4 which are heterogeneous in cell type (where cell type is either retrograde or the full DCN subset of nuclei). Violin plots were calculated using the VlnPlot

function in the Seurat vignette. For more details, the code can be found at https://github.com/stacci989/RNAseqData_SS2 (when published online).

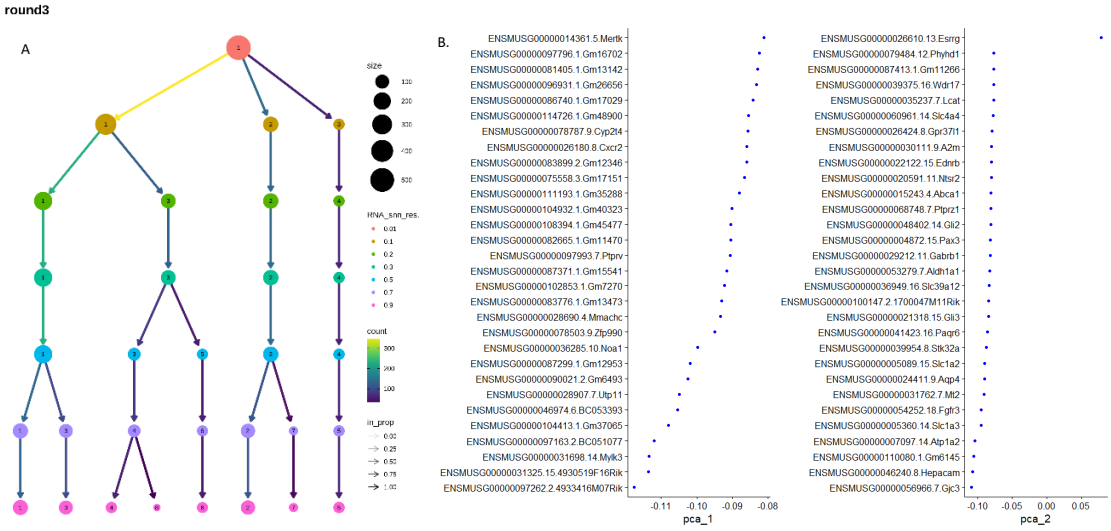

Supplemental Figure 4: A). Hierarchical clustering for SmartSeq2 Data. B). Identification, validation of PC1 and PC2.

RNAScope

For our *in situ* hybridization experiments of *ntsr1-cre* transgenic mouse lines, we used the RNAScope Multiplex Fluorescent Reagent Kit v2 Assay, (document Number 323100-USM), from Advanced Cell Diagnostics, Inc. Mice were transcardially perfused using the following paradigm: 20mL warm 1X Phosphate Buffer Solution (PBS), 20mL warm 4% PFA (plus 0.1% glutaraldehyde), 20mL cold 4% PFA (plus 0.1% glutaraldehyde). Dissected brains were fixed overnight at 4°C in 4% PFA. The next day, the brains were washed twice with PBS and incubated overnight at 4°C in 20% sucrose. Following this, the brains were incubated in 30% sucrose overnight at 4°, prior to embedding in OCT and sectioning with a cryostat. 20um sections were mounted onto glass slides and kept at -20° prior to the RNAScope protocol below.

For *in situ* hybridization, we followed the manufacturer's protocol. The probes used were the following: RNAScope Probe- CRE (Cat No. 312281) in Channel 1. RNAScope Probe – Mm- Slc17a6-C2 (Cat No. 319171-C2).

Mice

We used *vGlut2-cre* heterozygous mixed male and female mice between ages 2 and 5 months for anatomical tracing experiments. Heterozygous mice were maintained by crossing the homozygous *vGlut2-cre* mice (JAX Stock #028863) (Vong et al., 2011) to C57Bl6 wildtype mice. Mice were genotyped for *–cre*.

We used *vGlut2-cre* x *vGat-Flp* mixed male and female mice between ages 2 and 5 months were used for anatomical tracing experiments, where *vGlut2-cre* homozygous mice were crossed to heterozygous *vGat-flp* mice (B6.Cg-Slc32a1tm1.1(flpo)Hze/J, JAX Stock #029591). Mice were genotyped for *–cre* and –flp.

We used *ntsr1-cre* heterozygous mixed male and female mice between ages 2 and 5 months for anatomical tracing experiments. *Ntsr1-cre* heterozygous mice (B6-Tg(Ntsr1-cre)GN220Gsat/Mmucd) were crossed to C57Bl6. Mice were genotyped for –*cre*.

We used C57Bl6 mixed male and female mice for anatomical tracing experiments, ages 2 to 5 months.

All mice were housed on a 12 hours light-dark cycle, in ventilated cages, with temperature of 22 degrees Celsius with a humidity-controlled environment.

Viral Tracing

All of our adeno-associated viruses (AAV) were used according to the table below. Viruses used to label the cell bodies, retrograde infection, and synapses were used as described in previous work of the lab (Capelli et al., 2017; Ferreira-Pinto et al., 2021; Pivetta et al., 2014; Ruder et al., 2021).

VIRUS	SEROTYPE	REFERRED TO
AAV-flex-SynGFP	AAV(9)	AAV-Flex-SynTag
AAV-flex-SynMyc	AAV(9)	AAV-Flex-SynTag
AAV-frt-SynGFP	AAV(9)	AAV-Flex-SynTag
AAV-Flex-tdTomato	AAV(9)	AAV-Flex-cSynTag
Flex-H2B-GFP	PhP.eB	PHP.eB Flex H2B Tag
Flex-H2B-tdTomato	PhP.eB	PHP.eB Flex H2B Tag
AAV-retro-H2B-cre	AAV(2)	rAAV-cre
AAV-retro-Flex-H2B-GFP	AAV(2)	rAAV-flex-Tag
AAV-retro-Flex-H2B-tdTomato	AAV(2)	rAAV-flex-Tag

For both brainstem, thalamus, and deep cerebellar nuclei injections, surgeries were performed on a high precision stereotactic device (Kopf Instruments, Model 1900), under surgery protocols and anesthesia previously described and according to the approved permit (2106). After balancing the animal, the following coordinates were used for viral tracing, and injection of approximately 50-100nL virus: We incubated the viruses for two to three weeks, for viral expression. PHP.eB systemic viruses were delivered retro-orbitally (Gruntman et al., 2017) to mice aged between 1 and 2 months old. The titer for all viruses depended on the batch of production but ranged between 10^{12} and 10^{14}. Viral injections into the cervical spinal cord were injected into C1-C5 with an approximate volume of 300-500nL.

BRAIN REGION	COORDINATE (AP; ML; DV)
MedRM	-1.0, ±0.4, -4.8
LatRM	-1.4, ±1.55, -4.75
Interpositus DCN	-2.1, ±1.85, -2.25
Lateral DCN	-1.8, ±2.4, -2.4
Medial DCN	-2.1, ±0.8, -2.25
Ventrolateral Thalamic nuclei	+1.34, ±1.2, -3.3
Ventromedial Thalamic nuclei	+1.6, ±0.75, -4.0

Antibody Staining

All viral injections were visualized with immunohistochemistry. After mice were anesthetized (Ketamine/Xylazine) they were perfused with 4% paraformaldehyde and cold phosphate buffer saline (1X PBS). Brains were dissected and post fixed for 12-24 hours, prior to incubating brains in a 30% sucrose solution for at least 48 hours at 4°C for cryopreservation. Brains were sectioned with a cryostat at 80um thick slices and placed into individual wells filled with PBS. Slices were incubated in a 1% BSA solution with 0.1% TritonX100, in PBS. Primary antibodies were prepared and incubated again in BSA solution and incubated for three days. After primary incubation, slices were washed 2 times, blocked again for 30 minutes, and the secondary antibodies were added and incubated overnight, shaking at 4°C. Following this, slices were washed 2 times and mounted on glass slides with an in-house mounting media. Antibodies were used in the following manner:

ANTIBODY	CONCENTRATION	COMPANY
goat anti-ChAT	1:500	Chemicon/MM, lot#3305977
chicken anti-TH	1:500	Neuromics, lot#403512
rabbit anti-Calbindin D-28k	1:9000	Swant
mouse anti-Calbindin	1:1000	Swant, lot#07F
chicken anti-Myc IgY fraction	1:5000	Invitrogen/LifeTech, lot#1891012
mouse anti-V5 IgG2a	1:1000	Invitrogen/Life Tech, lot#46-1157
chicken anti-GFP	1:2000	Molecular Probes, Lot#1692920
sheep anti-GFP	1:1000	Biogenesis/Biorad, lot#25122051
rabbit anti-GFP, IgG fraction	1:5000	Molecular Probes, lot#57931A
rabbit anti-RFP	1:5000	Rockland, Lot#33754
488 donkey anti-Chicken IgY (H+L)	1:1000	JIR/LuBio, lot#703-545-155
488 donkey anti-Sheep IgG (H+L)	1:1000	JIR/LuBio, lot#713-545-147
488 donkey anti-Rabbit IgG (H+L)	1:1000	JIR/LuBio, lot#711-545-152
DyL405 donkey anti Chicken IgY (H+L)	1:500	JIR/LuBio, lot#703-475-155
DyL405 donkey anti-mouse IgG (H+L)	1:500	JIR/LuBio, lot#715-475-150
647 donkey anti-goat IgG (H+L)	1:1000	JIR/LuBio, lot#705-605-147
647 donkey anti rabbit IgG (H+L)	1:1000	JIR/LuBio, lot#711-605-152
647 donkey anti-mouse IgG (H+L)	1:1000	JIR/LuBio, lot#715-605-150
647 donkey anti-chicken IgG (H+L)	1:1000	JIR/LuBio, lot#703-605-155
Cy3 donkey anti-Chicken IgG (H+L)	1:1000	JIR/LuBio, lot#703-605-155
Cy3 donkey anti-Rabbit IgG (H+L)	1:1000	JIR/LuBio, lot#711-165-152

Imaging, Synaptic Quantification, 3D Registration

Imaging

After staining, brains were imaged at low resolution to get an overview of all sections with a Zeiss Axio Scan.Z1 slide scanner with a Hamamatsu Orca Flash 4.0 6.5um pixel size (fluorescence imaging). For these overviews, the Fluar5x/0.35 objective was used with a binning of 2.

For high resolution images, we used a spinning disk confocal microscope using the following components: Axio Imager M2 (upright microscope), Yokogawa CSU W1 Dual Camera T2 spinning disk confocal scanning unit, Visitron VS-Homogenizer, and ZPiezo drive stage. Laser lines used were 405nm, 488nm, 561nm, (all at 150mW type Obis) and 639nm (100mW power and type Obis). Horizontal and vertical detectors used were type sCMOS, camera PCO.EDGE4.2M, 2048x2048 format, with 6.5um x 6.5um pixel size, 13.3 x 13.3mm chip size, and 16-bit dynamic range (one vertical, one horizontal mounting). The acquisition settings of nuclei labeling was 20X objective, binning 4, step size 5.0 (pixel size 0.649). The acquisition settings of synaptic labeling was 20X or 40X objective, binning 4, step size 1.0 (pixel size 0.649 or 0.326). Multi-tile acquisitions were stitched using macros developed by the FMI Imaging Facility, built off of the Fiji stitching plugins, where an .stg file is created from the Acquire Multiple Tiled Region Visiview macro. This STG file was used to then stitch the Tile Configuration files.

Synaptic and Nuclear Quantification

Nuclei were quantified either manually, or with using TrackMate depending on the density (Ershov et al., 2021) using the Laplacian of Gaussian (LoG) filter, in which the calculations are made in the Fourier space and the maxima in the filtered image are found, where maxima too close to each other are suppressed. Detection option with a nuclei size of 13um, threshold of 25000, pre-processed with the median filter, and detected after sub-pixel localization. Synaptic terminals were quantified with TrackMate, with a diameter of 2um and threshold of 60000. To assess spatial location and quantitative distribution of the output of the DCN, two-dimensional density plots were made following spot detection with Imaris, using 2D kernel estimates, plotting 8 density lines over the space of 20-100% of the highest density equally using the kde1d function in python (adapted from MATLAB function kde2d (Botev et al., 2010), by Wuzhou Yang in the Arber Lab. Synapse positions were normalized to the reference of each brain, using three reference points including two to define the midline, and a third to the contralateral side of either the 5N, 7N, or ambiguous nucleus in the 12N). Scatter plots were where each point represents one synaptic terminal, and plotted with alpha 0.2. Contour density plots were made with the *contourf* function, and the kernel density plots (kde1d_1_plot) were made with bandwidth 0.1, kernel = Gaussian). Code can be found at https://github.com/stacci989/SynapticDensityMapping (when published online).

3D-Brain Registration

Each brain section of interest was registered to the Allen Brain Atlas according to a modified pipeline from the CortexLab, Allen CCF. (Adapted and optimized by Paola Patella and Chiara Pivetta from the Arber Lab). Briefly, each 80um section was individually cropped, rotated, and flipped so that all are in line with each other along the rostral to caudal axis of the brain. Sections were aligned and transformed to the matching sections from the Allen Brain Atlas, using SHARP-Track MATLAB user interface to register asymmetric slice images to the atlas with a manual input. Using the position of the nuclei quantified from either the Axio Scan or Spinning Disk Confocal (depending on density of nuclei and resolution), nuclei were added to the transformed and registered sections. Nuclei were then plotted in a 3D wire model of the brain, regions were tabulated according to the Allen CCF. Code adapted from the Allen CCF can be found at https://github.com/stacci989/3D_Registration (when published online).

References

Alonso, A., Merchán, P., Sandoval, J.E., Sánchez-Arrones, L., Garcia-Cazorla, A., Artuch, R., Ferrán, J.L., Martínez-de-la-Torre, M., and Puelles, L. (2013). Development of the serotonergic cells in murine raphe nuclei and their relations with rhombomeric domains. Brain Structure and Function *218*, 1229-1277.
Alstermark, B., and Isa, T. (2012). Circuits for skilled reaching and grasping. Annu Rev Neurosci *35*, 559-578.
Alstermark, B., Isa, T., Pettersson, L.G., and Sasaki, S. (2007). The C3–C4 propriospinal system in the cat and monkey: a spinal pre-motoneuronal centre for voluntary motor control. Acta Physiologica *189*, 123-140.
Altman, J., and Bayer, S.A. (1987). Development of the precerebellar nuclei in the rat: I. The precerebellar neuroepithelium of the rhombencephalon. Journal of Comparative Neurology *257*, 477-489.
Amezquita, R.A., Lun, A.T.L., Becht, E., Carey, V.J., Carpp, L.N., Geistlinger, L., Marini, F., Rue-Albrecht, K., Risso, D., Soneson, C*., et al.* (2020). Orchestrating single-cell analysis with Bioconductor. Nature Methods *17*, 137-145.
Ángeles Fernández-Gil, M., Palacios-Bote, R., Leo-Barahona, M., and Mora-Encinas, J.P. (2010). Anatomy of the Brainstem: A Gaze Into the Stem of Life. Seminars in Ultrasound, CT and MRI *31*, 196-219.
Apps, R., and Hawkes, R. (2009). Cerebellar cortical organization: a one-map hypothesis. Nat Rev Neurosci *10*, 670-681.
Arai, R., Jacobowitz, D.M., and Deura, S. (1994). Distribution of calretinin, calbindin-D28k, and parvalbumin in the rat thalamus. Brain Res Bull *33*, 595-614.
Aran, D., Looney, A.P., Liu, L., Wu, E., Fong, V., Hsu, A., Chak, S., Naikawadi, R.P., Wolters, P.J., Abate, A.R*., et al.* (2019). Reference-based analysis of lung single-cell sequencing reveals a transitional profibrotic macrophage. Nature Immunology *20*, 163-172.
Arber, S. (2012). Motor Circuits in Action: Specification, Connectivity, and Function. Neuron *74*, 975-989.
Arlt, C., Barroso-Luque, R., Kira, S., Bruno, C.A., Xia, N., Chettih, S.N., Soares, S., Pettit, N.L., and Harvey, C.D. (2021). Cognitive experience alters cortical involvement in navigation decisions. bioRxiv, 2021.2012.2010.472106.
Asahina, H., Masuba, A., Hirano, S., and Yuri, K. (2012). Distribution of protocadherin 9 protein in the developing mouse nervous system. Neuroscience *225*, 88-104.
Azim, E., and Alstermark, B. (2015). Skilled forelimb movements and internal copy motor circuits. Curr Opin Neurobiol *33*, 16-24.
Azim, E., Jiang, J., Alstermark, B., and Jessell, T.M. (2014). Skilled reaching relies on a V2a propriospinal internal copy circuit. Nature *508*, 357-363.
Bagnall, M.W., Zingg, B., Sakatos, A., Moghadam, S.H., Zeilhofer, H.U., and Lac, S.d. (2009). Glycinergic Projection Neurons of the Cerebellum. The Journal of Neuroscience *29*, 10104.
Bakken, T.E., Jorstad, N.L., Hu, Q., Lake, B.B., Tian, W., Kalmbach, B.E., Crow, M., Hodge, R.D., Krienen, F.M., Sorensen, S.A*., et al.* (2020). Evolution of cellular diversity in primary motor cortex of human, marmoset monkey, and mouse. bioRxiv, 2020.2003.2031.016972.
Basile, G.A., Quartu, M., Bertino, S., Serra, M.P., Boi, M., Bramanti, A., Anastasi, G.P., Milardi, D., and Cacciola, A. (2021). Red nucleus structure and function: from anatomy to clinical neurosciences. Brain Struct Funct *226*, 69-91.
Basler, K., Edlund, T., Jessell, T.M., and Yamada, T. (1993). Control of cell pattern in the neural tube: Regulation of cell differentiation by dorsalin-1, a novel TGFβ family member. Cell *73*, 687-702.

Batton III, R.R., Jayaraman, A., Ruggiero, D., and Carpenter, M.B. (1977). Fastigial efferent projections in the monkey: an autoradiographic study. Journal of Comparative Neurology *174*, 281-305.
Baumel, Y., Jacobson, G.A., and Cohen, D. (2009). Implications of functional anatomy on information processing in the deep cerebellar nuclei. Frontiers in cellular neuroscience *3*, 14-14.
Becker, M.I., and Person, A.L. (2019). Cerebellar Control of Reach Kinematics for Endpoint Precision. Neuron *103*, 335-348 e335.
Beitz, A.J., and Chan-Palay, V. (1979). The medial cerebellar nucleus in the rat: nuclear volume, cell number, density and orientation. Neuroscience *4*, 31-45.
Beitzel, C.S., Houck, B.D., Lewis, S.M., and Person, A.L. (2017a). Rubrocerebellar Feedback Loop Isolates the Interposed Nucleus as an Independent Processor of Corollary Discharge Information in Mice. The Journal of neuroscience : the official journal of the Society for Neuroscience *37*, 10085-10096.
Beitzel, C.S., Houck, B.D., Lewis, S.M., and Person, A.L. (2017b). Rubrocerebellar Feedback Loop Isolates the Interposed Nucleus as an Independent Processor of Corollary Discharge Information in Mice. J Neurosci *37*, 10085-10096.
Bjursten, L.M., Norrsell, K., and Norrsell, U. (1976). Behavioural repertory of cats without cerebral cortex from infancy. Experimental Brain Research *25*, 115-130.
Bohne, P., Schwarz, M.K., Herlitze, S., and Mark, M.D. (2019). A New Projection From the Deep Cerebellar Nuclei to the Hippocampus via the Ventrolateral and Laterodorsal Thalamus in Mice. Frontiers in Neural Circuits *13*.
Bosch-Bouju, C., Hyland, B., and Parr-Brownlie, L. (2013). Motor thalamus integration of cortical, cerebellar and basal ganglia information: implications for normal and parkinsonian conditions. Frontiers in Computational Neuroscience *7*.
Botev, Z.I., Grotowski, J.F., and Kroese, D.P. (2010). Kernel density estimation via diffusion. The Annals of Statistics *38*, 2916-2957.
Brennecke, P., Anders, S., Kim, J.K., Kołodziejczyk, A.A., Zhang, X., Proserpio, V., Baying, B., Benes, V., Teichmann, S.A., Marioni, J.C*., et al.* (2013). Accounting for technical noise in single-cell RNA-seq experiments. Nat Methods *10*, 1093-1095.
Briscoe, J., Pierani, A., Jessell, T.M., and Ericson, J. (2000). A homeodomain protein code specifies progenitor cell identity and neuronal fate in the ventral neural tube. Cell *101*, 435-445.
Brown, R.E., Basheer, R., McKenna, J.T., Strecker, R.E., and McCarley, R.W. (2012). Control of Sleep and Wakefulness. Physiological Reviews *92*, 1087-1187.
Bürk, K., Abele, M., Fetter, M., Dichgans, J., Skalej, M., Laccone, F., Didierjean, O., Brice, A., and Klockgether, T. (1996). Autosomal dominant cerebellar ataxia type I clinical features and MRI in families with SCA1, SCA2 and SCA3. Brain *119 (Pt 5)*, 1497-1505.
Buttner, U., Fuchs, A., Markert-Schwab, G., and Buckmaster, P. (1991). Fastigial nucleus activity in the alert monkey during slow eye and head movements. Journal of neurophysiology *65*, 1360-1371.
Caggiano, V., Leiras, R., Goñi-Erro, H., Masini, D., Bellardita, C., Bouvier, J., Caldeira, V., Fisone, G., and Kiehn, O. (2018). Midbrain circuits that set locomotor speed and gait selection. Nature *553*, 455-460.
Callaway, E.M., Dong, H.-W., Ecker, J.R., Hawrylycz, M.J., Huang, Z.J., Lein, E.S., Ngai, J., Osten, P., Ren, B., Tolias, A.S*., et al.* (2021). A multimodal cell census and atlas of the mammalian primary motor cortex. Nature *598*, 86-102.
Capelli, P., Pivetta, C., Soledad Esposito, M., and Arber, S. (2017). Locomotor speed control circuits in the caudal brainstem. Nature *551*, 373-377.
Catania, E.H., Pimenta, A., and Levitt, P. (2008). Genetic deletion of Lsamp causes exaggerated behavioral activation in novel environments. Behav Brain Res *188*, 380-390.
Chabrol, F.P., Blot, A., and Mrsic-Flogel, T.D. (2019). Cerebellar Contribution to Preparatory Activity in Motor Neocortex. Neuron *103*, 506-519.e504.

Chan-Palay, V. (1973a). Afferent axons and their relations with neurons in the nucleus lateralis of the cerebellum: a light microscopic study. Zeitschrift für Anatomie und Entwicklungsgeschichte *142*, 1-21.
Chan-Palay, V. (1973b). Neuronal plasticity in the cerebellar cortex and lateral nucleus. Z Anat Entwicklungsgesch *142*, 23-35.
Chan-Palay, V. (1973c). On the identification of the afferent axon terminals in the nucleus lateralis of the cerebellum an electron microscope study. Zeitschrift für Anatomie und Entwicklungsgeschichte *142*, 149-186.
Chan-Palay, V. (1977). Cerebellar Dentate Nucleus (Springer, Berlin, Heidelberg).
Chan, K.Y., Jang, M.J., Yoo, B.B., Greenbaum, A., Ravi, N., Wu, W.-L., Sánchez-Guardado, L., Lois, C., Mazmanian, S.K., Deverman, B.E*., et al.* (2017). Engineered AAVs for efficient noninvasive gene delivery to the central and peripheral nervous systems. Nature neuroscience *20*, 1172-1179.
Chen, K.H., Boettiger, A.N., Moffitt, J.R., Wang, S., and Zhuang, X. (2015). Spatially resolved, highly multiplexed RNA profiling in single cells. Science *348*.
Chung, S.H., Marzban, H., and Hawkes, R. (2009). Compartmentation of the cerebellar nuclei of the mouse. Neuroscience *161*, 123-138.
Conner, J.M., Bohannon, A., Igarashi, M., Taniguchi, J., Baltar, N., and Azim, E. (2021). Modulation of tactile feedback for the execution of dexterous movement. Science *374*, 316-323.
Cregg, J.M., Leiras, R., Montalant, A., Wanken, P., Wickersham, I.R., and Kiehn, O. (2020). Brainstem neurons that command mammalian locomotor asymmetries. Nature Neuroscience *23*, 730-740.
Czubayko, U., Sultan, F., Thier, P., and Schwarz, C. (2001). Two types of neurons in the rat cerebellar nuclei as distinguished by membrane potentials and intracellular fillings. Journal of Neurophysiology *85*, 2017-2029.
Dacre, J., Colligan, M., Clarke, T., Ammer, J.J., Schiemann, J., Chamosa-Pino, V., Claudi, F., Harston, J.A., Eleftheriou, C., Pakan, J.M.P*., et al.* (2021). A cerebellar-thalamocortical pathway drives behavioral context-dependent movement initiation. Neuron *109*, 2326-2338.e2328.
Darmohray, D.M., Jacobs, J.R., Marques, H.G., and Carey, M.R. (2019). Spatial and Temporal Locomotor Learning in Mouse Cerebellum. Neuron *102*, 217-231.e214.
De Zeeuw, C., and Berrebi, A. (1996). Individual Purkinje cell axons terminate on both inhibitory and excitatory neurons in the cerebellar and vestibular nuclei. Annals of the New York Academy of Sciences *781*, 607-610.
Dessaud, E., McMahon, A.P., and Briscoe, J. (2008). Pattern formation in the vertebrate neural tube: a sonic hedgehog morphogen-regulated transcriptional network. Development *135*, 2489-2503.
Dessaud, E., Yang, L.L., Hill, K., Cox, B., Ulloa, F., Ribeiro, A., Mynett, A., Novitch, B.G., and Briscoe, J. (2007). Interpretation of the sonic hedgehog morphogen gradient by a temporal adaptation mechanism. Nature *450*, 717-720.
Dum, R.P., and Strick, P.L. (1991). The origin of corticospinal projections from the premotor areas in the frontal lobe. J Neurosci *11*, 667-689.
Duò, A., Robinson, M.D., and Soneson, C. (2018). A systematic performance evaluation of clustering methods for single-cell RNA-seq data. F1000Res *7*, 1141-1141.
Eccles, J.C. (1973). The cerebellum as a computer: patterns in space and time. J Physiol *229*, 1-32.
Eccles, J.C., Sabah, N.H., and Táboříková, H. (1974a). Excitatory and inhibitory responses of neurones of the cerebellar fastigial nucleus. Experimental Brain Research *19*, 61-77.
Eccles, J.C., Sabah, N.H., and Táboříková, H. (1974b). The pathways responsible for excitation and inhibition of fastigial neurones. Experimental Brain Research *19*, 78-99.
Economo, M.N., Viswanathan, S., Tasic, B., Bas, E., Winnubst, J., Menon, V., Graybuck, L.T., Nguyen, T.N., Smith, K.A., Yao, Z*., et al.* (2018). Distinct descending motor cortex pathways and their roles in movement. Nature *563*, 79-84.

Ershov, D., Phan, M.-S., Pylvänäinen, J.W., Rigaud, S.U., Le Blanc, L., Charles-Orszag, A., Conway, J.R.W., Laine, R.F., Roy, N.H., Bonazzi, D.*, et al.* (2021). Bringing TrackMate into the era of machine-learning and deep-learning. bioRxiv, 2021.2009.2003.458852.
Esposito, M.S., Capelli, P., and Arber, S. (2014). Brainstem nucleus MdV mediates skilled forelimb motor tasks. Nature *508*, 351-356.
Ferreira-Pinto, M.J., Kanodia, H., Falasconi, A., Sigrist, M., Esposito, M.S., and Arber, S. (2021). Functional diversity for body actions in the mesencephalic locomotor region. Cell *184*, 4564-4578.e4518.
Fink, A.J., Englund, C., Daza, R.A.M., Pham, D., Lau, C., Nivison, M., Kowalczyk, T., and Hevner, R.F. (2006). Development of the deep cerebellar nuclei: transcription factors and cell migration from the rhombic lip. The Journal of neuroscience : the official journal of the Society for Neuroscience *26*, 3066-3076.
Fortin, M., Marchand, R., and Parent, A. (1998). Calcium-binding proteins in primate cerebellum. Neurosci Res *30*, 155-168.
Franklin, K.P., George. (2019). Paxinos and Franklin's the Mouse Brain in Stereotaxic Coordinates (Academic Press 2019).
Fujita, H., Kodama, T., and du Lac, S. (2020). Modular output circuits of the fastigial nucleus for diverse motor and nonmotor functions of the cerebellar vermis. eLife *9*, e58613.
Gao, Z., Davis, C., Thomas, A.M., Economo, M.N., Abrego, A.M., Svoboda, K., De Zeeuw, C.I., and Li, N. (2018). A cortico-cerebellar loop for motor planning. Nature *563*, 113-116.
Gehman, L.T., Meera, P., Stoilov, P., Shiue, L., O'Brien, J.E., Meisler, M.H., Ares, M., Jr., Otis, T.S., and Black, D.L. (2012). The splicing regulator Rbfox2 is required for both cerebellar development and mature motor function. Genes Dev *26*, 445-460.
Genis, D., Matilla, T., Volpini, V., Rosell, J., Dávalos, A., Ferrer, I., Molins, A., and Estivill, X. (1995). Clinical, neuropathologic, and genetic studies of a large spinocerebellar ataxia type 1 (SCA1) kindred: (CAG)n expansion and early premonitory signs and symptoms. Neurology *45*, 24-30.
Gerraty, R.T., Davidow, J.Y., Foerde, K., Galvan, A., Bassett, D.S., and Shohamy, D. (2018). Dynamic Flexibility in Striatal-Cortical Circuits Supports Reinforcement Learning. The Journal of neuroscience : the official journal of the Society for Neuroscience *38*, 2442-2453.
Glickstein, M. (1997). Chapter 14 Mossy-fibre sensory input to the cerebellum. In Progress in Brain Research, C.I. De Zeeuw, P. Strata, and J. Voogd, eds. (Elsevier), pp. 251-259.
Goldfarb, M., Schoorlemmer, J., Williams, A., Diwakar, S., Wang, Q., Huang, X., Giza, J., Tchetchik, D., Kelley, K., Vega, A.*, et al.* (2007). Fibroblast growth factor homologous factors control neuronal excitability through modulation of voltage-gated sodium channels. Neuron *55*, 449-463.
Grillner, S., Hellgren, J., Ménard, A., Saitoh, K., and Wikström, M.A. (2005). Mechanisms for selection of basic motor programs – roles for the striatum and pallidum. Trends in Neurosciences *28*, 364-370.
Gruntman, A.M., Su, L., and Flotte, T.R. (2017). Retro-Orbital Venous Sinus Delivery of rAAV9 Mediates High-Level Transduction of Brain and Retina Compared with Temporal Vein Delivery in Neonatal Mouse Pups. Hum Gene Ther *28*, 228-230.
Guo, J.-Z., Sauerbrei, B.A., Cohen, J.D., Mischiati, M., Graves, A.R., Pisanello, F., Branson, K.M., and Hantman, A.W. (2021). Disrupting cortico-cerebellar communication impairs dexterity. eLife *10*, e65906.
Guo, K., Yamawaki, N., Barrett, J.M., Tapies, M., and Shepherd, G.M.G. (2020). Cortico-Thalamo-Cortical Circuits of Mouse Forelimb S1 Are Organized Primarily as Recurrent Loops. J Neurosci *40*, 2849-2858.
Guo, Z.V., Inagaki, H.K., Daie, K., Druckmann, S., Gerfen, C.R., and Svoboda, K. (2017). Maintenance of persistent activity in a frontal thalamocortical loop. Nature *545*, 181-186.
Hamburgh, M. (1963). Analysis of the postnatal developmental effects of “reeler,” a neurological mutation in mice. A study in developmental genetics. Developmental Biology *8*, 165-185.
Hawkes, R. (1997). An anatomical model of cerebellar modules. Prog Brain Res *114*, 39-52.

He, Q., Versteeg, C.S., Suresh, A.K., Miller, L.E., and Bensmaia, S.J. (2021). Modulation of cutaneous responses in the cuneate nucleus of macaques during active movement. bioRxiv, 2021.2011.2015.468735.
Hinsey, J.C., Ranson, S.W., and McNattin, R.F. (1930). THE RÔLE OF THE HYPOTHALAMUS AND MESENCEPHALON IN LOCOMOTION. Archives of Neurology & Psychiatry *23*, 1-43.
Holmes, G. (1917). THE SYMPTOMS OF ACUTE CEREBELLAR INJURIES DUE TO GUNSHOT INJURIES. Brain *40*, 461-535.
Houck, B.D., and Person, A.L. (2015). Cerebellar Premotor Output Neurons Collateralize to Innervate the Cerebellar Cortex. J Comp Neurol *523*, 2254-2271.
Hounsgaard, J., and Midtgaard, J. (1989). Synaptic control of excitability in turtle cerebellar Purkinje cells. J Physiol *409*, 157-170.
Huang, C.-C., Sugino, K., Shima, Y., Guo, C., Bai, S., Mensh, B.D., Nelson, S.B., and Hantman, A.W. (2013). Convergence of pontine and proprioceptive streams onto multimodal cerebellar granule cells. eLife *2*, e00400.
Ichinohe, N., Mori, F., and Shoumura, K. (2000). A di-synaptic projection from the lateral cerebellar nucleus to the laterodorsal part of the striatum via the central lateral nucleus of the thalamus in the rat. Brain Research *880*, 191-197.
Ilicic, T., Kim, J.K., Kolodziejczyk, A.A., Bagger, F.O., McCarthy, D.J., Marioni, J.C., and Teichmann, S.A. (2016). Classification of low quality cells from single-cell RNA-seq data. Genome Biology *17*, 29.
Ito, M. (2006). Cerebellar circuitry as a neuronal machine. Prog Neurobiol *78*, 272-303.
Ito, M., and Itō, M. (1984). The cerebellum and neural control (Raven press).
Jessell, T.M. (2000). Neuronal specification in the spinal cord: inductive signals and transcriptional codes. Nature Reviews Genetics *1*, 20-29.
Joers, J.M., Deelchand, D.K., Lyu, T., Emir, U.E., Hutter, D., Gomez, C.M., Bushara, K.O., Eberly, L.E., and Öz, G. (2018). Neurochemical abnormalities in premanifest and early spinocerebellar ataxias. Ann Neurol *83*, 816-829.
Josset, N., Roussel, M., Lemieux, M., Lafrance-Zoubga, D., Rastqar, A., and Bretzner, F. (2018). Distinct Contributions of Mesencephalic Locomotor Region Nuclei to Locomotor Control in the Freely Behaving Mouse. Current Biology *28*, 884-901.e883.
Judd, E.N., Lewis, S.M., and Person, A.L. (2021). Diverse inhibitory projections from the cerebellar interposed nucleus. eLife *10*, e66231.
Kakei, S., Na, J., and Shinoda, Y. (2001). Thalamic terminal morphology and distribution of single corticothalamic axons originating from layers 5 and 6 of the cat motor cortex. J Comp Neurol *437*, 170-185.
Kebschull, J.M., Richman, E.B., Ringach, N., Friedmann, D., Albarran, E., Kolluru, S.S., Jones, R.C., Allen, W.E., Wang, Y., Cho, S.W.*, et al.* (2020). Cerebellar nuclei evolved by repeatedly duplicating a conserved cell-type set. Science *370*, eabd5059.
Keifer, J. (1996). Effects of red nucleus inactivation on burst discharge in turtle cerebellum in vitro: evidence for positive feedback. J Neurophysiol *76*, 2200-2210.
Kelly, R.M., and Strick, P.L. (2003). Cerebellar loops with motor cortex and prefrontal cortex of a nonhuman primate. J Neurosci *23*, 8432-8444.
Kennedy, P.R., and Humphrey, D.R. (1987). The compensatory role of the parvocellular division of the red nucleus in operantly conditioned rats. Neuroscience Research *5*, 39-62.
Kiselev, V.Y., Kirschner, K., Schaub, M.T., Andrews, T., Yiu, A., Chandra, T., Natarajan, K.N., Reik, W., Barahona, M., Green, A.R.*, et al.* (2017). SC3: consensus clustering of single-cell RNA-seq data. Nature Methods *14*, 483-486.
Kohlerman, N., Gibson, A., and Houk, J.C. (1982). Velocity signals related to hand movements recorded from red nucleus neurons in monkeys. Science *217*, 857-860.

Kumoi, K., Saito, N., Kuno, T., and Tanaka, C. (1988). Immunohistochemical localization of gamma-aminobutyric acid- and aspartate-containing neurons in the rat deep cerebellar nuclei. Brain Res *439*, 302-310.
Kuramoto, E., Furuta, T., Nakamura, K.C., Unzai, T., Hioki, H., and Kaneko, T. (2009). Two Types of Thalamocortical Projections from the Motor Thalamic Nuclei of the Rat: A Single Neuron-Tracing Study Using Viral Vectors. Cerebral Cortex *19*, 2065-2077.
Lalonde, R., Hayzoun, K., Derer, M., Mariani, J., and Strazielle, C. (2004). Neurobehavioral evaluation of Relnrl-orl mutant mice and correlations with cytochrome oxidase activity. Neuroscience Research *49*, 297-305.
Landmesser, L. (1978a). The development of motor projection patterns in the chick hind limb. J Physiol *284*, 391-414.
Landmesser, L. (1978b). The distribution of motoneurones supplying chick hind limb muscles. J Physiol *284*, 371-389.
Leclerc, N., Dore, L., and Hawkes, R. (1990). The compartmentalization of the monkey and rat cerebellar cortex: zebrin I and cytochrome oxidase. Brain research *506*, 70-78.
Leclerc, N., Schwarting, G.A., Herrup, K., Hawkes, R., and Yamamoto, M. (1992). Compartmentation in mammalian cerebellum: Zebrin II and P-path antibodies define three classes of sagittally organized bands of Purkinje cells. Proceedings of the National Academy of Sciences *89*, 5006-5010.
Lee, J., Wang, W., and Sabatini, B.L. (2020). Anatomically segregated basal ganglia pathways allow parallel behavioral modulation. Nature Neuroscience *23*, 1388-1398.
Leergaard, T.B., and Bjaalie, J.G. (2007). Topography of the complete corticopontine projection: from experiments to principal Maps. Front Neurosci *1*, 211-223.
Lein, E. (2017). What Is Your Conceptual Definition of "Cell Type"; in the Context of a Mature Organism? Cell Systems *4*, 255-259.
Lemon, R.N. (2008). Descending pathways in motor control. Annu Rev Neurosci *31*, 195-218.
Liao, Y., Smyth, G.K., and Shi, W. (2014). featureCounts: an efficient general purpose program for assigning sequence reads to genomic features. Bioinformatics *30*, 923-930.
Liem Jr, K.F., Tremml, G., Roelink, H., and Jessell, T.M. (1995). Dorsal differentiation of neural plate cells induced by BMP-mediated signals from epidermal ectoderm. Cell *82*, 969-979.
Low, A.Y.T., Thanawalla, A.R., Yip, A.K.K., Kim, J., Wong, K.L.L., Tantra, M., Augustine, G.J., and Chen, A.I. (2018a). Precision of Discrete and Rhythmic Forelimb Movements Requires a Distinct Neuronal Subpopulation in the Interposed Anterior Nucleus. Cell Rep *22*, 2322-2333.
Low, A.Y.T., Thanawalla, A.R., Yip, A.K.K., Kim, J., Wong, K.L.L., Tantra, M., Augustine, G.J., and Chen, A.I. (2018b). Precision of Discrete and Rhythmic Forelimb Movements Requires a Distinct Neuronal Subpopulation in the Interposed Anterior Nucleus. Cell Reports *22*, 2322-2333.
Lu, L., Cao, Y., Tokita, K., Heck, D., and Boughter, J. (2013). Medial cerebellar nuclear projections and activity patterns link cerebellar output to orofacial and respiratory behavior. Frontiers in Neural Circuits *7*.
Machado, A.S., Darmohray, D.M., Fayad, J., Marques, H.G., and Carey, M.R. (2015). A quantitative framework for whole-body coordination reveals specific deficits in freely walking ataxic mice. eLife *4*, e07892.
Macosko, Evan Z., Basu, A., Satija, R., Nemesh, J., Shekhar, K., Goldman, M., Tirosh, I., Bialas, Allison R., Kamitaki, N., Martersteck, Emily M*., et al.* (2015). Highly Parallel Genome-wide Expression Profiling of Individual Cells Using Nanoliter Droplets. Cell *161*, 1202-1214.
McCarthy, D.J., Campbell, K.R., Lun, A.T.L., and Wills, Q.F. (2017). Scater: pre-processing, quality control, normalization and visualization of single-cell RNA-seq data in R. Bioinformatics *33*, 1179-1186.
Mezey, E. (1977). QUANTITATIVE CYTOLOGY AND ELECTRON MICROSCOPY OF THE CEREBELLAR NUCLEI IN THE CAT.

Middleton, F.A., and Strick, P.L. (1997). Cerebellar Output Channels. In International Review of Neurobiology, J.D. Schmahmann, ed. (Academic Press), pp. 61-82.
Middleton, F.A., and Strick, P.L. (2001). Cerebellar Projections to the Prefrontal Cortex of the Primate. The Journal of Neuroscience *21*, 700.
Miller, L.E., and Houk, J.C. (1995). Motor co-ordinates in primate red nucleus: preferential relation to muscle activation versus kinematic variables. J Physiol *488 (Pt 2)*, 533-548.
Nelson, A., Abdelmesih, B., and Costa, R.M. (2021). Corticospinal populations broadcast complex motor signals to coordinated spinal and striatal circuits. Nature Neuroscience *24*, 1721-1732.
Neudert, F., Nuernberger, K.K., and Redies, C. (2008). Comparative analysis of cadherin expression and connectivity patterns in the cerebellar system of ferret and mouse. J Comp Neurol *511*, 736-752.
Noda, H. (1990). Sugita S, and Ikeda Y. Afferent and efferent connections of the oculomotor region of the fastigial nucleus in the macaque monkey J Comp Neurol *302*, 330-348.
Noga, B.R., Kettler, J., and Jordan, L.M. (1988). Locomotion produced in mesencephalic cats by injections of putative transmitter substances and antagonists into the medial reticular formation and the pontomedullary locomotor strip. The Journal of Neuroscience *8*, 2074.
Onodera, S., and Hicks, T.P. (2009). A comparative neuroanatomical study of the red nucleus of the cat, macaque and human. PLoS One *4*, e6623.
Opris, I., Dai, X., Johnson, D.M.G., Sanchez, F.J., Villamil, L.M., Xie, S., Lee-Hauser, C.R., Chang, S., Jordan, L.M., and Noga, B.R. (2019). Activation of Brainstem Neurons During Mesencephalic Locomotor Region-Evoked Locomotion in the Cat. Front Syst Neurosci *13*, 69.
Orr, H.T., Chung, M.Y., Banfi, S., Kwiatkowski, T.J., Jr., Servadio, A., Beaudet, A.L., McCall, A.E., Duvick, L.A., Ranum, L.P., and Zoghbi, H.Y. (1993). Expansion of an unstable trinucleotide CAG repeat in spinocerebellar ataxia type 1. Nat Genet *4*, 221-226.
Palkovits, M., Mezey, É., Hamori, J., and Szentagothai, J. (1977). Quantitative histological analysis of the cerebellar nuclei in the cat. I. Numerical data on cells and on synapses. Experimental Brain Research *28*, 189-209.
Parenti, R., Zappalà, A., Serapide, M.F., Pantò, M.R., and Cicirata, F. (2002). Projections of the basilar pontine nuclei and nucleus reticularis tegmenti pontis to the cerebellar nuclei of the rat. J Comp Neurol *452*, 115-127.
Patro, R., Duggal, G., Love, M.I., Irizarry, R.A., and Kingsford, C. (2017). Salmon provides fast and bias-aware quantification of transcript expression. Nature methods *14*, 417-419.
Picelli, S., Faridani, O.R., Björklund, Å.K., Winberg, G., Sagasser, S., and Sandberg, R. (2014). Full-length RNA-seq from single cells using Smart-seq2. Nature Protocols *9*, 171-181.
Pituello, F. (1997). Neuronal specification: Generating diversity in the spinal cord. Current Biology *7*, R701-R704.
Pivetta, C., Esposito, Maria S., Sigrist, M., and Arber, S. (2014). Motor-Circuit Communication Matrix from Spinal Cord to Brainstem Neurons Revealed by Developmental Origin. Cell *156*, 537-548.
Prekop, H.-T., Kroiss, A., Rook, V., Zagoraiou, L., Jessell, T.M., Fernandes, C., Delogu, A., and Wingate, R.J. (2018). Sox14 is required for a specific subset of cerebello–olivary projections. Journal of Neuroscience *38*, 9539-9550.
Prevosto, V., and Sommer, M.A. (2013). Cognitive control of movement via the cerebellar-recipient thalamus. Front Syst Neurosci *7*, 56-56.
Puelles, E., Acampora, D., Lacroix, E., Signore, M., Annino, A., Tuorto, F., Filosa, S., Corte, G., Wurst, W., and Ang, S.-L. (2003). Otx dose-dependent integrated control of antero-posterior and dorso-ventral patterning of midbrain. Nature neuroscience *6*, 453-460.
Puelles, E., Annino, A., Tuorto, F., Usiello, A., Acampora, D., Czerny, T., Brodski, C., Ang, S.-L., Wurst, W., and Simeone, A. (2004). Otx2 regulates the extent, identity and fate of neuronal progenitor domains in the ventral midbrain.

Puelles, L., Harrison, M., Paxinos, G., and Watson, C. (2013). A developmental ontology for the mammalian brain based on the prosomeric model. Trends in Neurosciences *36*, 570-578.
Puelles, L., Martínez, S., Martínez-De-La-Torre, M., and Rubenstein, J.L. (2015). Gene maps and related histogenetic domains in the forebrain and midbrain. In The rat nervous system (Elsevier), pp. 3-24.
Redgrave, P., Rodriguez, M., Smith, Y., Rodriguez-Oroz, M.C., Lehericy, S., Bergman, H., Agid, Y., DeLong, M.R., and Obeso, J.A. (2010). Goal-directed and habitual control in the basal ganglia: implications for Parkinson's disease. Nature Reviews Neuroscience *11*, 760-772.
Roh, J., Cheung, V.C.K., and Bizzi, E. (2011). Modules in the brain stem and spinal cord underlying motor behaviors. Journal of neurophysiology *106*, 1363-1378.
Rowland, N.C., and Jaeger, D. (2005). Coding of Tactile Response Properties in the Rat Deep Cerebellar Nuclei. Journal of Neurophysiology *94*, 1236-1251.
Rowland, N.C., and Jaeger, D. (2008). Responses to Tactile Stimulation in Deep Cerebellar Nucleus Neurons Result From Recurrent Activation in Multiple Pathways. Journal of Neurophysiology *99*, 704-717.
Ruder, L., Schina, R., Kanodia, H., Valencia-Garcia, S., Pivetta, C., and Arber, S. (2021). A functional map for diverse forelimb actions within brainstem circuitry. Nature *590*, 445-450.
Ruigrok, T.J.H., and Teune, T.M. (2014). Collateralization of cerebellar output to functionally distinct brainstem areas. A retrograde, non-fluorescent tracing study in the rat. Front Syst Neurosci *8*, 23-23.
Sathyamurthy, A., Barik, A., Dobrott, C.I., Matson, K.J.E., Stoica, S., Pursley, R., Chesler, A.T., and Levine, A.J. (2020). Cerebellospinal Neurons Regulate Motor Performance and Motor Learning. Cell Reports *31*, 107595.
Sathyamurthy, A., Johnson, K.R., Matson, K.J.E., Dobrott, C.I., Li, L., Ryba, A.R., Bergman, T.B., Kelly, M.C., Kelley, M.W., and Levine, A.J. (2018). Massively Parallel Single Nucleus Transcriptional Profiling Defines Spinal Cord Neurons and Their Activity during Behavior. Cell Reports *22*, 2216-2225.
Scala, F., Kobak, D., Bernabucci, M., Bernaerts, Y., Cadwell, C.R., Castro, J.R., Hartmanis, L., Jiang, X., Laturnus, S., Miranda, E.*, et al.* (2021). Phenotypic variation of transcriptomic cell types in mouse motor cortex. Nature *598*, 144-150.
Schäfer, C.B., Gao, Z., De Zeeuw, C.I., and Hoebeek, F.E. (2020). Cerebello-Thalamic Spike Transfer via Temporal Coding and Cortical Adaptation. bioRxiv, 2020.2001.2019.911610.
Shinoda, Y., Sugiuchi, Y., Futami, T., and Izawa, R. (1992). Axon collaterals of mossy fibers from the pontine nucleus in the cerebellar dentate nucleus. J Neurophysiol *67*, 547-560.
Sprague, J.M., and Chambers, W.W. (1953). Regulation of posture in intact and decerebrate cat. I. Cerebellum, reticular formation, vestibular nuclei. J Neurophysiol *16*, 451-463.
Srivastava, A., Malik, L., Smith, T., Sudbery, I., and Patro, R. (2019). Alevin efficiently estimates accurate gene abundances from dscRNA-seq data. Genome Biology *20*, 65.
Strick, P.L. (1983). The influence of motor preparation on the response of cerebellar neurons to limb displacements. The Journal of Neuroscience *3*, 2007.
Stuart, T., Butler, A., Hoffman, P., Hafemeister, C., Papalexi, E., Mauck, W.M., 3rd, Hao, Y., Stoeckius, M., Smibert, P., and Satija, R. (2019). Comprehensive Integration of Single-Cell Data. Cell *177*, 1888-1902.e1821.
Sugihara, I., and Shinoda, Y. (2007). Molecular, Topographic, and Functional Organization of the Cerebellar Nuclei: Analysis by Three-Dimensional Mapping of the Olivonuclear Projection and Aldolase C Labeling. The Journal of Neuroscience *27*, 9696-9710.
Sugihara, I., Wu, H.S., and Shinoda, Y. (1999). Morphology of single olivocerebellar axons labeled with biotinylated dextran amine in the rat. Journal of Comparative Neurology *414*, 131-148.
Sugiuchi, Y., Izawa, Y., Takahashi, M., Na, J., and Shinoda, Y. (2005). Physiological Characterization of Synaptic Inputs to Inhibitory Burst Neurons From the Rostral and Caudal Superior Colliculus. Journal of Neurophysiology *93*, 697-712.

Swenson, R.S., and Castro, A.J. (1983). The afferent connections of the inferior olivary complex in rats. An anterograde study using autoradiographic and axonal degeneration techniques. Neuroscience *8*, 259-275.
Terashima, T. (1983). Distribution and Morphology of Corticospinal Tract Neurons in Reeler Mouse Cortex by the Retrograde HRP Method. Journal of comparative neurology, 314-326.
Tervo, D.G.R., Hwang, B.-Y., Viswanathan, S., Gaj, T., Lavzin, M., Ritola, K.D., Lindo, S., Michael, S., Kuleshova, E., Ojala, D*., et al.* (2016). A Designer AAV Variant Permits Efficient Retrograde Access to Projection Neurons. Neuron *92*, 372-382.
Teune, T.M., van der Burg, J., van der Moer, J., Voogd, J., and Ruigrok, T.J.H. (2000). Topography of cerebellar nuclear projections to the brain stem in the rat. In Progress in Brain Research (Elsevier), pp. 141-172.
Thach, W.T. (1968). Discharge of Purkinje and cerebellar nuclear neurons during rapidly alternating arm movements in the monkey. Journal of Neurophysiology *31*, 785-797.
Thach, W.T. (1975). Timing of activity in cerebellar dentate nucleus and cerebral motor cortex during prompt volitional movement. Brain Research *88*, 233-241.
Thanawalla, A.R., Chen, A.I., and Azim, E. (2020). The Cerebellar Nuclei and Dexterous Limb Movements. Neuroscience *450*, 168-183.
Tolbert, D.L., Massopust, L.C., Murphy, M.G., and Young, P.A. (1976). The anatomical organization of the cerebello-olivary projection in the cat. J Comp Neurol *170*, 525-544.
Toyama, K., Tsukahara, N., Kosaka, K., and Matsunami, K. (1970). Synaptic excitation of red nucleus neurones by fibres from interpositus nucleus. Exp Brain Res *11*, 187-198.
Ulfig, N., and Chan, W.Y. (2002). Expression of a kinase anchoring protein 79 and synaptophysin in the developing human red nucleus. Neurosignals *11*, 95-102.
Van der Want, J., Wiklund, L., Guegan, M., Ruigrok, T., and Voogd, J. (1989). Anterograde tracing of the rat olivocerebellar system with Phaseolus vulgaris leucoagglutinin (PHA-L). Demonstration of climbing fiber collateral innervation of the cerebellar nuclei. Journal of Comparative Neurology *288*, 1-18.
Vong, L., Ye, C., Yang, Z., Choi, B., Chua, S., Jr., and Lowell, B.B. (2011). Leptin action on GABAergic neurons prevents obesity and reduces inhibitory tone to POMC neurons. Neuron *71*, 142-154.
Wallén-Mackenzie, Å., Dumas, S., Papathanou, M., Martis Thiele, M.M., Vlcek, B., König, N., and Björklund, Å.K. (2020). Spatio-molecular domains identified in the mouse subthalamic nucleus and neighboring glutamatergic and GABAergic brain structures. Communications Biology *3*, 338.
Wang, F., Flanagan, J., Su, N., Wang, L.-C., Bui, S., Nielson, A., Wu, X., Vo, H.-T., Ma, X.-J., and Luo, Y. (2012). RNAscope: a novel in situ RNA analysis platform for formalin-fixed, paraffin-embedded tissues. J Mol Diagn *14*, 22-29.
Wang, Q., Ding, S.-L., Li, Y., Royall, J., Feng, D., Lesnar, P., Graddis, N., Naeemi, M., Facer, B., Ho, A*., et al.* (2020a). The Allen Mouse Brain Common Coordinate Framework: A 3D Reference Atlas. Cell *181*, 936-953.e920.
Wang, X., Liu, Y., Li, X., Zhang, Z., Yang, H., Zhang, Y., Williams, P.R., Alwahab, N.S.A., Kapur, K., Yu, B*., et al.* (2017). Deconstruction of Corticospinal Circuits for Goal-Directed Motor Skills. Cell *171*, 440-455.e414.
Wang, X., Yu, S.-y., Ren, Z., De Zeeuw, C.I., and Gao, Z. (2020b). A FN-MdV pathway and its role in cerebellar multimodular control of sensorimotor behavior. Nature Communications *11*, 6050.
Watson, C. (2010). The presumptive isthmic region in a mouse as defined by fgf8 expression. Brain Behav Evol *75*, 315.
Watson, C., Kirkcaldie, M., and Puelles, L. (2017). Developmental gene expression redefines the mammalian brain stem.
Whelan, P.J. (1996). CONTROL OF LOCOMOTION IN THE DECEREBRATE CAT. Progress in Neurobiology *49*, 481-515.

Wolpert, D.M., Miall, R.C., and Kawato, M. (1998). Internal models in the cerebellum. Trends in Cognitive Sciences *2*, 338-347.
Wu, H.S., Sugihara, I., and Shinoda, Y. (1999). Projection patterns of single mossy fibers originating from the lateral reticular nucleus in the rat cerebellar cortex and nuclei. J Comp Neurol *411*, 97-118.
Yamada, M., and Hoshino, M. (2016). Precerebellar Nuclei. In Essentials of Cerebellum and Cerebellar Disorders: A Primer For Graduate Students, D.L. Gruol, N. Koibuchi, M. Manto, M. Molinari, J.D. Schmahmann, and Y. Shen, eds. (Cham: Springer International Publishing), pp. 63-67.
Yamaguchi, K., and Goto, N. (2008). Development of the human parvocellular red nucleus. A morphological study. Dev Neurosci *30*, 325-330.
Zappia, L., and Oshlack, A. (2018). Clustering trees: a visualization for evaluating clusterings at multiple resolutions. GigaScience *7*.
Zervas, M., Millet, S., Ahn, S., and Joyner, A.L. (2004). Cell behaviors and genetic lineages of the mesencephalon and rhombomere 1. Neuron *43*, 345-357.
Zhang, M., Eichhorn, S.W., Zingg, B., Yao, Z., Zeng, H., Dong, H., and Zhuang, X. (2020). Molecular, spatial and projection diversity of neurons in primary motor cortex revealed by in situ single-cell transcriptomics. bioRxiv, 2020.2006.2004.105700.
Zhang, X., Li, T., Liu, F., Chen, Y., Yao, J., Li, Z., Huang, Y., and Wang, J. (2019). Comparative Analysis of Droplet-Based Ultra-High-Throughput Single-Cell RNA-Seq Systems. Molecular Cell *73*, 130-142.e135.
Zhang, Z., Zhou, J., Tan, P., Pang, Y., Rivkin, A.C., Kirchgessner, M.A., Williams, E., Lee, C.-T., Liu, H., Franklin, A.D.*, et al.* (2021). Epigenomic diversity of cortical projection neurons in the mouse brain. Nature *598*, 167-173.